arXiv:astro-ph/0003219v2 22 Mar 2000

The Northern ROSAT All-Sky (NORAS) Galaxy Cluster Survey I: X-ray Properties of Clusters Detected as Extended X-ray Sources [1]

H. Böhringer[1], W. Voges[1], J.P. Huchra[2],B. McLean[3], R. Giacconi[4], P. Rosati[4], R. Burg[3], J. Mader[2], P. Schuecker[1], D. Simiç[1], S. Komossa[1], T.H. Reiprich[1], J. Retzlaff[1], J. Trümper[1]

Received ______________________; accepted ______________________

---

[1] Results reported here are based on observations made with the Multiple Mirror Telescope, a joint facility of the Smithonian Institution and the University of Arizona

[1] Max-Planck-Institut für extraterrestrische Physik, D-85740 Garching,Germany

[2] Harvard-Smithonian Center for Astrophysics, 60 Garden Street, Cambridge, MA 0213

[4] Space Telescope Science Institute, San Martin Drive, Baltimore, MA 02138

[3] ESO, D-85748 Garching,Germany

ABSTRACT

In the construction of an X-ray selected sample of galaxy clusters for cosmological studies, we have assembled a sample of 495 X-ray sources found to show extended X-ray emission in the first processing of the ROSAT All-Sky Survey. The sample covers the celestial region with declination $\delta \geq 0^\circ$ and galactic latitude $|b_{II}| \geq 20^\circ$ and comprises sources with a count rate ≥ 0.06 counts s^{-1} and a source extent likelihood of 7. In an optical follow-up identification program we find 378 (76%) of these sources to be clusters of galaxies.

It was necessary to reanalyse the sources in this sample with a new X-ray source characterization technique to provide more precise values for the X-ray flux and source extent than obtained from the standard processing. This new method, termed growth curve analysis (GCA), has the advantage over previous methods to be robust, easy to model and to integrate into simulations, to provide diagnostic plots for visual inspection, and to make extensive use of the X-ray data. The source parameters obtained assist the source identification and provide more precise X-ray fluxes. This reanalysis is based on data from the more recent second processing of the ROSAT Survey. We present a catalogue of the cluster sources with the X-ray properties obtained as well as a list of the previously flagged extended sources which are found to have a non-cluster counterpart. We discuss the process of source identification from the combination of optical and X-ray data.

To investigate the overall completeness of the cluster sample as a function of the X-ray flux limit, we extent the search for X-ray cluster sources to the data of the second processing of the ROSAT Survey for the northern sky region between 9^h and 14^h in right ascension. We include the search for X-ray emission of known clusters as well as a new investigation of extended X-ray sources. In the course of this search we find X-ray emission from additional 85 Abell clusters and 56 very probable cluster candidates among the newly found extended sources. A comparison of the X-ray cluster number counts of the NORAS sample with the REFLEX Cluster Survey results leads to an estimate of the completeness of the NORAS sample of RASS I extended clusters of about 50% at an X-ray flux of $F_x(0.1 - 2.4\mathrm{keV}) = 3 \times 10^{-12}$ erg s^{-1} cm^{-2}. The estimated completeness achieved by adding the supplementary sample in the study area amounts to about 82% in comparison to REFLEX. The low completeness introduces an uncertainty in the use of the sample for cosmological statistical studies which will be cured with the completion of the continuing Northern ROSAT All-Sky

(NORAS) cluster survey project.

Subject headings: Galaxies: Clusters of, X-ray: Galaxies, Cosmology: Large-Scale Structure of Universe - Surveys

1. Introduction

Galaxy clusters are important tracers of the large-scale structure of the matter distribution in the Universe. As the evolution of clusters is closely linked to the overall evolution of the cosmic large-scale structure, important tests of cosmological models can be performed with statistical data on the cluster population. The mass distribution and the spatial clustering of clusters are particularly interesting measures in such studies (e.g. Henry et al. 1992, Bahcall & Cen 1992, Eke et al. 1998, Thomas et al. 1998, Borgani et al. 1999). The construction of well defined cluster catalogues and the compilation of their properties is therefore an important task for observational cosmology.

Galaxy clusters were first detected and are continued to be cataloged from optical observations of galaxy density enhancements in the sky (e.g. Abell 1958, Abell et al. 1989 (ACO), Zwicky et al. 1961 - 68, Shectman 1985, Dalton et al. 1992, Lumbsden 1992, Collins et al. 1995, Couch et al. 1991, Bower et al. 1994, Postman et al. 1996, Olsen et al. 1999, Scodeggio et al. 1999). X-rays have also successfully been used to detect galaxy clusters and to conduct clusters surveys (e.g. Picinotti et al. 1982, Kowalski 1984, Lahav et al. 1989, Gioia et al. 1984, 1990, Edge et al. 1990, Henry et al. 1992, Romer et al. 1994, Pierre et al. 1994, Ebeling et al. 1996, 1998, Castander et al. 1995, Rosati et al. 1995, 1998, Burns et al. 1996 Collins et al. 1997, Burke et al. 1997, Vihklinin et al. 1998, Scharf et al. 1997, Jones et al. 1998, Böhringer et al. 1998, De Grandi et al. 1999, Ledlow et al. 1999, Romer et al. 1999). The use of samples of clusters detected and characterized by their X-ray emission for cosmological studies has two major advantages over samples based on optical observations. First, the optical observations (without very extensive redshift measurements) provide only the projected galaxy distribution and not all galaxy density enhancements in the sky are bound, three-dimensional entities. In fact, in the course of the ESO Nearby Abell Cluster Survey (Katgert et al. 1996, Mazure et al. 1996) it was found that of the order of 10% of the rich clusters from the catalogue of Abell, Corwin, and Olowin (1989) in the nearby redshift range $z \leq 0.1$ were spurious clusters without obvious clustering peaks in redshift space. For the optical surveys the reliability has improved, however, with the advent of multi-color surveys and machine based matched-filter selection techniques (e.g. Postman et al. 1996, Olsen et al. 1999). Extended X-ray emission from the hot intra-cluster plasma of galaxy clusters is a more clear indication of the presence of a large gravitationally bound mass aggregate since otherwise the hot plasma would have been dispersed immediately. And secondly, the X-ray luminosity is a parameter much more tightly correlated with the mass of clusters than the usual richness parameter measured in the optical (e.g. Reiprich & Böhringer 1999). Thus X-ray emission gives evidence for the presence of galaxy clusters within a certain mass interval. (The correlation of the X-ray luminosity and cluster mass actually shows a dispersion of about a factor of 1.6 if one wishes to determine the mass for a given luminosity - Reiprich & Böhringer, in preparation). The one exception is the case where the X-ray emission is not clearly extended and where the cluster emission could be confused with the emission of an AGN within the cluster or with a possible foreground or background source. This confusion is a problem for a very small fraction of the cluster sources, but in general X-rays are a very useful indicator of a true cluster. In addition projection effects are minimized in X-ray surveys since the X-ray surface brightness is more centrally concentrated than the galaxy distribution.

The ROSAT All-Sky Survey (RASS), the only large scale X-ray survey conducted with an X-ray telescope (Trümper 1993, Voges et al. 1999), provides an ideal data base to detect large numbers of clusters and to compile an all-sky cluster catalogue with homogeneously applied selection criteria. To exploit this unique data base we are conducting an optical follow-up identification program and redshift survey of RASS X-ray clusters in the northern hemisphere, the Northern ROSAT All-Sky (NORAS) Cluster Survey project. A complementary survey, the REFLEX (ROSAT-ESO Flux Limited X-ray) Cluster Survey, is conducted for the southern part of the RASS (Böhringer et al. 1998, Guzzo et al. 1999). The NORAS identification program was started in 1992 in a first step with a list of extended X-ray sources extracted from the general source list of the first RASS processing (RASS I; Voges et al. 1992). Apart from the selection for extent the following extraction criteria were used: northern declination, a minimum distance of 20 degrees to the galactic plane, and a minimum count rate of 0.06 cts s^{-1} in the ROSAT broad band (0.1 to 2.4 keV). The criterion of X-ray source extent was chosen for the selection of promising cluster candidates, because early tests have shown that such a sample would be highly enriched (by about 70 - 80%) in galaxy clusters. Contrary to the cluster selection scheme used for the REFLEX Survey which is based on the correlation of X-ray sources with galaxy overdensities, the present sample selection is purely based on X-ray information. With this different bias the NORAS Survey has also the potential to find more distant and possibly “opitcally dark” clusters.

The identification of these sources is now complete. In this paper we present a catalogue of the X-ray properties of the 378 cluster sources and 117 non-cluster sources of the primary candidate list. An accompanying paper by Huchra et al. (1999) provides a detailed catalogue of the optical identifications and redshift measurements of this sample, and scientific aspects of this survey are discussed in a paper by Giacconi et al. (1999). While this survey was ongoing some of the brighter sources of this sample as well as some X-ray emitting Abell and Zwicky clusters were spectroscopically observed for the ”BCS program” (Ebeling et al. 1998) by Allen et al. (1992) and Crawford et al. (1995, 1999). The region with the deepest exposure in the northern RASS, the north excliptic pole with exposure times ranging from 2000 to over 40000 sec, is also the subject of a dedicated survey which has identified all X-ray sources (c.f. Henry et al. 1995; Gioia et al. 1995; Bower et al. 1996; and Henry et al. 1997).

Further studies on the X-ray properties of a sample of these extended sources in $2^\circ \times 2^\circ$ sky fields extracted from the RASS revealed, that in the first standard processing of the RASS the count rate and the extent of the cluster sources are severely underestimated (see also Ebeling et al. 1996, DeGrandi et al. 1997). Therefore a detailed reanalysis of the sources in the present sample was necessary.

Here we also report the results of the detailed reanalysis of the sources using a new X-ray source characterization technique. In 1996, a second revised processing of the RASS (RASS II; Voges et al. 1999) with greatly improved attitude quality and with a fully merged photon data base became available. Our reanalysis is based on these new data.

Since the incomplete assessment of the X-ray count rate and extent in RASS I not only leads to an underestimate of the X-ray fluxes for extended sources but also to an incompleteness of the sample extracted from the data base with certain limiting parameters, we have also used the new RASS data base to explore the incompleteness of the present cluster sample in terms of a flux-limited X-ray selected sample of galaxy clusters. In this study we selected a subregion covering the right ascension range from 9^h to 14^h. In a first step we use the Abell cluster catalogue to study the completeness provided by the RASS I extent criterion. We further study the prospects of finding more clusters with a more comprehensive extent criterion based on the new X-ray source analysis technique. This study also points the way to a more complete selection of galaxy clusters from the RASS X-ray sources. We now apply this algorithm in the ongoing NORAS cluster redshift survey.

Since we will probably not be able tp rapidly complete the identifications of the newly found sources, we decided to publish the first part of the survey for which identifications are now complete and redshifts are nearly (all but 9) complete. The main emphasis here is not to publish a catalog of a complete, flux-limited sample, but to compile a cluster catalogue with reliable identifications based on a wealth of X-ray and optical data which are included in the identification process in a comprehensive way. The present sample contains many newly found objects, some of which are interesting targets for further astrophysical studies.

The paper is organized as follows. In Section 2 we summarize the properties of the primary RASS I source list of extended sources, and in Section 3 we describe the techniques used to reanalyze the X-ray properties of the sample sources. In Section 4 we present the X-ray source catalogue with detailed X-ray properties of the 495 sources. Major X-ray properties of the sources which help in the identification of the objects are discussed in

Section 5. The completeness of the sample is addressed in Sections 6 and 7 where we report the results of a rigorous search for X-ray emission from all ACO clusters and search for more extended X-ray sources with an improved analysis algorithm in a test region ranging in right ascensions from 9^h to 14^h. In Section 8 we compare the present results to the previous ROSAT Bright Cluster Survey by Ebeling et al. (1998). Section 9 provides a summary and conclusions. Throughout the paper we are using a Hubble parameter of $H_0 = 50$ km s^{-1} Mpc^{-1} and $h_{50} = H_0/(50$ km s^{-1} Mpc$^{-1})$ and further $\Omega_0 = 1$ for the density parameter and $\Lambda_0 = 0$ for the cosmological parameter.

2. The RASS I list of extended sources

During the ROSAT mission the first All-Sky Survey was conducted with an X-ray telescope (Trümper 1992, 1993). The RASS was performed over a period of six months from August 1990 to January 1991 with two follow-up auxiliary survey missions carried out to fill the gaps in the survey in February and August 1991. The first processing of the survey (RASS I) provided a source list of 49441 sources (Voges et al. 1992, 1996). For this first analysis the survey data received were sorted into one of 90 2-degree wide strips (oriented in the direction of constant ecliptic longitude) while the satellite was still scanning the sky. As a consequence of this, strips are overlapping in regions outside the equator. Photons are exclusively sorted into only one of the overlapping regions. Therefore the exposure time across the strips is quite homogenous, but no advantage can be taken of the high total exposure in the ecliptic pole regions. The survey product resulting from this first processing of the RASS will be referred to as RASS I data base. (The situation is different in RASS II, the second processing, where the $6.4° \times 6.4°$ sky regions contain the full exposure data from the RASS). The RASS was conducted with the X-ray telescope (Aschenbach et al. 1988) and Position Sensitive Proportional Counter (PSPC; Pfeffermann et al. 1986) providing a high sensitivity and a very low internal background. A histogram of the exposure time distribution of the NORAS survey area in RASS I is shown in Fig. 1 (where it is also compared to the exposure distribution in RASS II). For this statistic we use the maximum exposure in any of the strips for those cases where a sky pixel is covered by several survey strips. The mean and median exposure times are 397 and 402 sec, respectively.

The source detection procedure was based on detections using two alternative sliding window techniques plus a subsequent evaluation of the source detection significance and quality based on a maximum likelihood method (Voges et al. 1992, for aspects of the maximum likelihood method see also Cruddace et al. 1991). Only sources with a likelihood

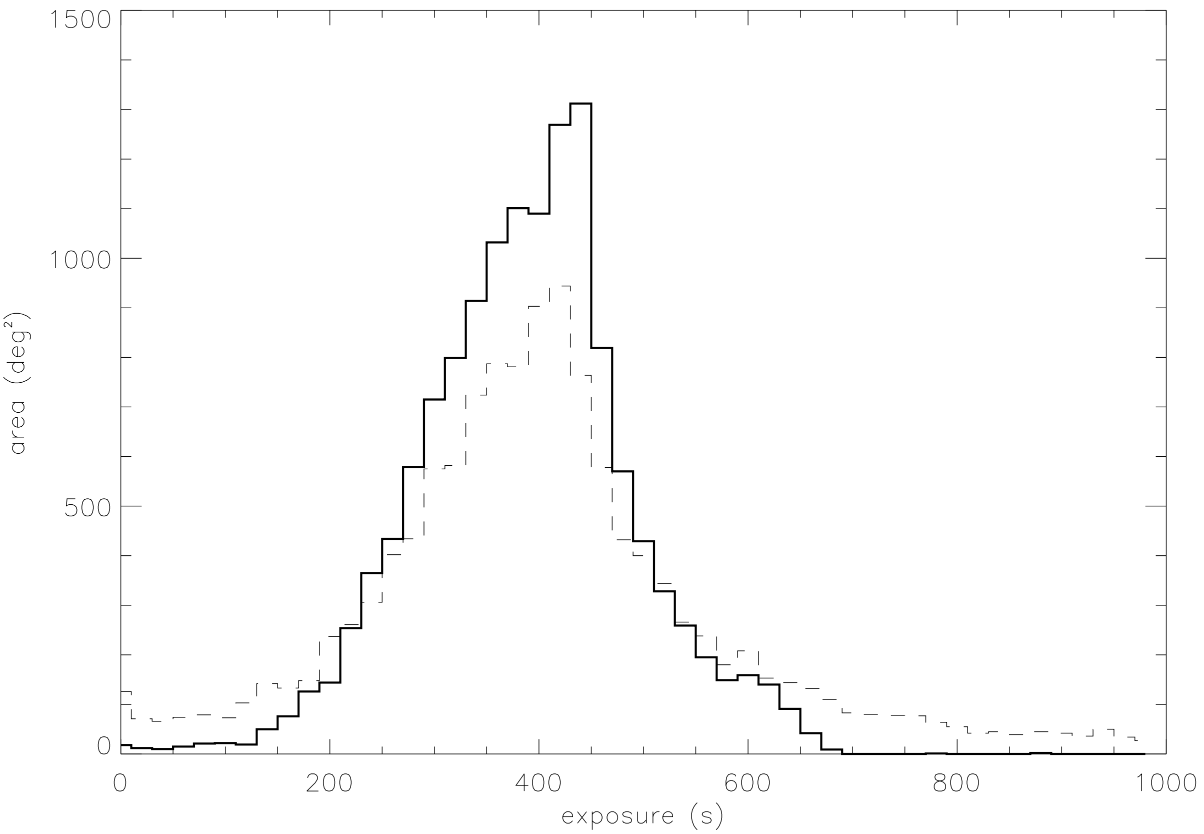

Fig. 1.— Exposure time distribution of the RASS I for the NORAS survey area. For comparison the distribution of the exposure time in the RASS II involving the merged photon data from all survey strips is also shown as broken line.

of detection larger than $L = 10$ were accepted into the RASS I source list. (The likelihood value here and throughout the paper is defined as $L = -\ln P$, where P is the probability for a spurious source detection – or a spurious extent detection in the case of the extent likelihood.) This threshold was chosen such that an estimated fraction of less than 1% spurious sources enter the source catalogue. The detections are based on the source counts in the broad ROSAT PSPC energy band covering the detector channels 11 – 240 which roughly corresponds to an energy range of 0.1 to 2.4 keV. Further qualities of the sources evaluated during the maximum likelihood assessment in three energy bands comprise the source count rate, an estimated source extent in excess of the broadening of the sources due to the telescope-detector point spread function (PSF), and two hardness ratios based on the counts measured in the soft (channel 11 – 40) and hard energy band (channel 52 – 201) or in the hard band 1 (channel 52 – 91) and hard band 2 (channel 92 – 201), respectively. The source extent which is of special importance here was determined within the maximum likelihood analysis by assuming for the source image shape a convolution of two two-dimensional Gaussian functions for the PSF and the source shape (Voges et al. 1999), respectively. The result of this analysis is then a value for the excess extent in terms of a σ-radius of the second Guassian. In this approximation the Gaussian wings are less extended than both the wings of the PSF and the wings of a King-type surface brightness model (e.g. Cavaliere & Fusco-Femiano 1976, Jones & Forman 1984). This is one, probably minor, reason for the effect that some of the X-ray flux in the outer X-ray halos is underestimated in the RASS standard analysis.

First tests of the source quality parameters in RASS I and ready identifications with existing source catalogues showed that many clusters of galaxies featured significantly extended X-ray emission in the RASS. It was known from previous X-ray surveys (e.g. the Einstein Medium Sensitivity Survey, e.g. Gioia et al. 1994, Stocke et al. 1994) that slightly more than about 10% of the X-ray sources at the depth of the RASS should be galaxy clusters emitting in X-rays (see also Böhringer et al. 1991). Therefore it was clear that an X-ray sample highly enriched in galaxy clusters could be obtained by selecting those RASS sources featuring a significant source extent. For example, this is demonstrated by a comparison of the extent properties of the X-ray sources for ACO clusters, stars, and AGN taken from the ROSAT Bright Source catalogue and the correlation with optical catalogues from Voges et al. (1999) shown in Fig. 2 for RASS II data (a comparable figure is also shown in Ebeling et al. 1996 for RASS I results). Even though the present study is concerned with RASS I results we are showing a statistic for RASS II in Fig. 2 because there is no principle difference and there is a larger data base of correlations with catalogued objects available for RASS II. About half of the galaxy clusters occupy an almost exclusive parameter space characterized by an excess source extent larger than 25

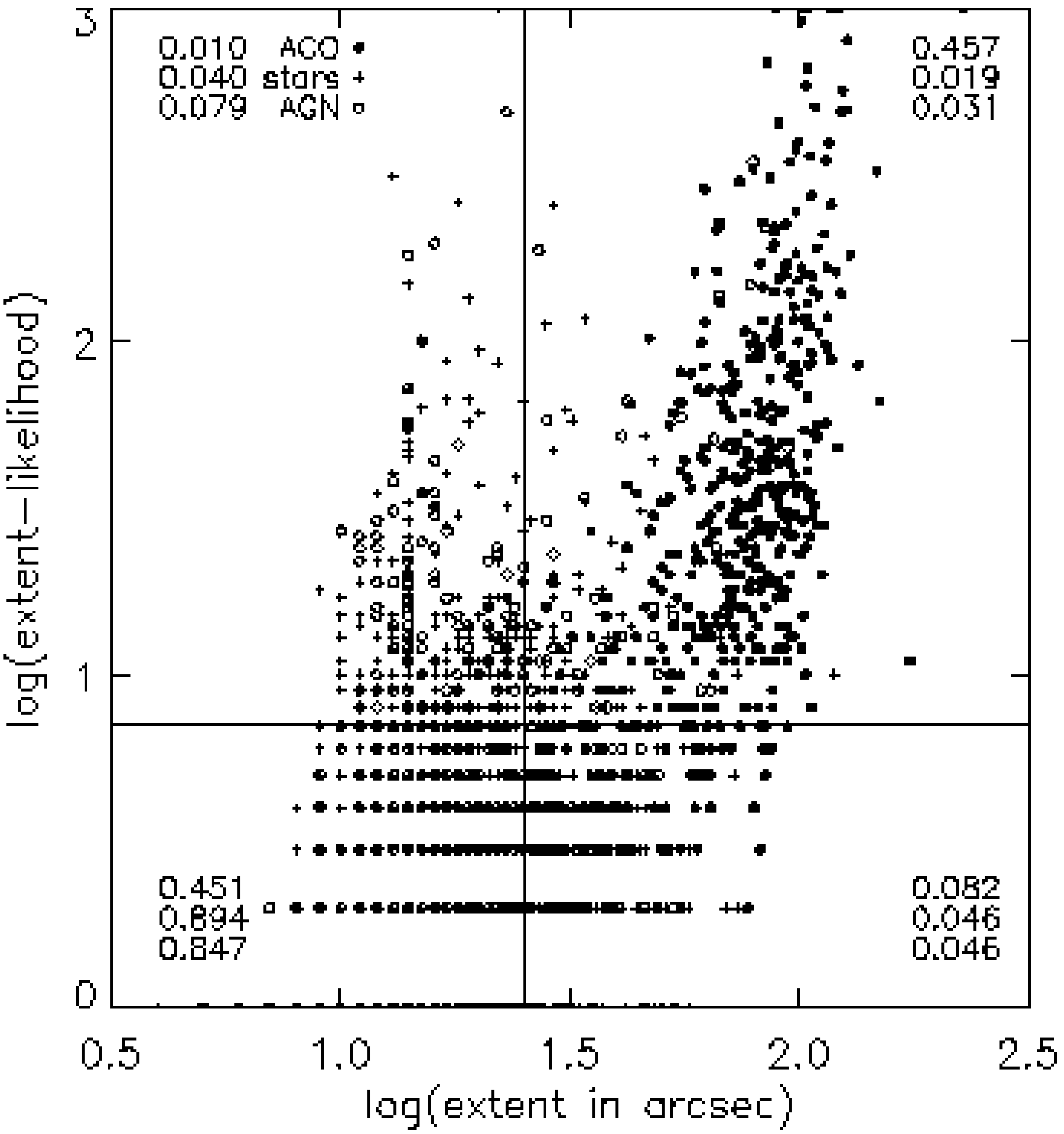

Fig. 2.— A comparison of the distribution of the values for the extent and extent likelihood for a set of RASS sources identified with ACO clusters, stars, and AGN. The data are taken from the ROSAT Bright Source catalogue compiled from RASS II and the cross identifications with optical catalogues as described by Voges et al. (1999). The coincidence radius used for the cross-identification is 5 arcmin. The vertical and horizontal lines give the extent limit of 25 arcsec and the extent likelihood limit of 7. The fraction of sources for each category located in the different quadrants is given in each quadrant. The upper number in each quadrant gives the fraction of all ACO clusters falling into this quadrant, the middle number gives the corresponding fraction for stars and the lower number the fractions for AGN. The fractions for each class summed for all quadrant adds up to unity, thus, for example, less than 2-3 % of the non-cluster sources are found in the upper right quadrant. The selection criteria for the present sample correspond to the upper right quadrant which is highly enriched in ACO clusters.

arcsec with a reasonably high extent likelihood (with a value of $L = 7$). Only about 2-3 % of the non-cluster sources are found in this region. Since galaxy clusters account for about $10 - 15\%$ of all X-ray sources we can expect a contamination of the order of $20 - 30\%$ by non-cluster sources if the sample is selected from the upper right quadrant. This is approximately what is found below. That this small value of 25 arcsec for the excess extent radius threshold shows a significant effect is somewhat surprising, since the mean half power radius of the survey point spread function is 70 arcsec, much larger than this threshold. This can be explained by the fact that in the RASS analysis likelihoods are calculated separately for each photon before they are summed and therefore each photon can be weighted by its own PSF according to the place in the detector where it was registered. In this way photons registered in the central part of the detector with a half power radius of the PSF of 15 - 20 arcsec give a high weight to the maximum likelihood analysis. This makes the RASS source analysis very sensitive to the recognition of small deviations from the expected shape of point sources. In the following analysis we will not make use of the information on the detector positions of individual photons. This is a disadvantage when compared to the standard RASS maximum likelihood analysis, but other advantages more than compensate for this.

A first search for X-ray selected clusters was made with RASS I sources flagged as extended. The selection criteria were as follows: For the extent parameters a minimum threshold of 25 arcsec for the extent radius and a minimum value of 7 for the extent likelihood was chosen, as indicated by the dividing lines in Fig. 2. Further a lower count rate limit of 0.06 cts s^{-1} in the ROSAT broad band was set and the sky area was restricted to the region $\delta \geq 0°$ and $|b_{II}| \geq 20°$. The sources at the count rate threshold are thus typically characterized by about 25 source photons. This leads to a source fraction of 76% galaxy clusters among the sources selected. The advantage of this approach is that it yields a low fraction of contaminating sources, provides an effective way to detect galaxy clusters, and involves relatively simple selection criteria. The disadvantage is that the selection by source extent is much more difficult to quantify and to model than for example a purely flux-limited selection technique.

In total 537 sources matching the selection criteria were extracted from the RASS I data base. 40 of these sources have been found to be detections of secondary maxima or fragments of clusters which are already in the list due to a detection at the main maximum. The largest fraction of these fragment sources is located in the very extended, diffuse emission region of the Virgo cluster (Böhringer et al. 1994). The fragment sources were removed from the list after a careful check that they are not associated with another distinct X-ray source in the line-of-sight. We have also excluded from the present catalogue the two detections in the Virgo cluster at the position of M87 and M86, because a useful flux measurement in the Virgo region requires a more detailed approach. Thus we report results for these parts of Virgo separately. In the following we will therefore discuss the analysis and identification of the remaining 495 sources.

Early 1996 a new ROSAT Survey product, RASS II, became available at MPE. This version which is based on a greatly revised attitude solution for the pointing of the satellite during the survey and also uses a much more stringent quality threshold for the times with acceptable attitudes was used to create a new RASS II source list from which the RASS Bright Source Catalogue (RASS BSC) was created (Voges et al. 1999). In this survey product the data are sorted in 1378 sky fields with sufficient overlap (~ 0.23 degrees) to guarantee an undiscriminating source assessment in the boundary regions. Each field now contains all the photons registered for this part of the sky during the entire survey. The resulting exposure distribution in the NORAS survey area is also shown in Fig. 1. As expected this distribution features a tail of high exposures up to about 40000 s. The reanalysis of the X-ray sources of the present sample makes almost exclusively use of the RASS II data base.

3. Reanalysis of the X-ray source properties

To reanalyse the sources we apply a novel technique that is essentially based on measuring background-corrected source counts as a function of a growing circular aperture and checking for saturation to determine the observed source counts. The growth curve of the counts as a function of aperture radius is also used subsequently to analyse further source properties. We therefore term this method the growth curve analysis, GCA. We preferred to apply this method over techniques applied in earlier studies. The Steepness Ratio Technique used in De Grandi et al. (1997) has some similarity to the present analysis, but makes only restricted use of the available photon data in only extracting the source counts in aperture radii of 3 and 5 arcmin. A comparison shows that the uncertainties in the determined count rates are usually higher for that technique than for GCA. Our preference of the GCA method over Voronoi-Tesselation and Percolation (Ebeling et al. 1996, 1998) is due to the fact that the GCA technique is simple to reproduce in models and simulations, the resulting count rates are quoted for a known aperture radius for each source allowing a better assessment of the results in subsequent modeling, and the GCA technique provides a set of very essential diagnostic plots which make the interactive evaluation of the reliability of the GCA results easy and transparent. In addition the VTP technique needs two counteracting steps to correct for the unobserved flux. The first step relies on an extrapolation based on the assumption of spherically symmetric sources and leads to a significant overcorrection which is then compensated in a second step with an *a posteriori* recalibration based on a comparison with pointed data. The present method achieves a good agreement with pointed data in one relatively minor *ab initio* correction in a first step as shown below. The presentation of more details and tests of the GCA method is planned for a future publication (Böhringer et al. in preparation), while the essential features of this method are described in the following.

The reanalysis of the X-ray properties was conducted for all 495 X-ray sources in the sample using RASS II data in fields of $1.5° \times 1.5°$ centered on each X-ray source. For 17 nearby clusters featuring a large extent the analysis is performed in larger fields of $4° \times 4°$ or $8° \times 8°$. For 7 sources, where the exposure in RASS II is less than 70 sec, data fields were extracted from RASS I which features a higher exposure for these cases. The reason for the reduced exposure in RASS II is the tight quality constraint which leads to the rejection of some RASS photon data in RASS II as compared to RASS I. The 7 fields of RASS I used here were carefully checked and did not show any peculiarities as e.g. double or otherwise distorted images of bright sources which would indicate a problem with the attitude control during the observation.

The primary data set used for each field consists of a photon event file containing all data of the photons registered in the field area and the corresponding exposure map, providing the exposure time as a function of sky position with a resolution of 45 arcsec pixels. The exposure maps include a broad band correction for vignetting and the effect of the shadowing of the support structure of the PSPC window. (The possible difference between the broad band vignetting correction and the proper correction for the specific source spectrum introduces an error no larger than 2% and no further correction is applied). The photon event files provide information on the sky position and energy channel as well as the time and the detector position for each registered photon. In the following analysis only the first two parameters are used.

The three energy bands defined for our data reduction procedure are identical to those used in the RASS analysis (Voges et al. 1999): broad band, soft band, and hard band. For the source count rate determination and the shape characterization we use exclusively the photon counts in the hard energy band. In this band the soft X-ray background is reduced to about one fourth, while – depending on the value of the interstellar column density – 60 to 100% of the cluster emission is detected. Therefore the analysis in this energy band provides the highest signal-to-noise ratio and the most reliable count rates. Another quite important aspect of the choice of this energy band is that it minimizes the contribution of contaminating sources to the count rate. Since the majority of all sources in the RASS are softer than the cluster X-ray sources, their contribution to the hard band is usually less significant than the contribution to the broad band counts.

3.1. Source position and count rate

Prior to the evaluation of the source count rate the source center position and the sky background brightness is determined. The input field centers chosen are the X-ray positions provided by the maximum likelihood technique of RASS II. These positions are not optimal for extended sources and in particular extended sources are sometimes multiply detected in the RASS. Therefore a redetermination of the source position is performed based on a moment method which determines the two-dimensional "center of mass" of the photon distribution within an aperture of 3 arcmin around the input value for the center. This procedure is iterated with the newly found center position until the process converges to a stable center position. The small aperture of 3 arcmin gives a high weight to local maxima. We check all the center positions interactively and correct those cases in which this method has settled on a secondary maximum or where the local maximum is obviously offset from the large scale symmetry of the cluster. Those 5 sources are marked in the catalogue. We have also applied the moment method for the determination of the center position using larger apertures (5 and 7.5 arcmin). In 7 cases we preferred to quote these centers in the catalogue. Also these cases are marked.

The background of the field is then determined from a ring area centered on the source with an inner and outer ring radius of 20 arcmin and 41.3 arcmin, respectively, as shown in Fig. 3. The inner ring size has been chosen such that it is outside the outer radius of the X-ray emission for the majority of the clusters. The outer radius is chosen to make almost full use of the 1.5 × 1.5 degree fields. This large background area ensures that the number of photons used for the determination of the background surface brightness is large and introduces an almost negligible Poissonian error into the source flux determination. There are 17 nearby clusters in the sample which exceed the inner background ring radius in size. For these clusters larger fields have been extracted from RASS II and larger background rings have been used in the analysis.

The ring is subdivided in 12 sectors. The photons in each of the three energy bands in all sectors are counted and the exposure time for each photon position is obtained from the exposure map. The count rate in each sector and the surface brightness are then calculated by averaging in count rate:

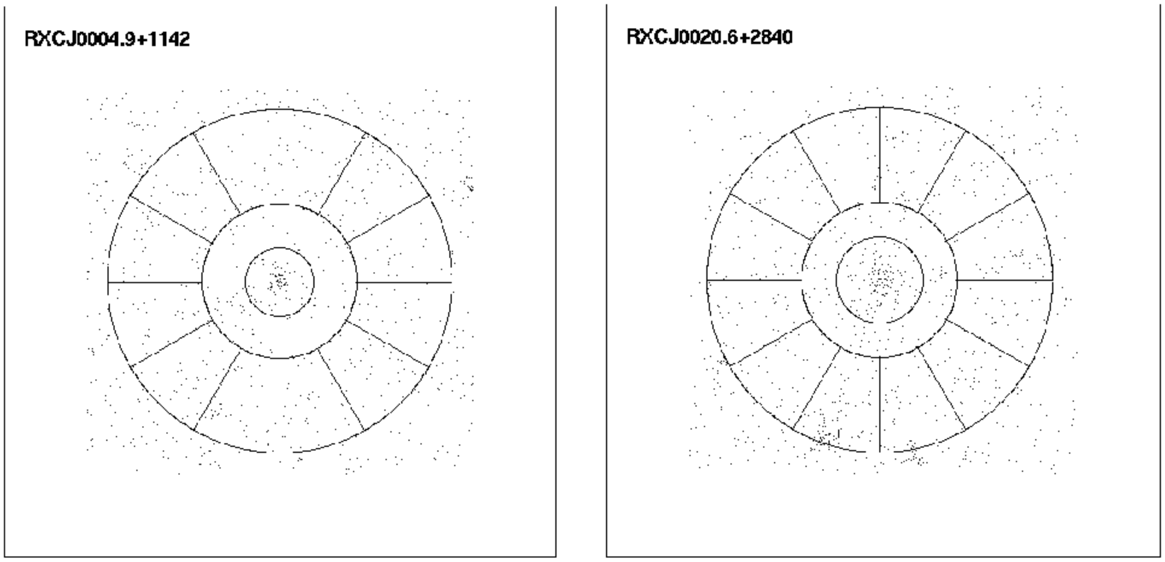

Fig. 3.— Distribution of the photons detected by the ROSAT PSPC in the hard band (∼0.5-2.0 keV) in the regions of the X-ray cluster sources RXCJ0004.9+1142 and RXCJ0020.6+2840. The ring segments of the area used for the background estimate and the source region as determined from the analysis are marked. The photon field extracted from the ROSAT All-Sky Survey as shown here covers an area of 90 by 90 square arcmin. The ring segment of the source field of RXCJ0020.6+2840 marked by a cross is excluded from the background determination due to contamination.

$$C = \sum_i \frac{1}{t_i}, \tag{1}$$

where C is the count rate, t_i is the exposure time at each photon position, and the summation is over all photon events in the sector. The surface brightness is obtained by division with the sector area. An uncertainty for the surface brightness in each sector is calculated from Poisson statistics.

To avoid that discrete sources located in the background ring are included in the background estimate, the median of the sector count rates is determined and sectors featuring a larger than 2.3σ deviation from the median are discarded from the further calculations. Even though sources are only expected to cause large enhancements, we also exclude sectors that have count rates which are too low by more than 2.3σ, since some of the positive deviations are due to fluctuations, and to avoid a negative bias in the background the negative fluctuations have to be discarded for reasons of symmetry. The clipping threshold of 2.3 σ guarantees a successful removal of sources with typical count

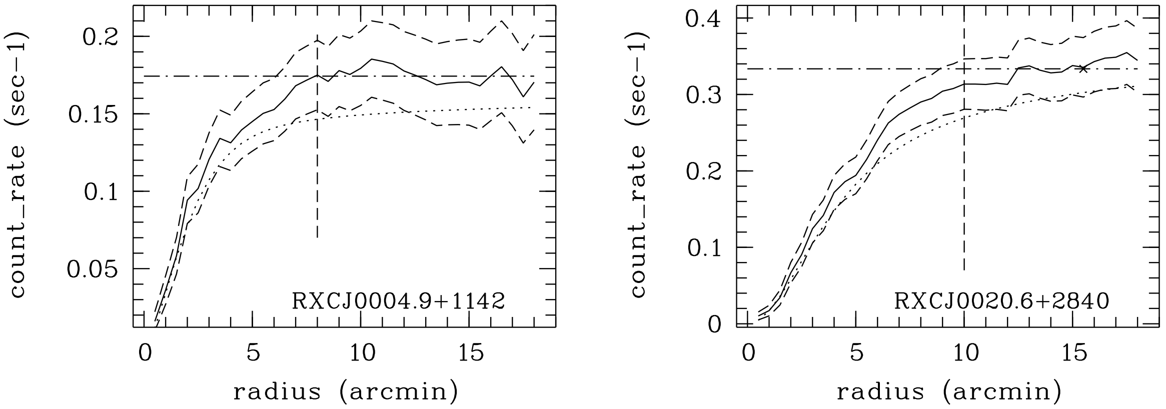

Fig. 4.— Radially integrated count rate for the cluster sources RXCJ0004.9+1142 and RXCJ0020.6+2840 in the hard band (∼0.5-2.0 keV). The two techniques used to determine the total observed source count rate are shown: the vertical dashed line shows the limiting radius outside which the 1σ uncertainty of the signal increases faster than the signal itself; the horizontal line shows the fit to the saturation plateau (as explained in the text below). Also shown as dotted line is the best fit of a β-model profile convolved with the PSF with a core radius of 0.5 arcmin and a normalization of 0.158 cts s^{-1} for RXCJ0004.9+1142 and 2.5 arcmin and 0.360 cts s^{-1} for RXCJ0020.6+2840, respectively. Note that the actual fits were performed to the differential count rate profiles and not to the cumulative ones as shown here. Thus the deviations of the fits at large radii have a low significance. They are often found and may indicate irregular structure at the outskirts of many clusters.

rates above about 0.04 s^{-1} which would otherwise introduce a typical error $\geq 1\%$ in the background determination. The chosen clipping threshold leads in general to the clipping of not more than 1 - 3 sectors which preserves most of the background area for averaging resulting in a small photon statistical error in the background of typically about 5%. This also shows that the variations in the background on that scale are generally small and hardly larger than what is expected from Poisson statistics.

The procedure of the background determination is illustrated in Fig. 3. For the data in Fig. 3a there is no interference of background sources and the background is smooth enough that all sectors were included in the background measurement, while for the data in Fig. 3b one of the sectors had to be discarded due to the presence of a significantly disturbing source. The two figures show the photon distribution of the hard band counts for each source field. The two sources, which have net source counts of 75.2 and 127.9, respectively, will be used in the following to illustrate the further analysis. (These two sources selected as the first sources in the list illustrating the features we like to show: RXCJ0004.9+1142 is the first source in the list with less than 100 photons which features a small but significant extent and RXCJ0020.6+2840 is the first source showing the search for the plateau in the count rate in the presence of steps in the plateau region, see below).

The cumulative source count rate as a function of radius starting from the earlier determined central position is then found by integrating the source counts in concentric rings outwards while subtracting the background contribution. The integration is performed using a ring-width of 0.5 arcmin (a reasonable resolution for the given PSF of the instrument). The source count rate is determined for each ring by weighting each photon with the local exposure time according to eq.(1). The integration is performed for the three selected energy bands. The results are count rate profiles as shown in Figs. 4a and 4b. The uncertainty corridors in these count rate profiles resulting from Poisson photon statistics are indicated as dashed lines in the figures. They also include the Poisson error of the background determination.

In most of these cumulative profiles the count rate levels off to a plateau value which gives the total observed source count rate. The total observed count rate is determined in the automated source characterization program in two alternative ways. In the first approach we determine the radius outside of which the source signal increases less than the 1σ uncertainty in the count rate. This radius, which we call the outer radius of significant X-ray emission, R_x, is indicated by the vertical dashed line in Figs. 4a and 4b. The count rate with its statistical uncertainty at this radius provides the value of the significantly detected count rate of the source. The radius R_x is shown for the two sources as the inner circle in Figs. 3a and 3b .

Alternatively the total source count rate is measured by getting an estimate of the plateau level. In the simplest case it is the average of the flat plateau outside R_x. In practice we determine the mean value of the plateau as well as the slope by means of a linear regression method for the profile part outside R_x. If the slope of the plateau is less than 0.8% of the total count rate per arcmin radius, the plateau value is accepted. If the plateau is decreasing the count rate is determined from the mean of three bins around R_x. If the plateau is increasing, another effort is made to find the best flat part of the plateau by iteratively excluding the outermost and in a second step also some of the innermost bins. This procedure helps in excluding an outer rise of the count rate profile due to a neighboring source or by skipping a few bins if the count rate curve has not completely saturated to a plateau at R_x. Both effects can be seen in Fig. 4b, where the outer radius of the considered plateau region before a secondary rise of the profile is indicated. The source analysis is checked in each case on the basis of diagnostic plots as those shown in Figs. 3 - 6. About 35% of the plateaus can be characterized by the first step and about 83% by the further iterative trials. There is a residual fraction of about 17% of the sources for which no satisfactory plateau can be established automatically often as a result of contaminating nearby sources. These cases are analysed individually. For all sources we determine the radius, R_{out}, out to which the plateau count rate was measured by simply following the profile until the plateau value is reached.

For the count rates and their uncertainties quoted in the present catalogue we have adopted the following approach. For the count rates we take the results from the fitted plateau values, which are in general higher by a few percent than the count rates determined at R_x. This is mainly due to an insignificant further rise of the cumulative count rate profile beyond R_x. This rise is in most cases much smaller than the statistical error in the count rate. The error in the count rate is then calculated from the root mean square of the shot noise error and the deviation of the plateau value from the value at R_x. Taking the root mean square would be justified for errors which are statistically independent and Gaussian distributed. Since the second error is a systematic deviation, this does not apply in this case. Nevertheless this is for the present case a practical approach which integrates the two errors by putting a larger weight on the larger one of the two uncertainties. The correction of the measured count rate of the source to a total count rate is discussed below.

3.2. Spectral hardness ratio and source extent

For the determination of the spectral hardness ratio the count rate in the soft band is also determined for the same radius as for the hard band value of R_x. The hardness ratio, HR, used here as well as in the RASS data base is defined as

$$HR = \frac{H - S}{H + S}, \tag{2}$$

where H is the hard band and S the soft band source count rate. The expected values for the hardness ratio for cluster sources is roughly in the range $0 - 1$ as shown in Fig. 8.

The source extent is addressed in two ways: quantifying the source size and testing the probability that the extent is real, respectively. In the first analysis a King profile with the surface brightness distribution,

$$S_x(R) = S_0 \left(1 + \frac{R^2}{r_c^2}\right)^{-1.5\beta+0.5} , \tag{3}$$

(where R is the projected radial distance from the soure center and r_c is the core radius of the X-ray surface brightness distribution) convolved with the averaged survey PSF (as calculated by G. Hasinger from the ROSAT XRT/PSPC PSF averaged over the detector area with a correction for the vignetting effect) and azimuthally integrated is fitted to the differential count rate profile. For the profile parameters a fixed value $\beta = 2/3$ is taken according to the most typical value found in X-ray cluster observations (e.g. Jones & Forman 1984). In the χ^2 fit the core radius is varied in steps of 0.5 arcmin, and the normalization is a free fitting parameter. Due to the very low count statistics we have thus limited the fitting parameters per step to one, the normalization, by choosing the most common value for β. The results for the two example sources are shown in Figs. 5a and 5b, and the best fitting profiles are indicated by dotted lines in Figs. 4a and 4b. Note that, while the figures show fits to the cumulative profiles for a better diagnosis of the results, the actual calculations are conducted for the differential profiles to assure statistical independence of the count rates in rings as required by the χ^2 fitting method. Together with the best fitting value we also keep the minimum radius which is still consistent within the 2σ uncertainty limit. Comparing the χ^2 values to the 1, 2, and 3σ limits shown in Fig. 5 we find that for the two examples the first source is only marginally extended (2σ result), while the second source features a clear and large extent.

The second, more sensitive method is used as a test for the probability that the source has an extent at all. For this we use a Kolmogorov-Smirnov test comparing the expected cumulative count rate profile of a point source including background with the given instrument PSF with the radially sorted, cumulative, and unbinned photon counts out to a radius of 6 arcmin. This radius is larger than the 90% power radius of the survey PSF and thus provides enough leverage to display the deviations of extended sources, but is small enough to minimize the influence of possible background errors. This test does not depend on the assumption that the uncertainties are Gaussian distributed. Since the pure photon counts also contain the background counts the previously determined background surface brightness has also to be added to the expected point source profile. Examples of the expected point source profile and measured curves are shown in Figs. 6a and 6b. The background contribution to the expected profile is also indicated and we can see that it is generally a minor contribution at these small source radii. Tests with known point sources have shown that the misclassification of point sources as extended sources is generally less than about 5% if we take an upper limit for the KS probability of 0.01 to classify a source as extended (see Böhringer 1999, in preparation). For the two examples we find probability values of 0.005 and 1.3×10^{-14}, respectively, and therefore both sources will be classified as extended in the catalogue. In the following we will use these results in the form of the extent parameter defined as $P_{ext} = -\log_{10}(\text{KS probability})$.

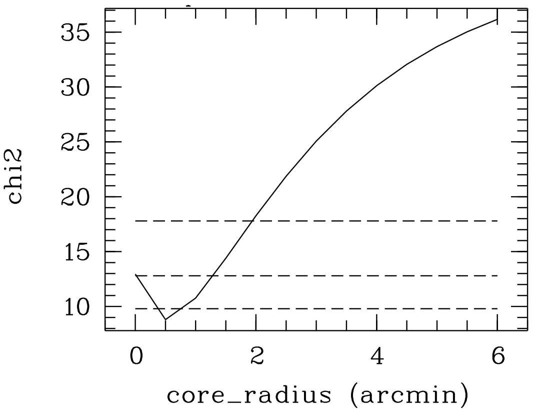

Fig. 5.— Evaluation of the source extent by means of a χ^2 fit of a King profile convolved with the mean RASS PSF. The χ^2 value is determined for varying core radii in steps of 0.5 arcmin. Here the best fitting core radii are found to be 0.5 and 2.5 arcmin. Only the second source is found by this test to be clearly extended with high significance. The horizontal dashed lines show the 1, 2, and 3σ uncertainty limits, respectively.

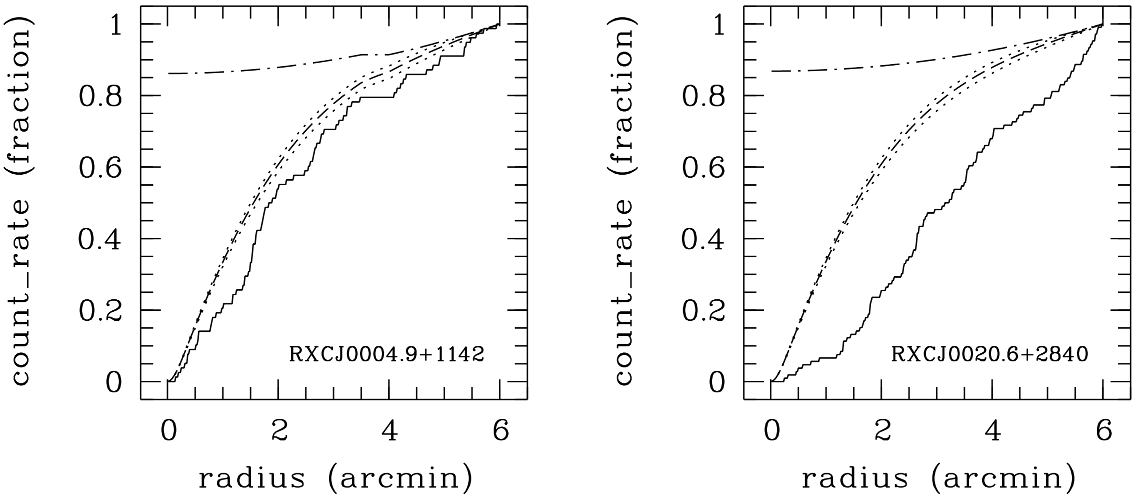

Fig. 6.— Test for the probability of a source extent by a KS test comparing the cumulative count rate profile out to a radius of 6 arcmin with the expected profile for a point source plus background. Both profiles are normalized to 1 at the outer radius. The long dashed curve gives the expected point source profile plus background and the dotted curves show the effect of a 30% background variation. The dotted-dashed curve indicates the background contribution.

3.3. Deblending and analysis of very extended sources

The visual inspection of the diagnostic plots of the GCA results for all the sources showed that in 19 cases the source analysis suffered from the blending of the cluster source with another nearby source probably not associated with the intracluster X-ray emission. These sources were scheduled for another analysis including a deblending technique. The correction by deblending was performed for all the sources where the contamination was clearly recognized as due to point sources. Tests show that a single contaminating source is usually easily recognized if its contribution to the total hard band count rate is larger than 5 - 10% and if the source is outside the central 3 arcmin radius. The deblending is not applied to irregular clusters or clusters with substructure where the non-symmetric emission region is most probably part of the diffuse intracluster X-ray emission (and not likely to be due to a point source). In this second analysis the source region is divided in two sets of twelve sectors for the radial region 3 to 8 and 8 to 15 arcmin. The variation of the surface brightness in the different ring sectors is analyzed in a similar way as done for the background ring sectors. Contaminating sources are best flagged by selecting those sectors with a more than 3.5σ deviation from the median. For weaker sources this detection threshold corresponds roughly to sources with fluxes larger than 3×10^{-13} erg s^{-1} cm^{-2} and in general guarantees the deblending of sources with contributions larger than 10%. The clipping technique is illustrated in Figs. 7a and 7b. In the further analysis the marked sectors are interpolated, that is, they are assigned a value for the surface brightness equal to the mean of the remaining sectors. The automated clipping works well for most sources but in about 30% of the cases the clipping either did not remove the contaminating source completely or removed in addition other parts of the cluster. For these cases we preferred to determine the count rate of the contaminating source directly (with the analysis centered directly on the contaminating source) with the same deblending algorithm and subtracted it from the blended source count rate. The 19 sources that required a deblending are marked in the catalogue.

Since the outer radius of the region in which the source profiles are analyzed is fixed in the automated source analysis routine, and since the cut out regions per source are restricted to a size of 1.5° × 1.5° , some nearby clusters are too extended to be covered completely by the analysis. For these clusters, 17 in total, larger files of photon data from RASS II were requested with fields covering 4° × 4° or even 8° × 8° around the source. To these data the same source analysis was applied as described above with an extended radial range. The clusters that required a reanalysis in a larger sky field are also marked in the catalogue and can also be recognized by their large values of R_x and R_{out}.

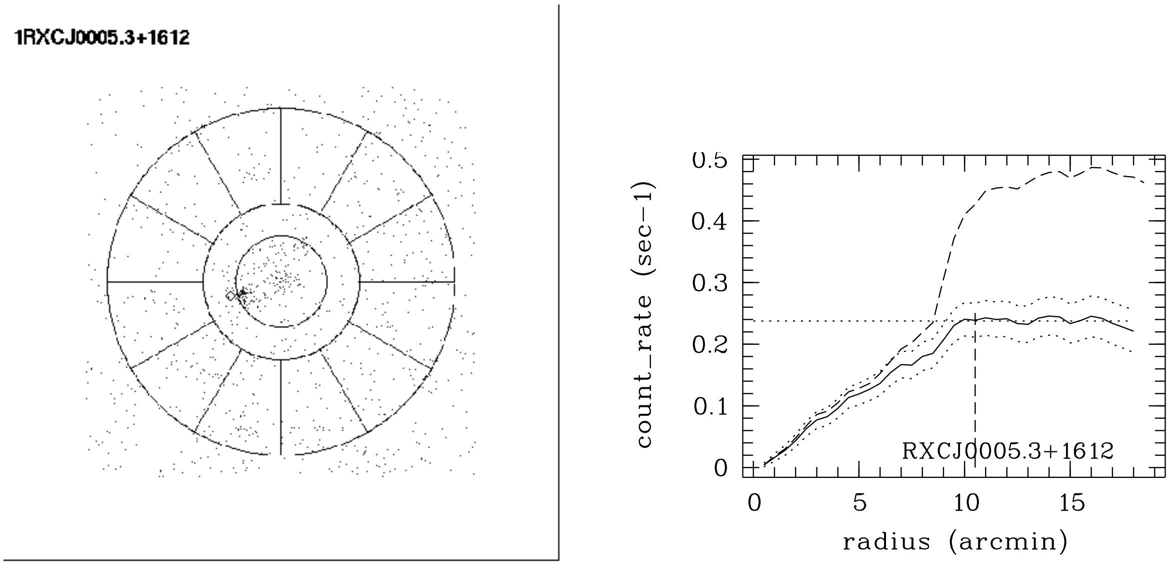

Fig. 7.— The left figure shows the photon distribution of a cluster X-ray source which is clearly contaminated by a point source. The small circle near the point source marks the sector which was excised from the source analysis to deblend the contaminating source. The right figure shows the result for the count rate analysis. The upper dashed curve gives the cumulative source count rate without deblending. The solid curve shows the result after the sector with the source was cut out and interpolated. The two dotted curves show again the 1σ Poisson error for the count rate including the effect of the interpolation. The horizontal short dashed curve indicates the plateau value determined and the vertical dashed curve shows the outer radius of significant X-ray emission from the source.

3.4. Flux and luminosity determination

To determine the flux and the luminosity of a source we first obtain the value of the interstellar hydrogen column density as measured at 21cm (Dickey & Lockman 1990, Stark et al. 1992) for the direction of the source by means of the EXSAS software package routine (Zimmermann et al. 1994). The flux is then determined in a first step by calculating the conversion factor from count rate to flux for a source with a thermal spectrum and a temperature of 5 keV (based on a modern version of the radiation code by Raymond & Smith 1977), a metal abundance of 0.3 of the solar value (Anders & Grevesse 1989), a redshift of zero, and an interstellar absorption according to the measured 21 cm value (Dickey & Lockman 1990) and the absorption tables of Morrison & McCammon (1983). We calculate the flux in the nominal ROSAT energy band: 0.1 - 2.4 keV. All fluxes and luminosities quoted in this paper and in the catalogue refer to this energy band. Fig. 8a shows the conversion factors as a function of absorbing column density for the three plasma temperatures 2.5, 5 and 8 keV. We note that the main dependence is on the column density. The variation with temperature makes a difference of less than 7% in the temperature range (2 - 10 keV). Only for temperatures below 1.5 keV larger corrections occur, which applies for the smallest groups of galaxies in the sample. The dependence on the metal abundances is even less, about 1%. Prior to any further knowledge about the redshift and the nature of the cluster source the estimated flux value represents a good first approximation. Note, however, that for non-cluster sources a different spectral shape and thus a different conversion factor is expected.

Once the redshift of the cluster source is known we can determine its luminosity. The luminosity is also calculated for the ROSAT energy band. The calculation is performed iteratively. In a first step we calculate a trial luminosity from the estimated flux value and the redshift and use its value to estimate a cluster plasma temperature using the X-ray luminosity-temperature relation of Markevitch (1998)

$$T_x = 2.34 \; L_{44}^{1/2} \times h_{50} \qquad , \tag{4}$$

where T_x is in keV, L_{44} is the X-ray luminosity in units of 10^{44} erg s^{-1} (in the 0.1 - 2.4 keV band). We make use of the relation which was derived by Markevitch without any correction for cooling flows in L_{44} and T_x. This applies to our case since we are only dealing with integral count rates and average spectral properties. (Note that we have approximated the exponent of 1/2.02 found by Markevitch by 1/2). The temperature estimate allows the calculation of a new count rate-flux conversion factor for which we now also take the redshift of the source spectrum into account and calculate the source rest frame value for the X-ray luminosity (which involves the equivalent to the cosmic "K-correction"). The K-correction term for example increases up to about 6% out to a redshift of $z = 0.3$ for clusters with a temperature of about 2 keV and up to about 15% for clusters with 10 keV. The iteration is repeated twice but found to actually converge to the final solution in the first step. The final rest frame X-ray luminosity is the value quoted in the catalogue.

We have compared our results for the count rate to flux conversion based on EXSAS software and special programs using a similar data base and radiation code as EXSAS with results obtained from XSPEC, the online PIMMS software, and the conversion factors used in Ebeling et al. (1998). The differences are always less than 3%. Thus the use of different flux evaluation software does not constitute a significant source of potential differences between different RASS cluster surveys.

3.5. Estimates of the total flux

The X-ray fluxes determined from the observations may still be biased low compared to the total flux coming from the cluster, since part of the flux in the faint outer regions is lost in the background. We can use the fact that we obtained the flux within a well defined angular aperture to make an estimate of the flux that may lie outside this aperture. Note that we use this approach here as a tentative estimate of the flux lost and we will therefore make no further effort in this paper to use the results for a correction, since the underlying assumption that all clusters have the same self-similar shape is not realized precisely enough to make a case by case correction useful without further tests and justifications. The aperture radius that corresponds to the generally used plateau value of the count rate is R_{out}.

To obtain a rough estimate of the flux possibly missed outside the aperture we adopt the following generic cluster model characterized by a β-model surface brightness distribution as given in eq.(3) with $\beta = 2/3$ to extrapolate the surface brightness profile outside R_{out}. For the core radius we are not using the results of the χ^2 fit, since they have too large uncertainties. We rather prefer to make a rough estimate of the cluster size from its X-ray luminosity. From the studies by Reiprich & Böhringer (1999) we find that the cluster mass is well correlated with the X-ray luminosity according to the relation

$$L_x \propto M_{grav}^{1.2} \qquad . \tag{5}$$

We further assume that the self-similar relation of the core radius and mass of the form $r_c \propto M_{grav}^{1/3} \propto L_x^{1/3.6}$ holds (see e.g. Kaiser 1986). Taking a Coma-type cluster with $L_x \sim 7 \times 10^{44}$ erg s^{-1} (0.1 - 2.4 keV) and a core radius of 300 kpc to normalize the relation we find

$$r_c = 0.3 \text{ Mpc} \left(\frac{L_x}{7 \times 10^{44} \text{ergs}^{-1}} \right)^{1/3.6} \quad . \tag{6}$$

Rather than integrating the X-ray flux of the β-model to infinite radius, we stop the integration at 12 core radii which is about as large as the virial radius of a Coma-type model cluster. The difference between an integration to infinity (as for example performed in Ebeling et al. 1998 and De Grandi et al. 1999) to the cut-off radius at 12 r_c is about 8%. This overestimate of the flux for integration to infinity is in general smaller than the individual uncertainties but not negligible if one is concerned with the global bias of the sample.

Applying this model to our cluster sample we can calculate the fraction of the X-ray flux missed for each of the sample sources. Fig. 9 shows these missing fractions as a function of the source luminosity and of the detected number of source photons. The mean missing flux is about 8.3%. (The most discrepant point with a missing flux of about 50% and $L_x \sim 10^{44}$ erg s^{-1} in Fig. 9a is for example a distant cluster observed at low flux ($0.5 \cdot 10^{-12}$ erg s^{-1} cm^{-2}) at low exposure which would be excluded in a proper flux limited sample).

The missing flux fraction, fr, features only a very weak dependence on X-ray luminosity. The linear regression fit to the function $fr = f(\log(L_x)$ shown in Fig. 9a decreases from 8.3% for $L_x = 10^{43}$ erg s^{-1} to 7.9% for $L_x = 10^{45}$ erg s^{-1}. A more significant dependence is found for the number of source photons, as could be expected since this is the main parameter determining the significance of the source detection and how far out the count rate integration can be performed. Here the linear regression fit of Fig. 9b, $fr = f(\log(N_{ph})$ shows a decrease of fr from 9.5% for 30 source photons to 6.7% for 500 source photons. Also this dependence is weak.

An exception to the relatively small values for the missing fraction constitute some of the low luminosity sources as displayed in Fig. 9a. These are elliptical galaxies or very small groups dominated by elliptical galaxies, which have much smaller core radii - as indicated by the GCA King-model fits - compared to the values assumed after eq.(6). Thus for these small objects the model assumption seems to break down and the actual values for the missing flux is much smaller than estimated here. The validity of this generic model for the extrapolation of the total flux will be pursued in more detail in a future publication.

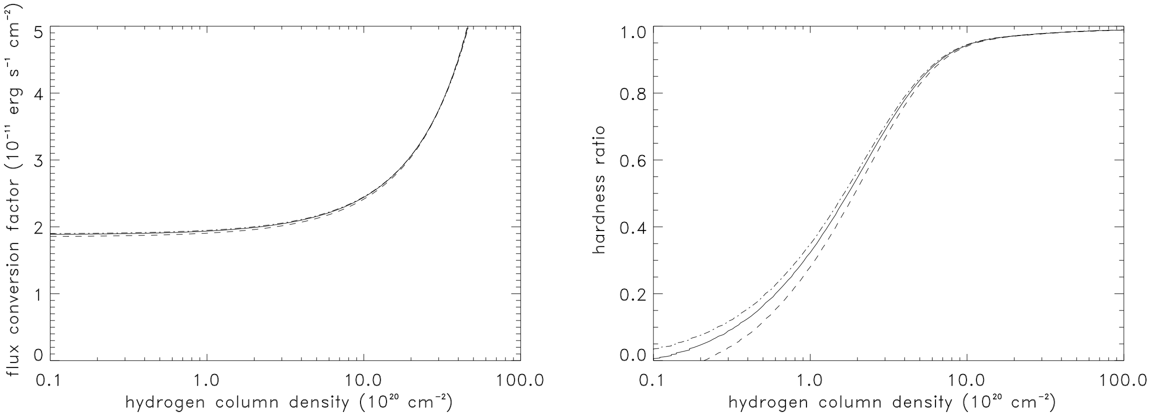

Fig. 8.— Flux conversion factor and hardness ratio as a function of the galactic hydrogen column density, N_H, for three different plasma temperatures: 2.5, 5, and 8 keV.

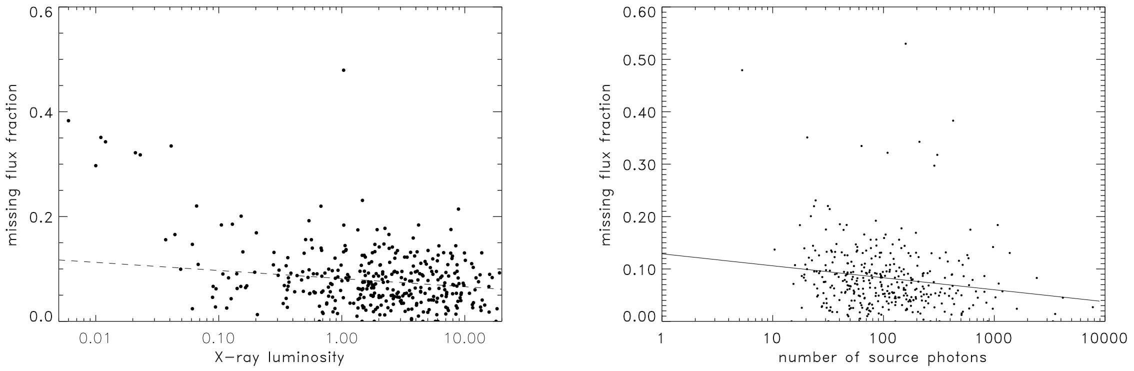

Fig. 9.— Estimated missing flux of the NORAS cluster sources as a function of a) the source luminosity (in units of 10^{44} erg s^{-1}) and b) the number of detected photons per source.

A comparison with pointed observations performed below gives already an encouraging confirmation of these estimates.

Alternatively we explore a second approach to estimate the missing X-ray flux by fixing the core radius in the β model to 250 kpc. This approach was used in earlier studies of X-ray cluster samples (e.g. Henry et al. 1992). Figs. 10a and 10b show the results corresponding to the results of Fig. 9. One clearly notes a very steep increase in the missing flux for decreasing X-ray luminosity in Fig. 10a. The dependence on the photon number for which we would expect the strongest dependence is much less pronounced and not essentially different from the results in Fig. 9. One notes, however, that the scatter in Fig. 10b has approximately doubled. The obvious interpretation of these results is that the strong dependence on X-ray luminosity seen in Fig. 10a is artificial and results from an overestimate of the core radius for the less luminous objects. This inappropriate choice of the core radius also increases the scatter in Fig. 10b. Thus we conclude that this approach is clearly inappropriate for our study and the above used scaling of the core radius is a reasonable choice.

3.6. Comparison with the results of RASS I

A comparison of the count rates measured in RASS I for the 378 cluster sources listed in Table 1 with the results of the GCA reanalysis is shown in Figs. 11a and 11b. For the comparison the RASS I count rates measured in the broad band have been converted to hard band counts by means of the measured hardness ratio. Sources which feature a significant extent according to our new analysis are marked in the plot. There is a large fraction of sources for which the count rates measured in RASS I or RASS II are underestimated by up to an oder of magnitude, which are essentially the sources marked as extended by the GCA method. The pointlike sources scatter around the line of equal count rate with an increasing scatter with decreasing count rate. The increase of the RASS I to GCA count rate ratio for low count rates seen in Fig. 11b is most probably an artefact produced by the previously set count rate limit in the selection of the RASS I sources for this sample (as indicated in the figure by the dotted line).

The source of disagreement for the extended sources results from the design of the source analysis technique used for the RASS which is tuned to work optimally for point sources. Two effects discriminate against the proper accounting of the count rate of extended sources: i) the Gaussian kernel of the source shape fitting of the maximum likelihood analysis is bound to miss the outer wings of a typical cluster surface brightness

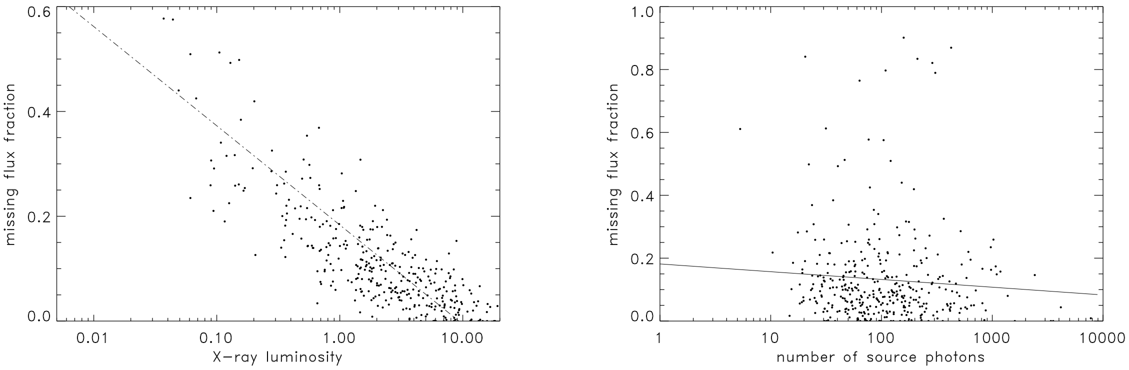

Fig. 10.— Estimated missing flux of the NORAS cluster sources as a function luminosity (left) and source photon number (right) if a constant core radius of 250 kpc is assumed. The straight lines show the results of linear regression fits to the data.

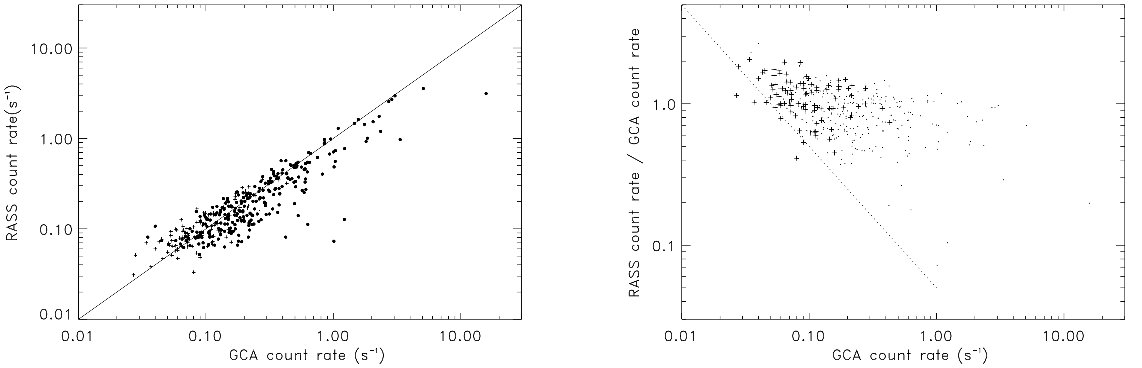

Fig. 11.— Comparison of the count rates determined by the maximum likelihood method applied in RASS I and the results of the GCA. The straight line in the left pannel indicates equality. The sources found to be extended in the new analysis are shown as filled circles and the point-like sources as crosses. In the right pannel the extended sources are shown as small dots. The dotted line in the right pannel indicates the approximate count rate limit for the RASS I source results (the count rate limit in the plot has a small uncertainty because the count rate conversion from broad band to hard band also includes a dependence on the interstellar column density).

distribution and ii) part of the outer X-ray halos of extended clusters may be treated as background by the background spline fitting process as used in the RASS standard analysis. A source analysis technique tuned to process the extended sources properly is therefore required to avoid these problems and to obtain correct X-ray parameters for the objects in our sample. The reanalysis of all the X-ray sources in the sample was therefore a necessary prerequisite for the compilation of an X-ray cluster catalogue to be used for astronomical and cosmological studies.

3.7. Comparison to pointed observations

To test the count rate determination of our new analysis technique against a more reliable standard we have analyzed 80 clusters of our sample in pointed observations in which the better photon statistics allows a more detailed and precise analysis. The results for the brighter sources were taken from the compilation of Reiprich & Böhringer (1999) of the ROSAT clusters with the highest flux. 13 of the clusters from this sample were also analyzed in very large RASS survey fields ($4^\circ \times 4^\circ$ or $8^\circ \times 8^\circ$) because of the large cluster sizes. In the analysis by Reiprich & Böhringer (1999) a more refined source analysis was performed (where contaminating sources are excised in a wide region in and around the cluster and a possibly badly measured background is iteratively corrected by parabolic fits to the azimuthally integrated background surface brightness profile outside the cluster). Therefore it is also interesting to keep these objects in the list for comparison. The other data were retrieved from the ROSAT archive. The analysis technique used is similar to the one described above with a main difference that contaminating sources are excised interactively. We are using the count rate at R_x. The values for R_x found in the pointed observations are generally larger than R_{out} found in the RASS data as the flux can usually be traced further out into the background in the deeper observations. Fig. 12 shows a comparison of the count rates found in the two data sets. The objects analyzed in large RASS fields are marked with open symbols. The mean deviation of the count rates determined for the pointed data and the present results is 8.6%. Thus we conclude that the missing flux is on average about $7 - 10\%$ without a significant bias as a function of X-ray flux. This result is in excellent agreement with the estimates for the missing flux in section 3.5. The validity of the GCA approach is thus confirmed in two ways: the missing flux fraction is relatively small compared for example to the measurement errors and the *ab initio* estimates for the missing fraction are approximately correct.

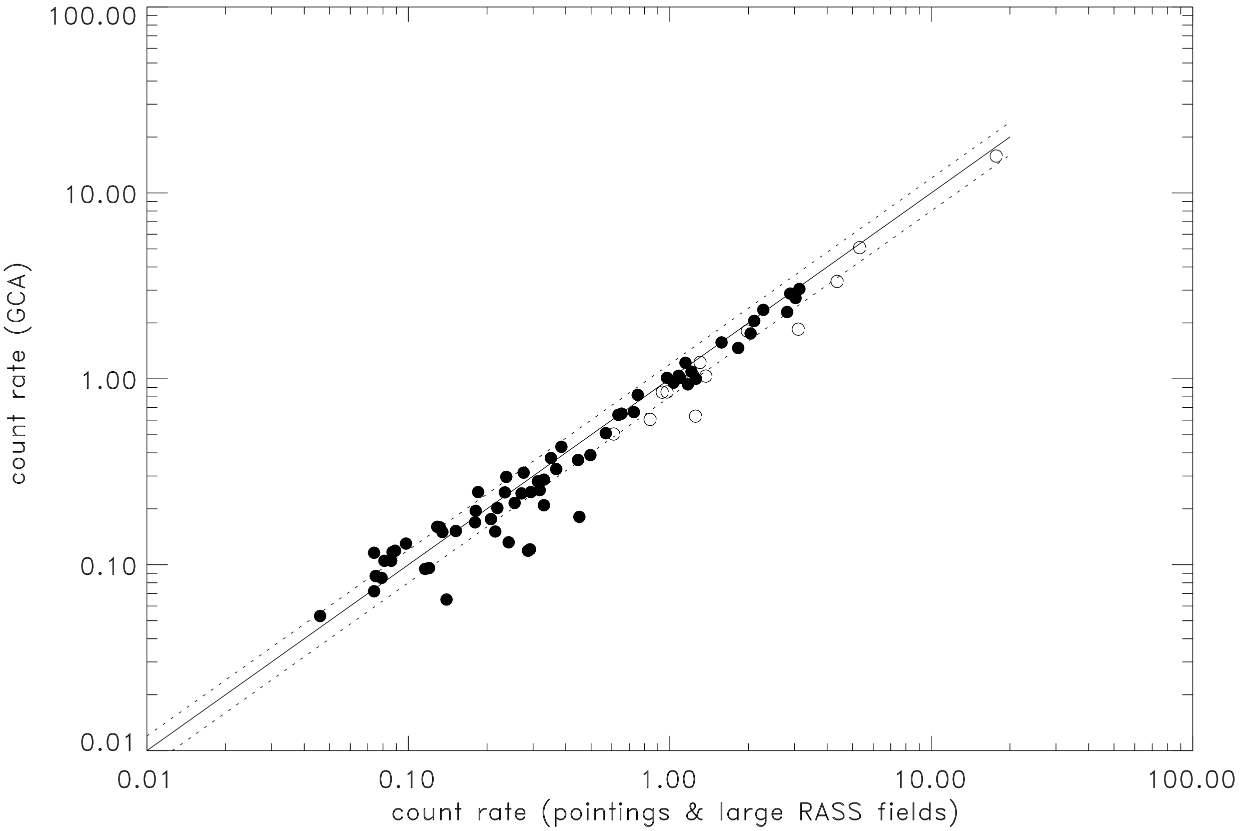

Fig. 12.— Comparison of the count rates for 67 clusters as determined in the present analysis and in deeper pointed observations (full circles). In addition we also show the comparison between the present results and the interactive analysis by Reiprich an Böhringer (1999) for 13 clusters in the same RASS fields (open symbols). The solid line indicates equality and the two dashed lines indicate deviations of 20%.

4. The catalogue of RASS I extended sources: clusters and non-cluster sources

In the following we are presenting the catalogue of the sample of 495 RASS I extended X-ray sources identified as galaxy clusters or as non-cluster X-ray sources. We discuss further characteristics of the source properties and the sample in the subsequent sections. We split the catalogue in three parts, the list of 378 sources identified as clusters, the list of 99 non-cluster sources, and a list of 17 X-ray AGN and one star located in clusters or in the line-of-sight of clusters, where the cluster is not the main source of the X-ray emission. The first tables, Table 1 - 4 list the major properties of the sources. Further X-ray parameters for the galaxy clusters are given in Table 5.

The parameters of the table columns of Table 1 are described as follows. Column (1) lists the source name given by the following scheme: we use the prefix RXCJ for the reanalyzed RASS sources that have been identified with a galaxy cluster, where the "C" stands for cluster. This prefix will be exclusively used for all RASS clusters analyzed by the above GCA technique. In particular this prefix has also been assigned to the RASS clusters identified within the REFLEX Survey (Böhringer et al. 1998, Guzzo et al. 1999). The remaining part of the name refers to the source coordinates for the epoch J2000 in hours (RA) or degrees (DEC), minutes, and fractions of a minute. Since the cluster sources are usually extended by more than one arcmin we use an arcmin precision in converting the cluster coordinates into the remaining part of the source name, thus the total name has 15 digits. Note that the coordinates in the cluster source name can deviate from the official RASS source catalogue coordinates reflecting the difference in the source analysis technique used. Column (2) gives alternative source names for previously catalogued optical counterparts to the X-ray sources, mainly Abell and Zwicky cluster names, names of NGC and UGC galaxies forming the central dominant galaxies of groups, and previously identified RASS or other X-ray sources. The Zwicky cluster names given in the table conform with the convention of the NED data base (note that the coordinate reference in the name refers here to epoch B1950). Columns (3) and (4) give the source position in decimal degrees for the epoch J2000. Column (5) gives the redshift of the cluster. Column (6) lists the measured count rate in units of counts s^{-1}. Columns (7) and (8) give the X-ray flux in units of 10^{-12} erg s^{-1} cm^{-2} for the flux estimated for a temperature of 5 keV in the first step and the finally calculated corrected flux, respectively. This correction includes the recalculation of the count rate flux conversion for the best temperature estimate and the redshift of the spectrum, but not the addition of the estimated missing flux. The fractional uncertainty in percent for the count rate, the fluxes and the luminosity are given in Column (9). Column (10) gives the rest frame X-ray luminosity of the clusters in the 0.1 - 2.4 keV energy band. Column (11) lists the value assumed for the absorbing column density in the line-of-sight to the source in units of 10^{20} cm^{-2}, and column (12) indicates with the sign "?" if the identification as a cluster leaves some residual doubts. In some cases a second flag provides information on the way the source position was determined as explained below. Column (12) also lists the flags for the sources which have been deblended, flag B, analyzed in extra large fields, flag L, and sources which may be contaminated, flag C. The last column, (13), gives the reference number for the redshift as listed in the table caption. The objects marked by "?" or C are commented below.

For the position we have used the coordinates determined by the moment method with a 3 arcmin aperture radius. As an exception in the case of 12 cluster sources we have chosen to either redetermine the center position by a moment method with a larger aperture of 5 or 7.5 arcmin or we have determined a center position by hand. In these sources the automatic detection has selected a maximum which is significantly offset from the global center of symmetry of the clusters. These clusters are marked by the flags b, c, o in column (13) for the 5 arcmin and 7.5 arcmin moment method and the determination by eye, respectively.

Table 2 lists the equivalent parameters for the RASS I extended sources identified as non-cluster objects. Here column (2) gives the source type of the identification except for cases with popular object names. A more detailed identification will be given in the second paper by Huchra et al. (1999). Columns (3) to (8) have the same definition as these columns in Table 1. Columns (9) to (14) give the extent parameter P_{ext} from the KS test, the best fitting core radius, its minimal value consistent with the 2σ uncertainty limit, the hardness ratio, its error, and the deviation from the expected value of HR in units of σ. The hardness ratio does occationally exceed the value of one in the tables, which occurs when the soft photon counts in the source region fall short of the background expectation. Note that for the parameters P_{ext} and ΔHR an upper limit to the numerical value of 30 and 10, respectively, was set, which was also used in plotting the data. Column (15) gives the interstellar HI column density. In the last column (16) objects with no certain optical identification are marked with "?". The identification strategy for the non-cluster sources is explained in section 5. The last column also contains the flag for the alternative center determination.

Table 3 lists X-ray sources where the X-ray emission is obviously originating from an AGN and in one case from a star, but where a cluster or group of galaxies is also visible on the Palomar Sky Survey images or on the CCD frames taken for this project. In several cases which are commented in Table 4 the redshift information indicates in addition the existence of a cluster and that the AGN is at the same redshift. The meaning of the columns of Table 3 is the same as that for Table 2. Table 4 provides the redshifts of the AGN as far as known and comments on the source identification.

Figure 13 shows the distribution of the sources from Table 1 - 3 in the sky. Since we have not yet imposed a strict flux limit to the survey and also due to the incompleteness of the sample we cannot necessarily expect a homogeneous coverage of the sources in the sky. Near the coordinates $RA = 270°$ and $DEC = 70°$ we note a significant concentration of sources, which is due to the concentration of overlapping survey strips at the north ecliptic pole (NEP). (Note that this is not due to a pile up of exposure time at the NEP, since each survey strip was analysed independently, but due to the fact that the chance for detection of low flux, extended sources is increased in the multiple strips. A homogeneous coverage is achieved here only after imposing a proper flux cut.) There are also several low density regions in the source distribution as for example at the northern tip of the south galactic cap region.

The distribution in X-ray luminosity and redshift of the sources in the cluster sample is shown in Fig. 14. The parabolic curves indicate limiting fluxes of 10^{-12} erg s^{-1} cm^{-2} and 3×10^{-12} erg s^{-1} cm^{-2}, respectively. There are 5 clusters with redshifts larger than 0.4 and 18 clusters with redshifts between 0.3 and 0.4. About half (11) of these clusters have luminosities in excess of 10^{45} erg s^{-1} and belong to the most X-ray luminous clusters in the Universe.

4.1. Comments on individual objects

RXCJ0106.8+0103 has an active galaxy in the cluster noted in the survey by Romer et al. (1994). The RASS image is consistent with a point source and a cluster spectrum. The available ROSAT HRI image has a small but significant extent. If the emission is mainly due to the cluster it would be very compact for the given high luminosity. A CCD exposure shows a nice cluster image and therefore we expect that this object is an X-ray cluster with a severe X-ray contamination by the AGN.

RXCJ0255.8+0918 is a pointlike X-ray source with spectral properties consistent with intracluster medium emission centered on an elliptical galaxy. The galaxy is also classified as Sy2/LINER (Pietsch et al. 1999). They also note that the galaxy is located in a group. Without further information it is difficult to distingish between AGN or hot gas halo emission. The X-ray luminosity of $L_x = 0.7 \times 10^{43}$ erg s^{-1} could well be that of a small group.

RXCJ0311.5+0714 is not certainly confirmed as an X-ray cluster and the redshift is uncertain since only one galaxy redshift is available.

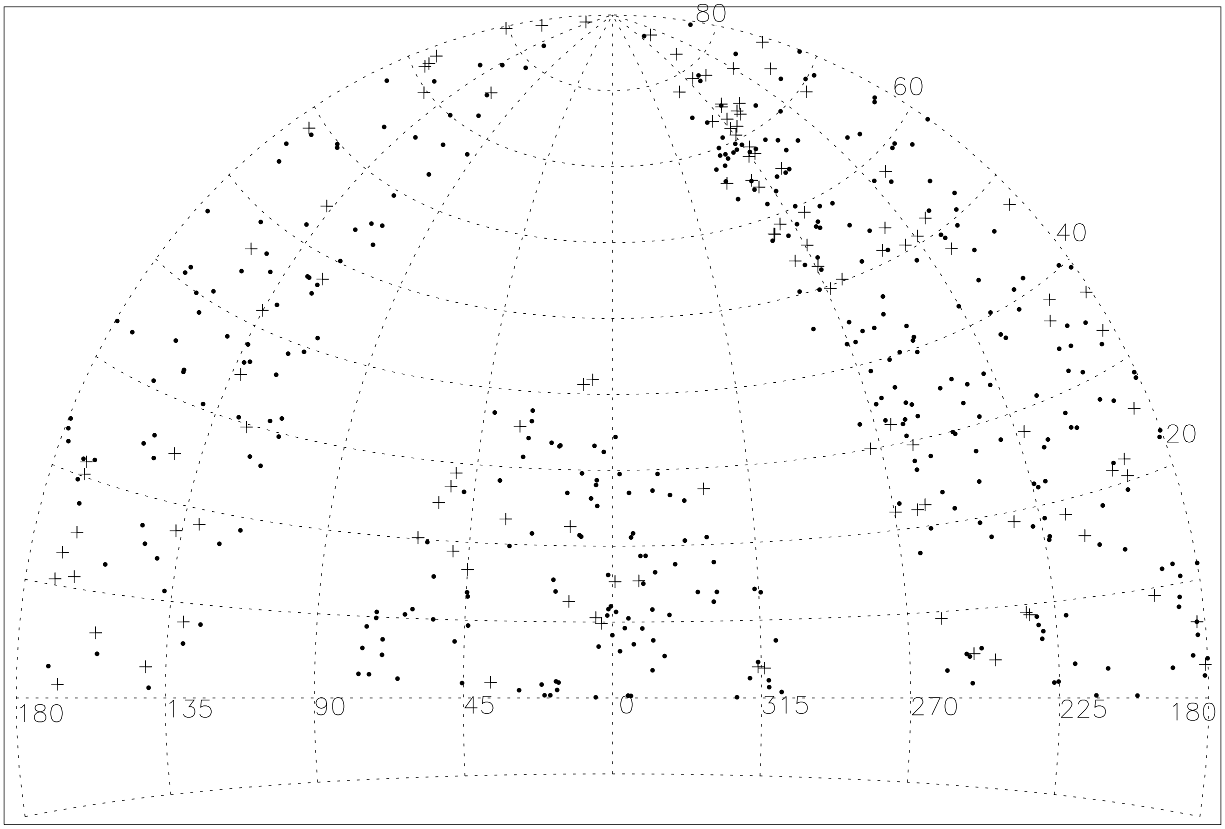

Fig. 13.— Distribution of the RASS I extended sources selected for the NORAS sample. The dots mark the NORAS cluster sources while the crosses mark the non-cluster sources identified in the course of the NORAS survey.

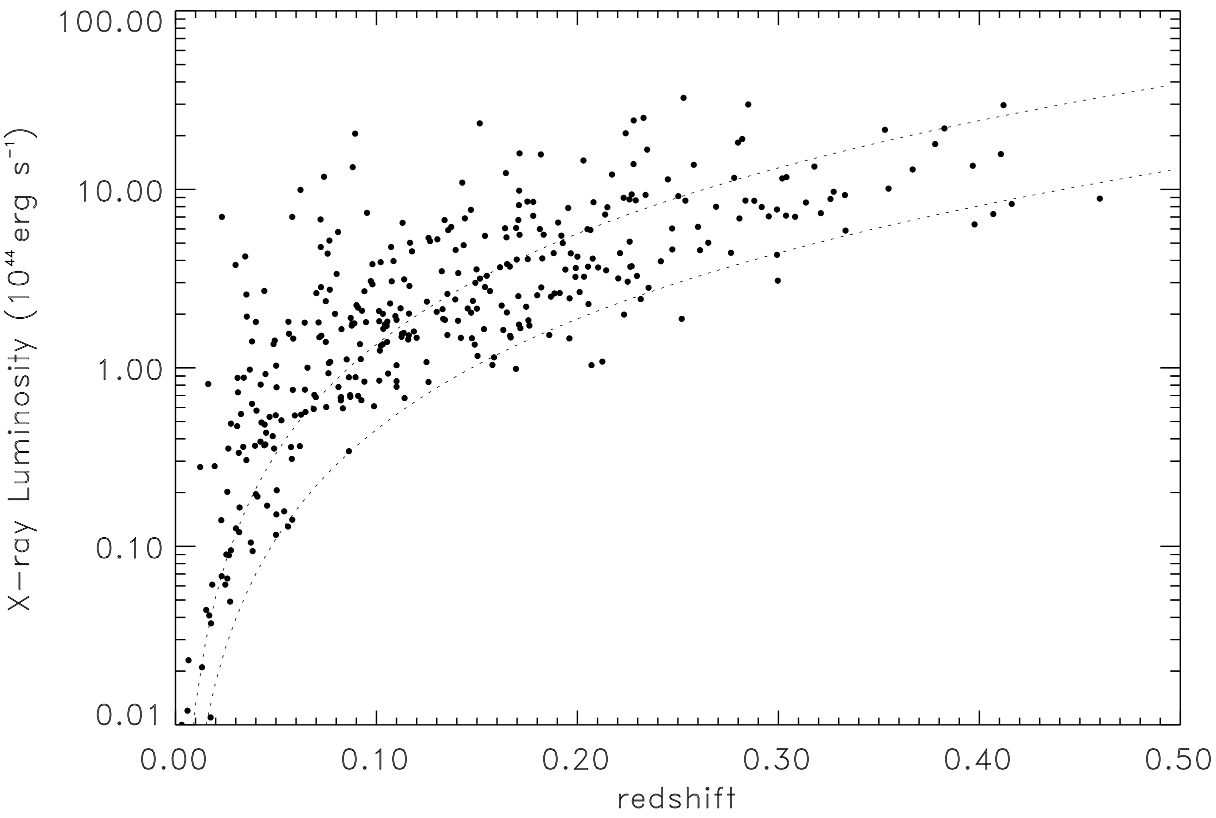

Fig. 14.— X-ray luminosity and redshift distribution of the NORAS cluster sources. The two dotted lines indicate flux limits of 10^{-12} and 3×10^{-12} erg s^{-1} cm^{-2}.

RXCJ0728.9+2935 is a cluster candidate in a crowded stellar field featuring a pointlike X-ray source. Only one galaxy redshift is available for the X-ray source region.

RXCJ0736+3925 shows extended X-ray emission, mostly due to intracluster medium emission, but obviously also some contribution by a softer central point source.

RXCJ0921.1+4538 coincides with the radio galaxy 3C219. The X-ray source is point like but the hardness ratio is consistent with hot gas emission. 3C219 is located in a galaxy group. Without further information we cannot definitely decide if the X-ray emission comes from the AGN or the group.

RXCJ1009.3+7110 is a case similar to RXCJ0106.8+0103 where a Seyfert 2 galaxy is listed in the Veron catalogue (Veron-Cetti & Veron 1998) and the ROSAT HRI image shows most probably a point source with a very compact halo. Thus this object is also classified as cluster contaminated by an X-ray AGN.

RXCJ1122.2+6712 shows in the available HRI image a small extended halo around the galaxy VII Zw 392. The RASS source is contaminated by a nearby point source. The X-ray halo is with a luminosity of less than 10^{43} erg s^{-1} quite faint corresponding to a very small group. It is one of the faintest sources in the sample.

RXCJ1157.3+3336: For this X-ray source two cluster identifications are possible. It is associated with Abell 1423 at a redshift of 0.0761 but there is also the possibility that a cluster is associated with the radio galaxy 7C 1154+3353 located at the center of the X-ray emission. The 7C galaxy is classified as cD galaxy. We adopt the identification of an X-ray cluster associated to the 7C galaxy because of the better positional coincidence. Crawford et al. (1999) note the same identification.

RXCJ1229.7+0759 and **RXCJ1243.6+1133** are the X-ray halos of the two Virgo cluster galaxies M49 and M60, respectively. They are included in this catalogue, even though these halos are embedded within the low surface brightness structure of the Virgo cluster emission. But since the two local halos stand out from the low surface brightness emission environment and can be reasonably characterized by the present source characterization technique we have not excluded them from our catalogue as we have excluded M86 and M87.

RXCJ1510.1+3330, RXCJ1556.1+6621, RXCJ1700.7+6412 show a contamination by a point source in the available HRI image by no more than 10 - 15%.

RXCJ1518.7+0613 is contaminated by X-ray emission from an AGN in the cluster, which is also indicated by a softer hardness ratio than expected for a galaxy cluster.

RXCJ1554.2+3237 is not yet definitely confirmed as cluster and the redshift is uncertain since there is only one galaxy redshift.

RXCJ1644.9+0140 and **RXCJ1647.4+0441** are cluster candidates in a crowded stellar field where no conclusive redshift has been ontained so far. RXCJ1644.9+014 is possibly a distant cluster.

RXCJ1738.1+6006 is also a cluster candidate in a crowded stellar field with extended X-ray emission at the significance threshold. No redshift has yet been obtained. A Seyfert galaxy is known with a distance of 1 arcmin from the X-ray maximum which is most probably not the X-ray source because the offset would be unusually large.

RXCJ1800.5+6913 has a complex structure and is obviously contaminated by emission from point sources. But these sources contribute less than 20% to the overall emission from the cluster.

RXCJ1832.5+6848 contains a BL Lac in the cluster center, which most probably severely contaminates the cluster X-ray emission.

RXCJ1854.1+6858 is a cluster candidate featuring an extended X-ray source. The redshift is uncertain since only one galaxy redshift is available.

RXCJ2035.7+0046 is an extended low surface brightness source with a detection significance of 3 to 4 σ. It is a cluster candidate in a very crowded stellar field for which no redshift is available yet.

RXCJ2041.7+0721 is a cluster candidate in a crowded stellar field with only one available redshift.

5. Discussion of the major source properties

Further properties of the X-ray cluster sources are provided by Table 5. The columns of the table are as follows. Column (1) and (2) repeat the name and rest frame ROSAT band X-ray luminosity of the sources from the previous tables. Columns (3) and (4) give the radius out to which the source count rate has been integrated, R_{out}, in units of arcmin and Mpc, respectively. Column (5) gives the probability result of the Kolmogorov-Smirnov test for the source to be a point source in terms of the parameter P_{ext}. For very low probabilities for the consitency with a point source the parameter P_{ext} was limited to a value of 30 for the entry in the table. A source is considered very likely to be extended if this parameter has at least a value of 2 (point source excluded with 99% probability). Column (6) and (7) give the best fitting core radius for the King model fit and the minimal core radius still consistent within 2σ error limits, respectively. Note that the core radii determined here are a only qualitative measure for the source extent, since in general the errors are very large and the fitting grid was coarsely spaced. Therefore we do not recommend to use the results for r_c as a measure of the statistics of the cluster shapes at this point. Column (8) and (9) give the spectral hardness ratio defined by eq.(2) and its Poissonian error. Column (10) finally indicates the deviation of the measured hardness ratio from the expectation value calculated for the given N_H and for a temperature of 5 keV. This deviation parameter is given in units of the 1σ-error of the hardness ratio and the listed and plotted values were limited to a maximum numerical value of 10.

One of the most interesting first questions about these parameters concerns the discrimination power of the spectral and extent parameters in distinguishing between cluster and non-cluster sources. This is analysed in detail for statistical samples of sources with known identifications in the forthcoming paper by Böhringer et al. (in preparation). The present source sample should be highly biased since it was preselected from the RASS I data with the criterion of showing a significant extent in the RASS I analysis. We have to expect for example that the subsample of point sources within the present sample is already enriched in pathological cases including e.g. double and very bright sources. Therefore the present sample is used here only for a qualitative discussion while statistical numbers can only be obtained from the analysis to be published in the following paper.

Fig. 15 displays the distribution of the spectral and spatial extent parameters for the cluster and non-cluster sources for comparison. For the spectral discrimination we plot the difference of the actually observed hardness ratio to the theoretically expected hardness ratio as calculated for a 5 keV cluster as shown in Fig. 8. The difference is thereby quantified in terms of the σ-deviation accounting for the uncertainty of the hardness ratio measurement. To quantify the extent we use the probability result of the KS-test for a point source in terms of the extent parameter P_{ext}. As we can see most of the clusters occupy the upper part of the figure and cover a wide range of extent values. As expected, non-cluster sources are concentrated in the region of small values of P_{ext}. Clusters have harder spectra than the average of the other X-ray sources being mostly stars or AGN, and therefore clusters should be separable by the hardness ratio from the softer part of the non-cluster population. On the other hand the extent parameter should help in the discrimination against the non-cluster sources since they are to the vast majority point-like sources at the angular resolution of ROSAT.

This is clearly seen in Figs. 16 and 17 which show a blow-up of Fig. 15 and display the cluster and non-cluster sources separately. Only 12 clusters out-off 378 show a more than 3σ deviation to the X-ray soft side. These are to about one half very bright clusters (including Coma) where the relative deviation is small in absolute sense and could reflect for example an incorrect value for the column density. For some of the sources we suspect some contamination by AGN to the overall emission. One of these cases is for example A1722 for which the HRI observation confirms the contribution of a point source to the extended cluster emission by an amount of about 30 - 40%. Anyway these pathological cases comprise only about 3% of the sample and the hardness ratio provides indeed a very powerful diagnostics for the source identification.

A similarly interesting result is found for the extent parameter, P_{ext} for the case of the non-cluster sources shown in Fig. 17. Only 22 out-off 117 sources show an extent if we adopt the extent threshold criterion defined above, that is, a value of $P_{ext} \geq 2$. Some of these sources are very bright and soft and are far from the expectation for a cluster type spectrum. If we exclude these sources with deviations larger than -8σ, there are only 13 sources for which the nature of the extent should be investigated to rule out a cluster nature. For more than half of these sources we find a reason why they are featuring an extent: 2 are nearby galaxies, M82, M106, which show extended X-ray emission, 7 of the sources are double sources where the main, catalogued source is consistent with a point source. Some of the remaining sources are very bright in the RASS (more than 500 photons) and, therefore, the relative deviation corresponds to a very small absolute deviation which can be caused by small systematic effects. A pathological object in this subsample is the BL Lac RXJ1456.0+5048 which has a value for P_{ext} of 5.4. It has been analyzed in a RASS-follow-up HRI observation by Nass (1998) and shows at most a very marginal extent in this observation with a ten times higher angular resolution. Therefore the extent seen in the present RASS analysis has to be spurious. We have also checked the mean off-axis position of the source photons as a signature of an imperfect scanning of the source which could produce a deviation of the mean PSF for the source observation compared to the average survey PSF, but found no obvious deviation. Therefore this case demonstrates that systematic effects in the broadening of the PSF for individual sources in the RASS exist, but they are obviously extremely rare. Subtracting the cases for which the extent is real, we find that less than 10% of the sources feature a spurious extent. Applying a similar test to an unbiased point source sample shows that the misclassification is usually less than about 5% (see Böhringer 1999 in preparation).

In Fig. 17 we have also marked the non-cluster X-ray sources which seem to be associated with an optical cluster either in projection or located in the cluster. There is no indication that these sources show a different distribution in the source quality parameters. Therefore the identification that in most of these sources the AGN or star is clearly the dominant X-ray source is supported by this result.

These results on the source quality can be compared with the prime selection criteria of this sample as extracted from RASS I. We recall that only sources which were characterized by a significantly large extent parameter obtained in the maximum likelihood analysis were included in the present sample. Using the new technique $\sim 25\%$ of the sources do not feature an extent. This could be partly due to the fact that the present method is sometimes less sensitive in recognizing the source extent for very compact sources since it does not use the detector position information and thus does not weight for photons imaged with different sharpness as does the maximum likelihood method. Looking at the nature of the sources we conclude that about 23% of the sources are genuine point sources and thus the failure rate of the RASS I extent classification is at least about 20%. The results displayed in Figs. 15 - 17 show that the present method provides a great improvement concerning the failure rate of the method. This justifies the use of these source quality parameters to assist the identification of the sources.

We have made use of the above results in the identification process. The criterion for classifying a source as a non-cluster source was one of the following:

i) The optical counterpart is a bright star (≥ 12.5 mag) and the source is not extended. This is justified by the finding of Voges et al. 1999 (in preparation) that there is a much less than 1% chance coincidence of a RASS X-ray source with such a bright star.

ii) There is an optically identified AGN at the source position and the source is not extended. No cluster is seen on the CCD images taken for this project.

iii) The source is a known, previously identified non-cluster X-ray source.

iv) The source is clearly point-like and has a soft hardness ratio deviation larger than 3σ. There is no signature of an optical cluster in the digitized Palomar Sky Survey image or the CCD images taken for the project.

We noted 17 cases, where there is a signature of an optical cluster, but the other criteria are inconsistent with a cluster identification. These cases have been listed separately in Tables 3 and 4.

This identification scheme is only made possible by the extensive spectroscopic follow-up and almost complete CCD imaging of the targets in the sample of extended sources (no spectroscopy was done for those objects for which this information is already available from the literature or the CfA archives). A classification only by identification of clusters on optical images or exclusion of sources with spectroscopically identified AGN without further inspection would have failed in several cases.

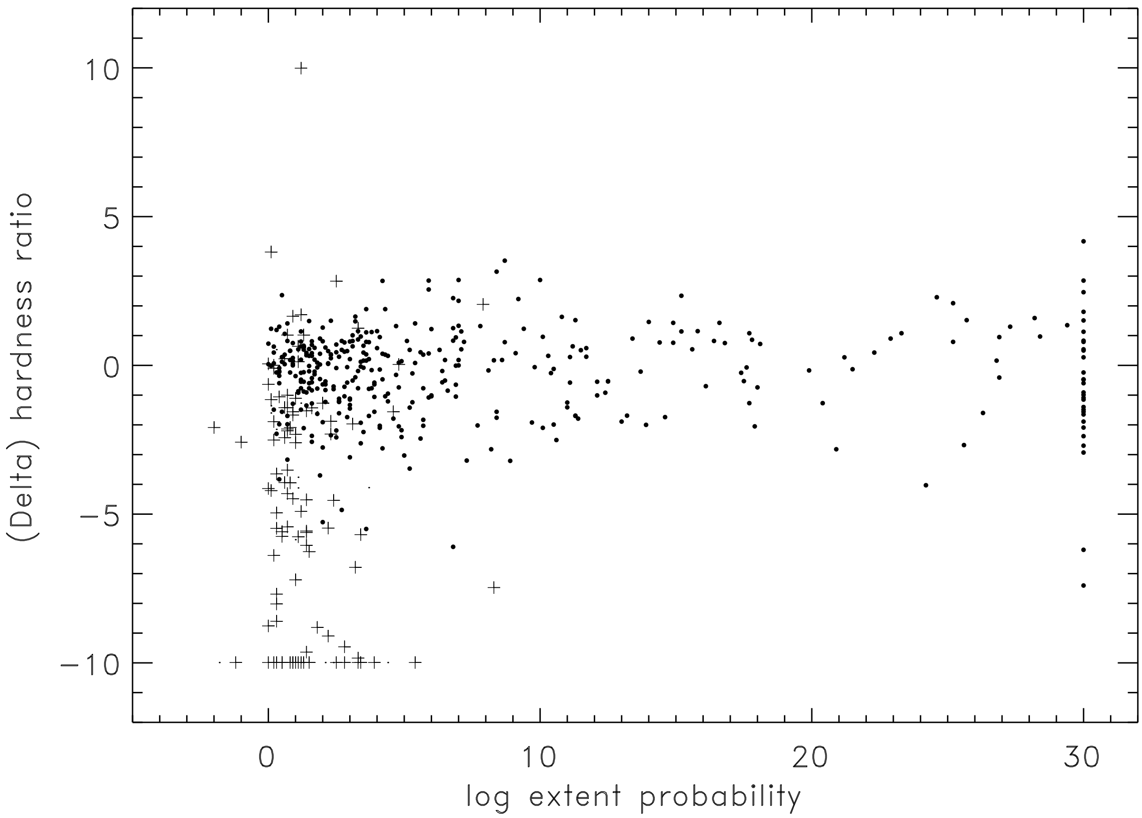

Fig. 15.— Distribution of the values of the negative logarithmic probability for the KS-test for a point source (labeled log extent probability) and for the sigma deviation of the hardness ratio from the expectation for given hydrogen column density and for a 5 keV cluster spectrum. Filled circles mark the cluster sources while crosses label the non-cluster sources.

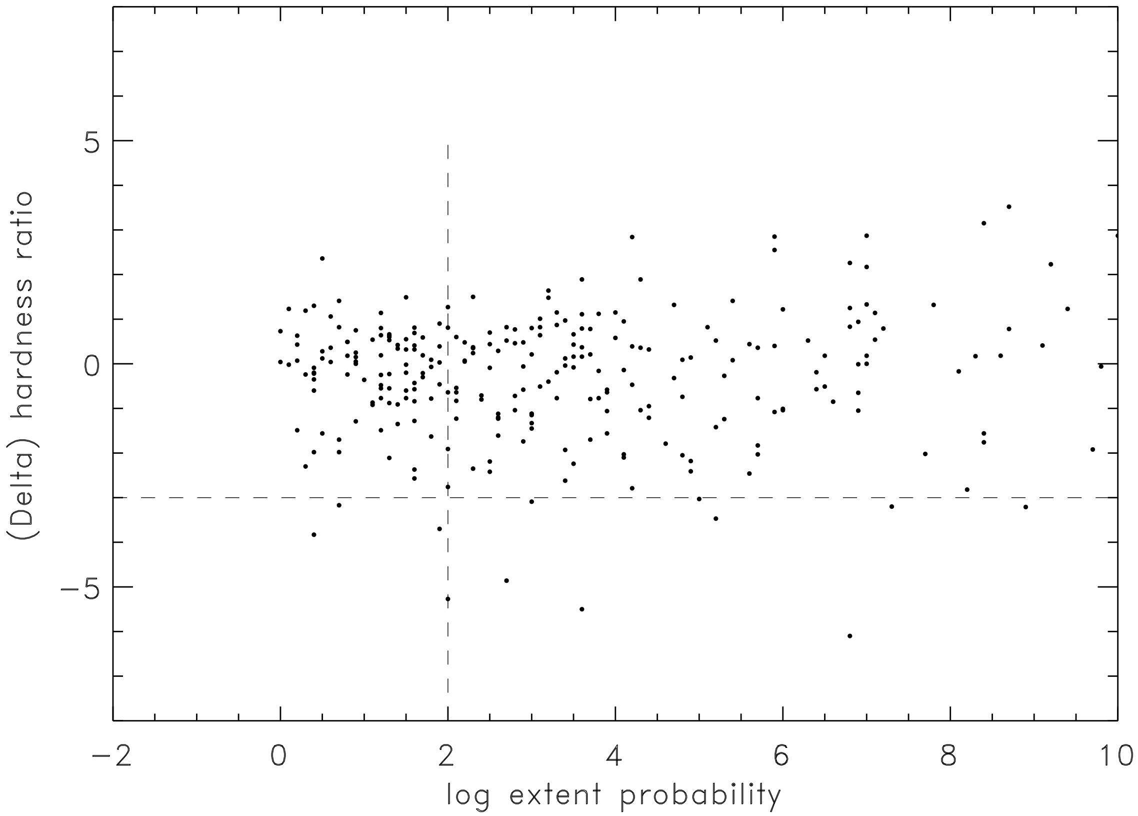

Fig. 16.— Distribution of the log extent probability and the sigma deviation of the hardness ratio from the expectation for the cluster sources only. Only about 3% of the clusters show a more than 3σ deviation to the soft side. This hardness threshold and the threshold for the extent parameter are marked by dashed lines.

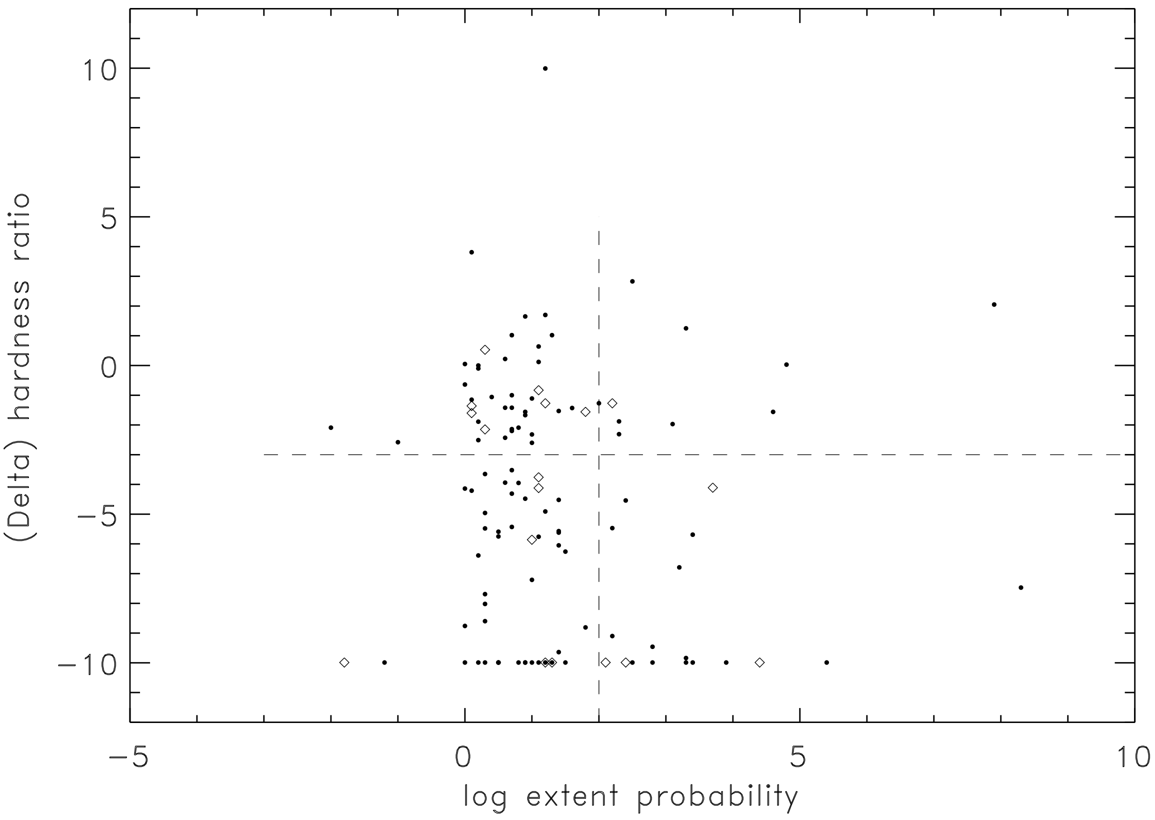

Fig. 17.— Distribution of the log extent probability and the sigma deviation of the hardness ratio from the expectation for the non-cluster sources only. Less than 19% of the non-cluster sources show a log extent probability value larger than 2.

6. Further analysis of the 9 - 14^h study region

While the above results show that the source identification has reached a high level of reliability, there are serious concerns about the completeness of the present sample in terms of a purely flux-limited X-ray cluster sample, because the sample rests on the RASS I source extent selection criterion. There are two principle sources of incompleteness: i) medium distant and distant clusters may have too compact X-ray emission regions to be resolved as extended X-ray objects in the RASS and ii) the RASS maximum likelihood analysis may fail to recognize all the spatially resolved sources in the RASS as extended X-ray sources. Both sources of incompleteness affect the present sample. Figs. 2 and 16 show that there are galaxy clusters which appear as point-like X-ray sources for both analysis techniques, the standard RASS analysis and the method used here. In addition we will find below that there is a large fraction of significantly extended sources which are missed by RASS I.

In an attempt to check for the incompleteness of the RASS I sample we conduct two studies: we investigate what fraction of ACO clusters with X-ray emission is missing in the present sample and we search for extended sources in the RASS II data base with the new analysis technique and inspect their nature to find additional clusters or cluster candidates. Since this is meant as a statistical test we restrict the analysis to a subregion of the study area: the region of the northern sky between 9^h and 14^h. The sky area of this region is 1.309 ster as compared to the total NORAS survey area of 4.134. In this right ascension range the $|b_{II}| \leq 20°$ band of the Milky Way is completely located at negative declinations. We restrict the cluster search by imposing an X-ray flux limit of 1.6×10^{-12} erg s^{-1} cm^{-2}.

Thus in the first step we have run our analysis on the sky positions in RASS II of the 901 clusters listed by Abell, Corwin, & Olowin (1989) in the sub-survey region. Ten clusters of this sample were missed in the analysis since RASS II has a too low exposure in the corresponding sky fields for a significant source detection (these clusters are: A917, A974, A986, A996, A999, A1011, A1042, A1057, A1128, A1554). 93 additional ACO clusters are detected above the flux limit. A closer inspection of the detections with the same procedures as described above revealed that 8 of the detections have most probably an AGN as the dominant X-ray source. These ACO clusters are: A763, A924, A1030, A1225, A1575, A1593, A1739, A1774. The results for the other 85 detections, where we identify the X-ray emission to originate in the cluster, are listed in Tables 6 and 7. The columns of these tables have the same meaning as those of Tables 1 and 5, respectively.

In the second step we have selected all the sources from the RASS II data base in the sub-survey region, reanalyzed them, and extracted all the sources with a flux $\geq 1.6 \times 10^{-12}$ erg s^{-1} cm^{-2} and an extent parameter $P_{ext} \geq 2$. In total there are 377 sources of which a large fraction is already contained in the NORAS I sample and the supplementary ACO sample. Again we find another fraction which is identified as double point sources or very bright point sources having a small absolute extent.

An inspection of all the remaining sources on the digitized sky images and literature data from data bases leads to a sample of 52 very promising candidates of which 21 can readily be identified as previously listed galaxy clusters. The latter list of identified cluster sources is given in Table 8 and 9. For the positive identification of the remaining candidates further optical observations within the ongoing NORAS survey are in progress.

To understand which of the two sources of incompleteness discussed above is more important for the loss of these additional cluster sources in the primary candidate list of the NORAS Survey, we plot in Fig. 18 the distribution of the extent parameters of the X-ray clusters of the two additional cluster lists. As we can see most of the additionally found ACO clusters (74.2%) feature an extent according to the new analysis technique. The second supplementary list consists by definition only of extended cluster sources. Therefore we have to conclude, that the extent flag in the RASS I data base is not only not very reliable but a large fraction of the well extended sources is also missed.

7. Discussion of the sample completeness

To test the completeness of the catalogue, a comparison can be made to the southern RASS cluster survey project, the REFLEX Survey (Böhringer et al. 1998). This sample has been constructed in a different way making extensive use of the COSMOS data base to correlate X-ray sources with the galaxy distribution. Therefore this sample does not rely on existing cluster catalogues nor on the selection of X-ray sources featuring an extent. Internal statistical estimates for the REFLEX sample suggest a completeness larger than 90% for the flux limit of $F_X = 3 \times 10^{-12}$ erg s^{-1} cm^{-2}. The number counts of the REFLEX survey and the NORAS survey are compared in Fig. 19. We note that the NORAS sample reaches a fraction of 50% of the REFLEX number counts at the REFLEX flux limit.

A large fraction of the missing clusters has been recovered by the supplementary sample in the study area. In Fig. 20 various subsamples of the combined cluster catalog in the 9^h to 14^h region are compared to the REFLEX Survey. While the cluster sample from Table 1 recovers with 40% an even smaller fraction of the sky density compared to the REFLEX Survey, 70% are reached if the ACO clusters are added and 82% are obtained for the combined sample. Thus there is still a fraction of clusters missing. This is easily

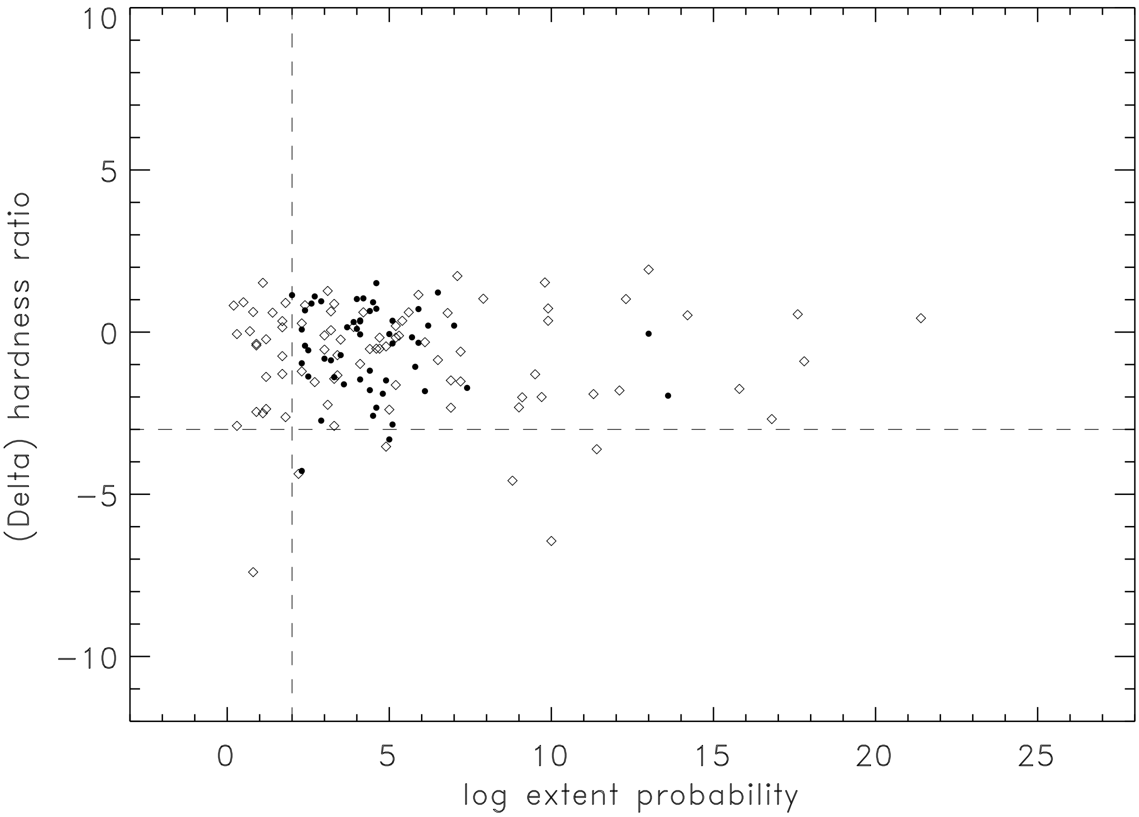

Fig. 18.— Distribution of the log extent probability and the sigma deviation of the hardness ratio from the expectation for the additionally found ACO clusters (diamonds) and extended sources (dots) from the 9^h to 14^h study region.

understood, since the REFLEX sample contains a fraction of 22% of all objects which are not resolved as extended by the GCA analysis. We can expect that about 10 - 20% of the clusters for the REFLEX flux limit are neither listed as ACO clusters nor recognized as extended sources. Note that the combined sample in the study region completely recovers the previous RASS cluster sample by Ebeling et al. (1998) as discussed below. Most clusters not contained in Table 1 are easily found as ACO clusters and 7 further clusters show a clear extent.

Therefore to achieve a higher completeness in our continuing northern cluster survey we are, in addition to including known catalogued clusters with X-ray emission and newly classified extended X-ray sources, conducting further imaging of promising non-identified X-ray sources to recover the compact X-ray clusters missed in the previous searches.

8. Comparison with the northern Brightest Cluster Sample

In total 166 X-ray sources analyzed here overlap with the previous RASS galaxy cluster compilation by Ebeling et al. (1998). 142 sources coincide with the sources of Table 1, 22 sources with sources in Tables 6 and 8 for the 9^h to 14^h region, and two sources are identified with AGN in our analysis. Thus 40 sources compiled by Ebeling et al. are not included here (including the Virgo cluster). Since the two compilations are made with the same intention we compare the results of the two samples in some detail.

Fig. 21 shows a comparison of the X-ray fluxes determined by the two different methods used in the two surveys for the 166 cluster in common. Note that in our compilation the fluxes have not been corrected for the missing flux outside the measurement aperture. Therefore we show both results from the work of Ebeling et al. in the plots: the uncorrected measured fluxes (with open circles) and the corrected final fluxes (full circles). The agreement at high fluxes is very good and there is also quite good agreement for most sources. The scatter is increasing, however, towards lower fluxes. Mostly at lower fluxes we find a few sources with fluxes larger by factors up to 2 as determined by the VTP method compared to the present results. Note the bias introduced at low fluxes by the flux limit set in the Ebeling et al. sample that suppresses the cases where the VTP to GCA flux ratio is lower than one. Thus, what appears like a high bias of the VTP results at low flux in Fig. 21b is most probably explained by an increased scatter in the flux ratio with decreasing flux. Thus in general the agreement is good.

Two sources in the cluster list by Ebeling et al. (1998), A2318 and Z2701, are classified as AGN in our work. The first source appears as RXJ1905.7+7804 in Table 3. We have

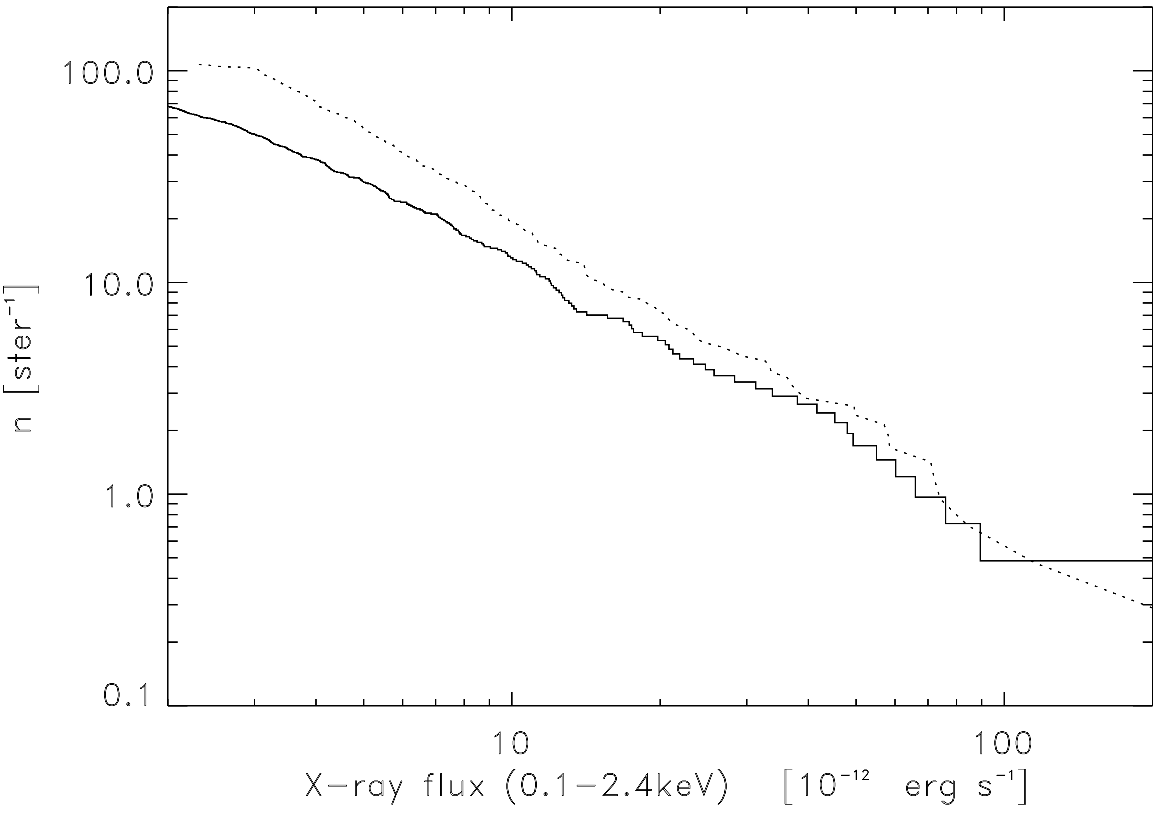

Fig. 19.— LogN-logS for the NORAS I sample (continous line) compared to the REFLEX Cluster Survey (dotted line).

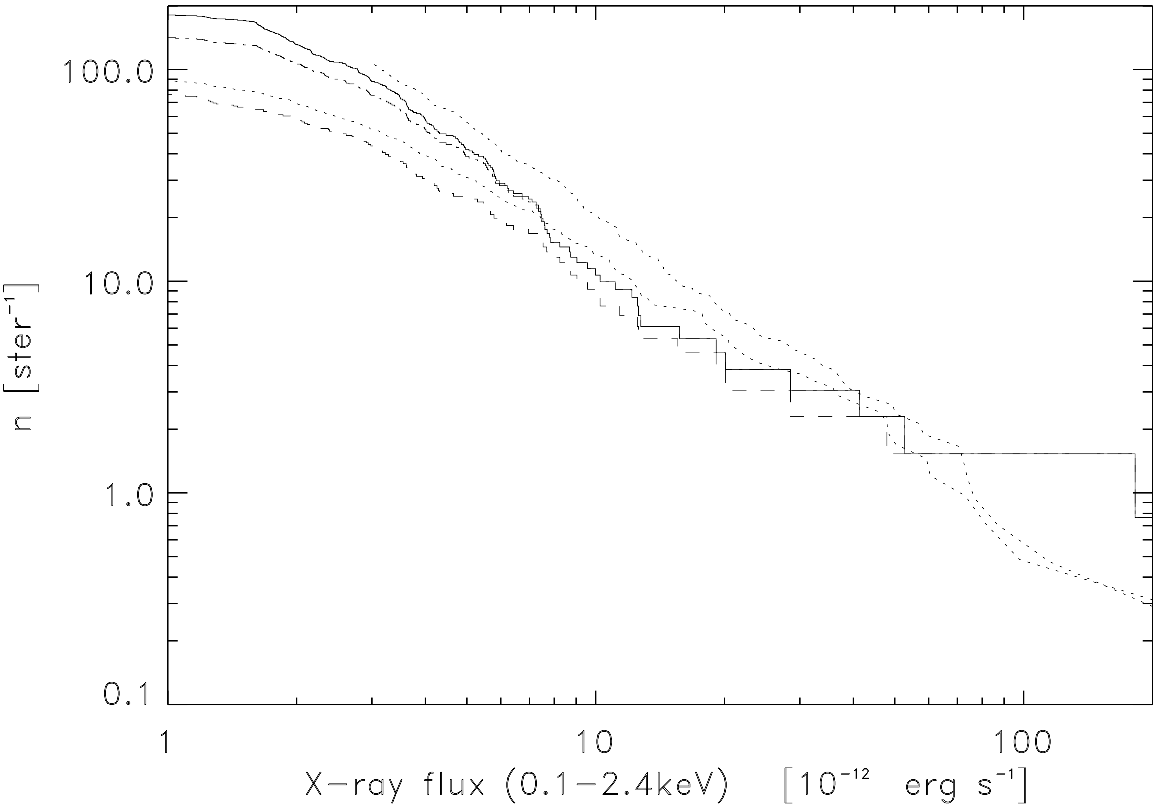

Fig. 20.— LogN-logS for the NORAS 9-14 hour region. NORAS I main sample (lower dashed curve), NORAS I and ACO clusters (dashed-dotted curve), NORAS I, ACO, and supplementary extended cluster candidates (continuous curve), NORAS I sample for the whole northern sky (lower dotted curve), REFLEX Survey (upper dotted curve).

optically identified a Seyfert 1 galaxy at the source position. The X-ray source is pointlike and has a spectral hardness ratio that is too soft for a cluster with a 3.8σ deviation. The X-ray source is also significantly offset from the optical cluster center. Thus we identify the X-ray source with the AGN. The second source was found in our search for additional extended sources in the 9^h - 14^h region and is not catalogued here. It was dismissed because it is identified by as AGN by Bade et al. 1998. The spectral hardness ratio shows again a 4.5σ deviation to the soft side. The KS-test yields a small extent of the source and an inspection of the X-ray image indicates a smaller emission contribution from the region of the optical cluster center. But the main contribution comes obviously from the AGN.

We can also make a comparison of the completeness of both surveys in the 9^h - 14^h region. While we recover all the clusters in Ebeling et al. (except for Z2701 which is classified as AGN), two additional clusters are found in our search with a flux larger than $L_X \geq 4.7 \times 10^{-12}$ erg s^{-1} cm^{-2} (in addition the two Virgo galaxies M60 and M49 which are summed into the Virgo cluster in Ebeling et al.). Over the whole right ascension range we find 12 additional objects above the flux limit of Ebeling et al. These sources are RXCJ0005.3+1612 (A2703), RXCJ0209.5+1946 (A311), RXCJ0736.4+3925 (contains a BL Lac), RXCJ1121.7+0249 (SHK352), RXCJ1242.8+0241 (NGC4636), RXCJ1447.4+0827, RXCJ1501.2+0141, RXCJ1506.4+0136, RXCJ1617.5+3458 (NGC6107), RXCJ1718.1+7801 (A2271), RXCJ1742.8+3900, RXCJ1900.4+6958 (A2315). All the sources except for RXCJ1447.4+082 have a significant extent. The Abell clusters have fluxes within about 15% of the flux limit of Ebeling et al. (1998) and most of the remaining sources are nearby groups of galaxies being less rich than Abell clusters. This number of extra sources is still compatible with the claimed completeness of the Ebeling et al. (1998) sample. The above comparison with the results of the southern RASS analysis in the REFLEX sample indicates, however, that both samples are still less complete than the southern survey.

9. Discussion and Summary

Using the early results of the RASS we compiled an X-ray sample of galaxy clusters by selecting the RASS sources which featured a significant extent in the first standard processing of the RASS. The complete spectroscopic identification of these sources (as far as no identification was already available) leads to a compilation of a catalogue of 378 X-ray cluster sources.

A reanalysis of the X-ray properties of these sources shows that the X-ray source properties can successfully be used in the source identification process. In particular we found that in many cases the hardness ratio can be used to flag sources which are severely contaminated by an AGN. In this way we could also exclude previously identified X-ray clusters – as for example the two cases discussed in the previous section – from identification as cluster sources.

One of the major points of concern of such catalogs of X-ray clusters is the contamination of the observed X-ray luminosity by AGN. As commented in Section 4.1 there are all combinations of clusters and optically identified AGN or radio galaxies: AGN which do not provide a significant contribution to the cluster X-ray flux, AGN that contribute partially, and AGN which completely outshine the clusters. These cases can only definitely be distinguished if high resolution X-ray images or X-ray spectra of high quality are available. E.g. ROSAT HRI observations provide the means for this distinction, but they are only available for a small fraction of the sources for survey sizes of the present survey. Lack of additional X-ray data creates a twofold danger. Since X-ray sources are often identified with the most plausible nearby optical counterpart, there is a significant risk that the cluster ID will be discarded when an AGN is found near or within the error circle. Conversely, an AGN which is the primary X-ray emitter may not be recognized and the emission falsely associated to the cluster.

Also in the present case this problem of AGN cluster associations cannot be solved in each case and we still expect some hidden misclassifications which will be hard to find until the whole sample is probed more deeply in X-rays. However, we believe that the remaining uncertainties are small and not harmful for the application of our sample for cosmological statistical studies and we will substantiate this believe in the following. First of all we note that 74.4% of the sources in the catalog in Table 1 are sources recognized as significantly extended. This requires a major contribution to the X-ray emission from diffuse cluster sources. Thus for this source population we have a very high reliability that these sources are true X-ray clusters. We can now - as shown in Fig. 22 - compare the spectral properties of these extended cluster sources to those cluster sources where no significant extent could be established in terms of the parameter P_{ext}. We note that the two distributions are hardly different. Also both distributions are almost symmetric around unity, as would be ideally expected. For some reason the larger sample of extended sources shows a broader distribution of the ΔHR parameter. This seems to be caused by clusters with a larger number of photons for which a small systematic error in the HR estimate leads to a significant additional scatter in ΔHR in units of σ and also the low temperature groups will add to this scatter. A comparison to the non-cluster sources shows a very large difference in the spectral parameter distribution, however. While the non-cluster sources have a median deviation of the parameter ΔHR of -4.6σ the X-ray pointlike sources identified as clusters have a median $\Delta HR \sim -0.02\sigma$.

We can explore the contamination effect in somewhat more detail by considering the effect on a typical cluster source. The median number of source photons for the clusters listed in Table 1 is about 94 source photons. For such a source the typical uncertainty in the measured hardness ratio is about $\delta HR \sim 0.12$. An AGN with median properties easily shows a deviation of $3 - 4\sigma$ in the ΔHR parameter. Even if the contamination fraction by AGN is only 50% or 25% the typical shift in the parameter of $\Delta HR \sim 1.7\sigma$ and $\sim 0.9\sigma$ still constitutes a recognizable distortion of the ΔHR-distribution. Another test is shown in Fig. 22b. Here we compare the distribution of the ΔHR values for the clusters with the sample of point like clusters artificially contaminated by removing 20% of the cluster sources and replacing them by a statistical sample of non-cluster sources. There is a clearly visible change in the distribution of the spectral parameters. A KS test shows that the two distributions are still only distinguishable at the $\sim$ 90% level. A test with a similar contamination of 40%, however, leads to a clear difference with a KS probability for the two samples being statistically the same of $\sim 10^{-4}$. Since a 20% contamination of the point like clusters corresponds to a contamination of about 5% of the total sample we expect that the real misclassification fraction is not larger than this percentage.

The present X-ray cluster catalog provides a wealth of new data. 98 new cluster sources are listed in Table 1 and in addition new X-ray luminous groups associated with known giant ellipticals are reported in Table 1 and 8.

Test searches for additional X-ray clusters in the 9^h - 14^h region have shown that both, the selection of extended sources by the RASS standard analysis and the finding of X-ray clusters by selecting extended sources is quite incomplete in terms of the compilation of flux-limited X-ray cluster catalogues - except for very high flux limits. We have shown that probably most of the missing clusters can be recovered by using a better search algorithm for extended sources and by screening the optically known clusters. This may not be sufficient to produce a high quality, highly complete catalogue. Further screening of RASS sources, including CCD imaging of sources not visibly extended in X-rays, is required. The completion of the NORAS sample thus requires additional imaging and spectroscopic observations.

We like to thank first of all the ROSAT Team who helped in providing the RASS data fields, in discussions about the RASS source properties, and by providing the EXSAS software which was essential for the studies. We like to thank in particular J. Engelhauser, A. Vogler, C. Rosso, and C. Izzo for help with the data and programs. We would also like to thank the remote observers at FLWO, Perry Berlind and Jim Peters, for observations made on the 1.5-m telescope, and Susan Tokraz for help in the data reduction. This work has made use of the SIMBAD data base operated at CDS, Strasbourg. In addition this research

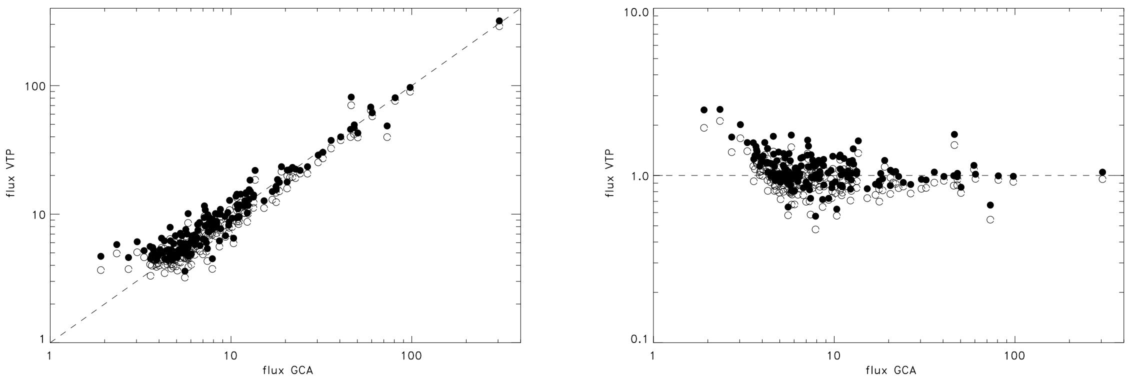

Fig. 21.— Comparison of the X-ray fluxes derived in the present analysis with the results of Ebeling et al. (1998) for the 164 sources which are common to both samples.

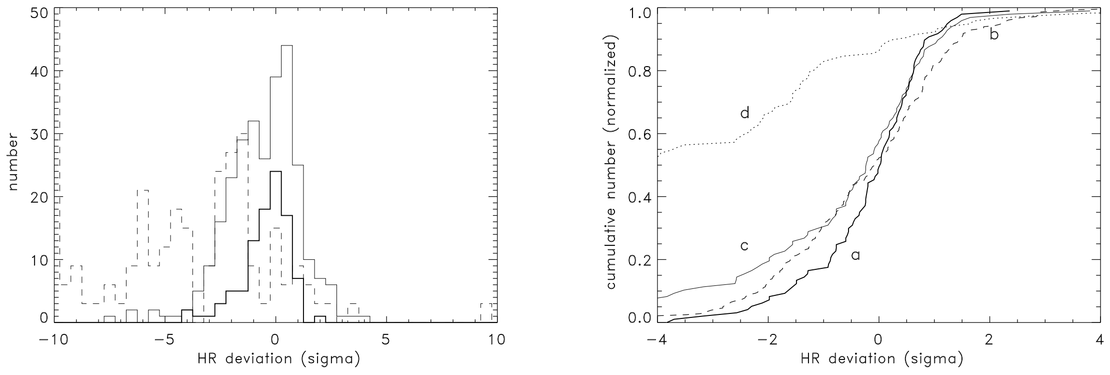

Fig. 22.— Distribution of the spectral parameter, ΔHR in units of sigma, for different subsamples of the present study. The parameter ΔHR is the difference of the measured from the estimated hardness ratio of the source for given interstellar absorption scaled by the $1sigma$-uncertainty of the hardness ratio determination. The right pannel shows histograms of the parameter ΔHR for pointlike cluster sources (thick line), extended cluster X-ray sources (thin line), and non-cluster sources (broken line). The right pannel shows normalized, cumulative histograms for (a) the pointlike cluster sources, (b) the extended cluster sources, (c) the sample of pointlike cluster sources artificially contaminated by 20% of non-cluster sources, and (d) the non-cluster sources. The samples (b) and (c) have an about 10% KS probability of being sampled from the same parent distribution as (a).

also made use of the NASA/IPAC Extragalactic Database (NED), which is operated by the Jet Propulsion Laboratory, California Institute of Technology, under contract with NASA. H.B. and P.S. acknowledge the support by the Verbundforschung under grant No. 50 OR 93065 and 50 OR 970835, respectively. JPH and JM were supported by the Smithonian Institution.

REFERENCES

Abell, G.O., 1958, ApJS, 3, 211

Abell, G.O., Corwin, H.G. & Olowin, R.P., 1989, ApJS, 70, 1

Allen, S.W., Edge, A.C., Fabian, A.C., Böhringer, H., Crawford, C.S., Ebeling, H., Johnstone, R.M., Taylor, T., & Schwarz, R.A., 1992, MNRAS, 259, 67

Anders, E. & Grevesse, N., 1989, Geochimica et Cosmochimica Acta, 53, 197

Andersen, V. & Owen, F. N. 1994, AJ, 108, 361

Appenzeller, I., Thiering, I., Zickgraf, F. -J., Krautter, J., Voges, W., Chavarria, C., Kneer, R., Mujica, R., Pakull, M., Rosso, C., Ruzicka, F., Serrano, A., & Ziegler, B., 1998, ApJS, 117, 319

Aschenbach, B., 1988, Appl. Optics, 27, 1404

Bade, N., Engels, D., Voges, W., Beckmann, V., Boller, Th., Cordis, L., Dahlem, M., Englhauser, J., Molthagen, K., Nass, P., Studt, J., & Reimers, D., 1998, A&AS, 127, 145

Bahcall, N.A. & Cen, R., 1992, ApJ, 407, L49

Barton, E., Geller, M., Ramella, M., Marzke, R. O., & Da Costa, L. N., 1996, AJ, 112,871

Batuski, D. J., Burns, J. O., Newberry, M. V., Hill, J. M., Deeg, H.-J., Laubscher, B. E., & Elston, R. J., 1991, AJ, 101, 1983

Beers, T. C., Kriessler, J. R., Bird, C. M. & Huchra, J. P. 1995, AJ, 109, 874

Böhringer, H., Voges, W., Ebeling, H., Schwarz, R.A., Edge, A.C., Briel, U.G., & Henry, J.P., 1991,in: *Observational Tests of Inflation* T. Shanks *et al.* (eds.), Kluwer Academ. Publ., p.293

Böhringer, H., Briel, U.G., Schwarz, R.A., Voges, W., Hartner, G., & Trümper, J., 1994, Nat, 368, 828

Böhringer, H., Guzzo, L., Collins, C.A., Neumann, D.M., Schindler, Schuecker, P., Cruddace, R.G., DeGrandi, S., Chincarini, G., Edge, A.C., MacGillivray, H.T., Shaver, P., Vettolani, G., & Voges, W., 1998, The Messenger, No. 94, 21 - 25

Bower, R.G., Böhringer, H., Briel, U.G., Ellis, R.S., Castander, & F.J., Couch, W.J., 1994, MNRAS, 268, 345

Bower, R.G., Hasinger, G., Castander, F.J., Aragon-Salamanca, A., Ellis, R.S., Gioia, I.M., Henry, J.P., Burg, R., Huchra, J.P., Böhringer, H., Briel, U.G., & McLean, B., 1996, MNRAS, 281, 59

Braine, J. & Dupraz, C., 1994, A&A, 283, 407

Brandt, W. N., Fabian, A. C., Nandra, K., Reynolds, C. S., & Brinkmann, W., 1994, MNRAS, 271, 958

Burke, D.J., Collins, C.A., Sharples, R.M., Romer, A.K., Holden, B.P., & Nichol, R.C., 1997, ApJ, 488, L83

Burns, J.O., Ledlow, M.J., Loken, C., Klypin, A., Voges, W., Bryan, G.L., Norman, M.L., White, R.A., ApJ, 467, L49

Caballo, R., Warwick, R.S., Barcons, X., Gonzales-Serrano, J.I., Barbar, C.R., Martinez-Gonzales, E., Perez-Serrano, I., & Burgos, J., 1995, MNRAS, 277, 1312

Cao, L., Wei, J. -Y. & Hu, J. -Y., 1999, A&AS, 135, 243

Capelato, H. V., Mazure, A., Proust, D., Vanderriest, C., Lemonnier, J. P., & Sodre, L., JR, 1991, A&AS, 90, 355

Castander, F.J., Bower, R.G., Ellis, R.S., Aragon-Salamanca, A., Mason, K.O., Hasinger, G., McMahon, R.G., Carrera, F.J., Mittaz, J.P., Perez-Fournon, I., & Letho, H.J., 1995, Nat, 377, 39

Cavaliere, A. & Fusco-Femiano, R., 1976, A&A, 49, 137

Chapman, G. N. F., Geller, M. J., & Huchra, J. P., 1988, AJ, 95, 999

Chincarini, G. & Rood, H. J., 1976, PASP, 88, 388

Collins, C.A., Guzzo, L., Nichol, R.C., & Lumsden, S.L., 1995, MNRAS, 274, 1071

Collins, C.A., Burke, D.J., Romer, A.K., Sharples, R.M., & Nichol, R.C., 1997, ApJ, 479, L117

Cooray, A. R., Grego, L., Holzapfel, W. L., Joy, M., & Carlstrom, J. E., 1998, AJ, 115, 1388

Crawford, C.S., Edge, A.C., Fabian, A.C., Allen, S.W., Böhringer, H., Ebeling, H., McMahon, R.G., & Voges, W., 1995, MNRAS, 274, 75

Cruddace, R., Hasinger, G., Trümper, J., Schmitt, J.H.M.M., & Hartner, G., 1991, Experimental Astronomy, 1, 365

Crawford, C.S., Allen, S.W., Ebeling, H., Edge, A. C., & Fabian, A.C. 1999, MNRAS, 306, 857

Couch, W.J., Ellis, R.S., Malin, D.F., & MacLaren, I., 1991, MNRAS, 249, 606

Dale, D. A., Giovanelli, R., Haynes, M. P., Scodeggio, M., Hardy, E., & Campusano, L. E., 1997, AJ, 114, 455

Dalton, G.B., Efstathiou, G., Maddox, S.J., & Sutherland, W.J., 1992, ApJ, 390, L1

Davidge, T. J. & Grinder, M., 1995, AJ, 109, 1433

Davoust, E. & Considere, S., 1995, A&AS, 110, 19

De Grandi, S., Molendi, S., Böhringer, H., & Voges, W., 1997, ApJ, 486, 738

De Grandi, S., Böhringer, H., Guzzo, L., Molendi, S., Chincarini, G., Collins, C.A., Cruddace, R.G., Neumann, D., Schindler, S., Schuecker, P., & Voges, W., 1999, ApJ, 514, 148

Dell'Antonio, I. P., Geller, M. J., & Fabricant, D. G., 1994, AJ, 107, 427

de Vaucouleurs, G., de Vaucouleurs, A., Corwin, H., Buta, R., Paturel, G., & Fouque, P., 1991, Third Reference Catalogue of Bright Galaxies

Dickey, J.M. & Lockman, F.J., 1990, ARAA, 28, 215

Dressler, A. & Shectman, S. A. 1988, AJ, 95, 284

Ebeling, H., Voges, W., Bohringer, H., Edge, A. C., Huchra, J. P., & Briel, U. G., 1996, MNRAS, 281, 799

Ebeling, H., Edge, A.C., Böhringer, H., Allen, S.W., Crawford, C.S., Fabian, A.C., Voges, W., & Huchra, J.P., 1998, MNRAS, 301, 881

Edge, A.C., Stewart, G.C., Fabian, A.C., & Arnaud, K.A., 1990, MNRAS, 245, 559

Eke, V.R., Cole, S., Frenk, C.S., & Henry, J.P., 1998, MNRAS, 298, 1145

Elvis, M., Plummer, D., Schachter, J., & Fabbiano, G., 1992, ApJS, 80, 257

Falco, E. E., Kochanek, C. S., & Munoz, J. A., 1998, ApJ, 494, 47

Fisher, D. , Fabricant, D. , Franx, M. & Van Dokkum, P. 1998, ApJ, 498, 195

Fetisova, T. S., Kuznetsov, D. Y., Lipovetskii, V. A., Starobinskii, A. A., & Olovin, R. P., 1993, AstL, 19, 198

Fisher, K. B., Huchra, J. P., Strauss, M. A., Davis, M., Yahil, A., & Schlegel, D., 1995, ApJS, 100, 69

Fouque, P., Durand, N., Bottinelli, L., Gouguenheim, L., & Paturel, G., 1992, Catalogue of Optical Radial Velocities, Observatoires de Lyon et Paris-Meudon, Vol. 1, 1

Frenk, C.S., White, S.D.M., Efstathiou, G., & Davis, M., 1990, ApJ, 351, 10

Gioia, I.M., Maccacaro, T., Schild, R.E., Stocke, J.T., Liebert, J.W., Danziger, I.J., Kunth, D., & Lub, J., 1984, ApJ, 283, 495

Gioia, I.M., Henry, J.P., Maccacaro, T., Morris, S.L., Stocke, J.T., & Wolter, A., 1990, ApJ, 356, L35

Gioia, I.M., Henry, J.P., Luppino, G.A., Clowe, D.I., Böhringer, H., Briel, U.G., Voges, W., Huchra, J.P., MacGillivray, H.T., 1995, A&A, 297, L75

Grogin, N.A., Geller, M.J, & Huchra, J.P., 1998, ApJS, 119, 277

Gubanov, A. G. & Reshetnikov, V. P., 1999, AstL, 25, 380

Gunn, J. E., Hoessel, J. G., & Oke, J. B., 1986, ApJ, 306, 30

Guzzo, L., Böhringer, H., Schuecker, P., Collins, C.A., Schindler, S., Neumann, D.M., DeGrandi, S., Cruddace, R.G., Chincarini, G., Edge, A.C., Shaver, P., & Voges, W., 1999, The Messenger, No. 95, 27

Henry, J.P., Gioia, I.M., Maccacaro, T., Morris, S.L., Stocke, J.T., & Wolter, A., 1992, ApJ, 386, 408

Henry, J. P., Gioia, I. M., Huchra, J. P., Burg, R., McLean, B., Böhringer, H., Bower, R. G., Briel, U. G., Voges, W., MacGillivray, H., & Cruddace, R. G., 1995, ApJ, 449, 422

Henry, J.P., Gioia, I.M., Mullis, C.R., Clowe, D.I., Luppino, G.A., Böhringer, H., Briel, U.G., Voges, W., Huchra, J.P., 1997, AJ, 114, 1293

Henstock, D. R., Browne, I. W. A., Wilkinson, P. N., & McMahon, R. G., 1997, MNRAS, 290, 380

Hewitt, A. & Burbidge, G., 1991, ApJS, 75, 297

Hill, J. M. & Oegerle, W.R., 1993, AJ, 106, 83

Hickson, P., Mendes de Olivera, C., Huchra, J.P., & Palumbo, G.G., 1992, ApJ, 399, 353

Hopp, U., Kuhn, B., Thiele, U., Birkle, K., Elsasser, H., & Kovachev, B., 1995, A&AS, 109, 537

Huchra, J. P., Geller, M. J., Henry, J. P., & Postman, M., 1990, ApJ, 365, 66

Huchra, J. P., Geller, M. J. & Corwin, H. G. , Jr. 1995, ApJS, 99, 391

Huchra, J. P., Vogeley, M. S., & Geller, M. J., 1999, ApJS, 121, 287

Huchtmeier, W. K., Sage, L. J. & Henkel, C. 1995, A&A, 300, 675

Jones, C. & Forman, W., 1984, ApJ, 276, 38

Jones, L.R., Scharf, C., Ebeling, H., Perlman, E., Wegner, G., Malkan, M., & Horner, D., 1998, ApJ, 495, 100

Kaiser, N., 1986, MNRAS, 222, 323

Katgert, P., Mazure, A., Prera, J., Den Hartog, R., Moles, M., Le Fevre, O., Dubath, P., Focardi, P., Rhee, G., Jones, B., Escalera, E., Biviano, A., Gerbal, D., & Giuricin, G., 1996, A&A, 310, 8

Katgert, P., Mazure, A., Den Hartog, R., Adami, C., Biviano, A., & Perea, J., 1998, A&AS, 129, 399

Klemola, A.R., Jones, B.F., & Hanson, R.B., 1987, AJ, 94, 501

Kowalski, M., Cruddace, R.G., Wood, K.S., & Ulmer, M.P., 1984, ApJS, 56, 403

Lacy, M., Hill, G. J., Kaiser, M. E., & Rawlings, S., 1993, MNRAS, 263, 707

Lahav, O., Edge, A.C., Fabian, A.C., Putney, A., 1989, MNRAS, 238, 88

Ledlow, M. J. & Owen, F. N., 1995, AJ, 109, 853

Ledlow, M. J., Loken, C., Burns, J. O., Hill, J. M., & White, R. A., 1996, AJ, 112, 388

Ledlow, M. J., Loken, C., Burns, J. O., Owen, F.N., Voges, W., 1999, ApJ, 516, L53

Lin, W. & Daly, R.A., 1996, ApJ, 467, 145

Lozinskaya, T. A., Silchenko, O. K., Helfand, D. J., & Goss, W. M., 1998, AJ, 116, 2328

Lumbsden, S.L., Nichol, R.C., Collins, C.A., & Guzzo, L., 1992, MNRAS, 258, 1

Mahtessian, A.P., 1998, Astrofizika, 41, 308

Markevitch, M, 1998, ApJ, 504, 27

Marzke, R. O., Huchra, J. P., & Geller, M. J., 1996, AJ, 112, 1803

Maurogordato, S., Proust, D., Cappi, A., Slezak, E., & Martin, J.M., 1997, A&AS, 123, 411

Mazure, A., Katgert, P., den Hartog, R., Biviano, A., Dubath, P., Escalera, E., Focardi, P., Gerbal, D., Giuricin, G., Jones, B., Le Fevre, O., Moles, M., Perea, J., & Rhee, G., 1996, A&A , 310, 31

Merrifield, M.R. & Kent, S.M., 1991, AJ, 101, 783

Michel, A. & Huchra, J., 1988, PASP, 100, 1423

Moran, E. C., Helfand, D. J., Becker, R. H., & White, R. L., 1996, ApJ, 461, 127

Morrison, R & McCammon, D., 1983, ApJ, 270, 119

Nass, P., Ph. D. Thesis, Universität Hamburg, 1998

Olsen, L. F., Scodeggio, M., Da Costa, L., Benoist, C., Bertin, E., Deul, E., Erben, T., Guarnieri, M. D., Hook, R., Nonino, M., Prandoni, I., Slijkhuis, R., Wicenec, A., & Wichmann, R., 1999, A&A, 345, 681

Owen, F. N., Ledlow, M. J., & Keel, W. C., 1995, AJ, 109, 14

Owen, F. N. & Ledlow, M. J., 1997, ApJS, 108, 41

Pfeffermann, E., Briel, U.G., Hippmann, H., Kettenring, G., Metzner, G., Predehl, P., Reger, G., Stephan, K.H., Zombeck, M.V., Chappell, J., & Murray, S.S., 1986, Proc. SPIE, 733, 519

Piccinotti, G., Mushotzky, R.F, Boldt, E.A., Holt, S.S., Marshall, F.E., Sermelitsos, P.J., & Shafer, R.A., 1982, ApJ, 253, 485

Pierre, M., Böhringer, H., Ebeling, H., Voges, W., Schuecker, P., Cruddace, R.G., & MacGillivray, H.T., 1994, A&A, 290, 725

Pietsch, W., Bischoff, K., Boller, TH., Doebereiner, S., Kollatschny, W., & Zimmermann, H.-U., 1998, A&A, 333, 48

Postman, M., Huchra, J. P., & Geller, M. J., 1992, ApJ, 384, 404

Postman, M., Lubin, L.M., Gunn, J.E., Oke, J.B., Hoessel, J.G., Schneider, D.P., & Christensen, J.A., 1996, AJ, 111, 615

Quintana, H. & Ramirez, A., 1995, ApJS 96, 343

Ramella, M., Geller, M.J., Huchra, J.P., & Thorstensen, J.R., 1995, AJ, 109, 1458

Raymond, J.C. & Smith, B.W., 1977, ApJS, 35, 419

Reiprich T.H. & Böhringer, H., 1999, in *Heating and Acceleration in the Universe*, H. Inoue, T. Ohashi, T. Takahashi (eds.), Astron. Nachr., 320, 296

Romer, A.K., Collins, C.A., Böhringer, H., Cruddace, R.G., Ebeling, H., MacGillivray, H.T., & Voges, W., 1994, Nat, 372, 75

Romer, A.K., Nichol, R.C., Holden, B.P., Ulmer, M.P., Pildis, R.A., Merrelli, A.J., Adami, C., Burke, D.J., Collins, C.A., Metevier, A.J., Kron, R.G., & Commons, 1999, preprint (astro-ph/9907401)

Rosati, P., Della Ceca, Norman, Burg, R., C., & Giacconi, R., 1995, ApJ, 445, L11

Rosati, P., Della Ceca, Norman, C., & Giacconi, R., 1998, ApJ, 492, L21

Sakai, S., Giovanelli, R, & Wegner, G., 1994, AJ, 108, 33

Schade, D. , Barrientos, L. F. & Lopez-Cruz, O. 1997, ApJ, 477, L17

Scharf, C.A., Jones, L.R., Ebeling, H., Perlman, E., Malkan, M., & Wegner, G., 1997, ApJ, 477, 79

Schmidt, M., Schneider, D. P., & Gunn, J. E., 1986, ApJ, 306, 411

Scoddegio, M., Olsen, L. F., Da Costa, L., Slijkhuis, R., Benoist, C., Deul, E., Erben, T., Hook, R., Nonino, M., Wicenec, A., Zaggia, S., 1999, A&AS, 137, 83

Shectman, S.A., 1985, ApJS, 57, 77

Slinglend, K., Batuski, D., Miller, C., Haase, S., Michaud, K., & Hill, J. M, 1998, ApJS, 115, 1

Smith, R. J., Lucey, J. R., Steel, J., & Hudson, M. J., 1997, MNRAS, 291, 461

Spinrad, H., Marr, J., Aguilar, L., & Djorgovski, S., 1985, PASP, 97, 932

Stocke, J.T., Morris, S.L., Gioia, I.M., Maccacaro, T., Schild, R., Wolter, A., Fleming, T.A., & Henry, J.P., 1991, ApJS, 76, 813

Stark, A.A., Gammie, C.F., Wilson, R.W., Bally, J., Linke, R.A., Heiles, C., Hurwitz, M., 1992, ApJS, 79, 77

Stoll, D., Tiersch, H., & Cordis, L., 1997, Astron. Nachr., 318, 149

Struble, M.F.& Rood, H.J., 1987 ApJS, 63, 543

Struble, M.F.& Rood, H.J., 1991a, ApJS, 77, 363

Struble, M.F.& Rood, H.J., 1991b, ApJ, 374, 359

Struble, M.F.& Rood, H.J., 1999, ApJS, 125, 35

Thomas, P.A. Colberg, J.M., Couchman, H.M.P., Efstathiou, G.P., Frenk, C.S., Jenkins, A.R., Nelson, A.H., Hutchings, R.M., Peacock, J.A., Pearce, F.R., & White, S.D.M., 1998, MNRAS, 296, 119

Tomita, A., Nakamura, F. E., Takata, T., Nakanishi, K., Takeuchi, T., Ohta, K., & Yamada, T., 1996, AJ, 111, 42

Trasarti-Battistoni, R., 1998, A&AS, 130, 341

Trümper, J., 1992, Royal Astron. Soc. Quart. J., 33, 165

Trümper, J., 1993, Science, 260, 1769

Tucker, W.H., Tananbaum, H., & Remillard, R.A., 1995, ApJ, 444, 532

Ulrich, M.-H., 1976, ApJ, 206, 364

Veron-Cetty, M.P. & Veron, P., 1998, ESO Scientific Report 18

Vikhlinin, A., McNamara, B.R., Forman, W., Jones, C., Quintana, H., & Hornstrup, A., 1998, ApJ, 502, 558

Voges, W., et al., 1992, Proc. of Satellite Syposium 3, ESA International Space Year 3, p. 9 & p. 223

Voges, W., Boller, T., Dennerl, K., Engelhauser, J., Gruber, R., Haberl, F., Paul, J., Pietsch, W., Trümper, J., & Zimmermann, H.U., 1996, Proc. of the Conference *Röntgenstrahlung from the Universe*, H.U. Zimmermann, J.E. & Trümper, H. Yorke (eds.), MPE Report No. 263, 637

Voges, W., Aschenbach, B., Boller, T., Bräuninger, H., Briel, U., Burkert, W., Dennerl, K., Englhauser, K., Gruber, R., Haberl, F., Hasinger, G., Kürster, M., Pfeffermann, E., Pietsch, W., Predehl, P., Rosso, C., Schmitt, J.H.M.M., Trümper, J., & Zimmermann, H.U., 1999, A&A, 349, 389

Wegner, G., Colless, M., Baggley, G., Davies, R. L., Bertschinger, E., Burstein, D., McMahan, R. K., Jr., & Saglia, R. P., 1996, ApJS, 106, 1

Zabludoff, A. I., Geller, M. J., Huchra, J. P., & Vogeley, M. S., 1993, AJ, 106, 1273

Zimmermann, H.U., Becker, W., Belloni, T., Döbereiner, S., Izzo, C., Kahabka, P., & Schwentker, O., 1994, *EXSAS User's Guide*, MPE Report No. 257

Zwicky, F., Herzog, E., Wild, P., Karpowicz, M., & Kowal, C.T., 1961 - 1968, *Catalogue of Galaxies and Clusters of Galaxies*, Vol. 1 - 6

This manuscript was prepared with the AAS LaTeX macros v3.0.

APPENDIX

NORAS Cluster Survey Tables

Table 1
The NORAS cluster X-ray source catalogue

name	alt.name	RA	DEC	z	ctr	F_x	F_x^*	err	L_x	N_H	ID	ref
RXCJ0000.1+0816	UGC12890	0.0295	8.2744	0.0396	0.26	5.80	5.39	12.4	0.37	5.9		1,3
RXCJ0001.9+1204	A2692	0.4877	12.0730	0.2033	0.08	1.82	1.81	17.9	3.24	5.1		1
RXCJ0004.9+1142	UGC00032	1.2473	11.7006	0.0761	0.17	3.78	3.68	12.7	0.93	5.3		2,4
RXCJ0005.3+1612	A2703	1.3440	16.2105	0.1164	0.24	4.96	4.94	11.8	2.88	3.7	B	2,5
RXCJ0006.3+1052	a)	1.5906	10.8677	0.1698	0.15	3.28	3.28	19.3	4.05	5.6		1
RXCJ0011.7+3225	A0007	2.9350	32.4170	0.1073	0.44	9.60	9.60	9.1	4.75	5.5		2,6,3
RXCJ0016.7+0646	A0016	4.1895	6.7736	0.0833	0.09	2.00	1.95	20.2	0.59	4.1		1,6
RXCJ0019.6+2517	-	4.9128	25.2908	0.1353	0.16	3.29	3.28	21.6	2.60	3.6		1
RXCJ0020.1+0005	-	5.0444	0.0917	0.2124	0.03	0.55	0.53	35.1	1.08	2.8		1
RXCJ0020.6+2840	A0021	5.1705	28.6751	0.0940	0.33	7.10	7.08	11.6	2.68	4.5		2,6,7
RXCJ0021.5+2803	IV Zw015	5.3997	28.0513	0.0948	0.22	4.68	4.64	20.9	1.80	4.2		1
RXCJ0024.5+3312	-	6.1327	33.2087	0.2260	0.11	2.33	2.33	18.4	5.10	5.3		1
RXCJ0027.8+2616	-	6.9573	26.2738	0.3668	0.11	2.30	2.31	20.1	12.93	3.9		1
RXCJ0039.6+2114	A0075	9.9000	21.2390	0.0619	0.11	2.34	2.17	40.8	0.36	3.4	b	2,6
RXCJ0040.4+2933	A0077	10.1140	29.5593	0.0712	0.38	8.26	8.19	9.8	1.80	5.3		2,5
RXCJ0041.7+2124	A0084	10.4462	21.4140	0.1014	0.20	4.13	4.09	16.7	1.82	3.4		2,6
RXCJ0058.9+2657	b)	14.7258	26.9507	0.0451	0.23	5.05	4.92	12.9	0.43	5.7		1,41
RXCJ0105.0+0201	IC1613	16.2595	2.0301	0.1967	0.13	2.64	2.64	15.4	4.38	2.8		2,39
RXCJ0106.8+0103	-	16.7094	1.0546	0.2537	0.15	3.16	3.18	13.6	8.65	3.2	C	1
RXCJ0108.2+0210	A0147	17.0533	2.1800	0.0447	0.23	4.62	4.29	16.0	0.37	3.0		2,6
RXCJ0110.0+1358	A0152	17.5229	13.9804	0.0581	0.06	1.26	0.95	29.5	0.14	3.9		2,27
RXCJ0110.9+3308	NGC0410	17.7419	33.1494	0.0177	0.17	3.73	2.68	24.1	0.04	5.9		2,43
RXCJ0112.2+3302	a)	18.0721	33.0384	0.1249	0.07	1.61	1.57	18.0	1.08	5.9		1
RXCJ0113.0+1531	A0160	18.2741	15.5170	0.0442	0.22	4.67	4.34	14.1	0.37	4.4		2,6
RXCJ0114.9+0024	A0168	18.7397	0.4056	0.0448	0.53	10.93	10.63	10.0	0.92	3.3	cL	2,30,37
RXCJ0121.9+0021	A0181	20.4929	0.3575	0.1756	0.07	1.38	1.37	31.1	1.85	3.3		1,9
RXCJ0123.1+3327	c)	20.7970	33.4620	0.0153	0.28	6.10	4.36	11.7	0.04	5.3	B	35,2
RXCJ0124.5+0145	N0533	21.3744	1.7629	0.0183	0.33	6.74	4.71	15.0	0.06	3.1		2,10
RXCJ0142.0+2130	-	25.5128	21.5109	0.0698	0.14	3.32	3.23	14.5	0.69	7.3		1
RXCJ0152.7+0100	A0267	28.1817	1.0160	0.2270	0.21	4.28	4.30	12.7	9.37	2.8		1,32,29
RXCJ0152.7+3609	A0262	28.1948	36.1513	0.0163	3.34	73.07	71.13	4.0	0.81	5.5	L	2,6,43
RXCJ0152.9+3732	A0263	28.2451	37.5354	0.2993	0.09	2.03	2.03	20.4	7.71	5.4		1
RXCJ0155.1+3355	A0272	28.7897	33.9222	0.0872	0.26	5.79	5.75	14.8	1.90	5.7	B	2,6
RXCJ0200.2+3126	NGC0777	30.0687	31.4365	0.0168	0.22	4.69	3.36	14.0	0.04	5.5		2,17
RXCJ0209.5+1946	A0311	32.3796	19.7695	0.0657	0.23	5.47	5.34	17.9	1.00	8.9		2,18
RXCJ0228.1+2811	a)	37.0401	28.1943	0.0353	0.26	6.03	5.62	13.8	0.30	7.9		2,41
RXCJ0246.0+3653	A0376	41.5108	36.8879	0.0488	0.59	13.30	13.20	6.6	1.36	6.8		2,6,13
RXCJ0255.8+0918	IC1867	43.9639	9.3134	0.0258	0.12	2.93	2.26	20.7	0.07	11.8	?	2,36
RXCJ0257.8+1302	A0399	44.4574	13.0492	0.0722	1.23	30.36	30.41	5.4	6.78	10.6		2,6
RXCJ0258.9+1334	A0401	44.7396	13.5795	0.0739	2.05	50.29	50.45	6.5	11.76	10.2	L	2,6
RXCJ0301.6+0155	Zw0258.9+0142	45.4083	1.9205	0.1695	0.22	4.96	4.97	15.8	6.07	7.7		1,29
RXCJ0311.5+0714	-	47.8992	7.2380	0.1420	0.06	1.69	1.68	20.9	1.47	14.0	?	1
RXCJ0313.3+2624	-	48.3437	26.4068	0.1649	0.07	1.74	1.73	20.6	2.04	11.9		1
RXCJ0338.6+0958	2A0335	54.6699	9.9745	0.0347	2.72	80.91	80.91	3.1	4.21	18.6		2,22
RXCJ0341.2+1524	-	55.3206	15.4074	0.0311	0.62	17.78	17.42	7.5	0.73	16.7		2,29
RXCJ0352.9+1941	d)	58.2492	19.6895	0.1085	0.29	7.83	7.83	10.7	3.96	13.9		1,29
RXCJ0404.6+1109	a)	61.1558	11.1658	0.3548	0.07	1.90	1.91	22.50	10.1	14.0		1
RXCJ0413.4+1028	A0478	63.3565	10.4669	0.0882	1.47	40.45	40.51	5.1	13.31	15.3		2,6
RXCJ0419.6+0224	N1550	64.9067	2.4144	0.0123	1.81	45.84	42.78	8.0	0.28	11.6	L	2,41
RXCJ0439.0+0520	d)	69.7598	5.3439	0.2080	0.19	4.59	4.61	12.9	8.47	9.8		1,29
RXCJ0439.0+0715	e)	69.7528	7.2625	0.2450	0.18	4.51	4.52	13.2	11.38	10.6		1,38
RXCJ0448.0+1037	-	72.0016	10.6183	0.0940	0.08	2.22	2.17	26.9	0.84	14.4		1
RXCJ0448.2+0952	a)	72.0619	9.8736	0.0000	0.13	3.60	3.60	14.9	0.00	14.1		1
RXCJ0454.1+0255	A0520	73.5458	2.9180	0.2030	0.36	8.33	8.37	10.6	14.52	7.8		2,5
RXCJ0459.1+0846	A0523	74.7757	8.7804	0.1034	0.14	3.59	3.57	16.4	1.65	11.8		1,3
RXCJ0503.1+0607	d)	75.7802	6.1272	0.0880	0.22	5.35	5.31	13.6	1.77	9.4		1,29
RXCJ0506.9+0257	-	76.7253	2.9523	0.1475	0.07	1.56	1.55	22.8	1.47	8.6		1
RXCJ0618.5+6724	A0554	94.6500	67.4070	0.1127	0.12	2.85	2.83	17.7	1.55	7.5		1
RXCJ0704.4+6318	A0566	106.1022	63.3161	0.0980	0.33	7.13	7.11	11.7	2.94	5.1		2,6
RXCJ0708.1+7151	A0565	107.0316	71.8570	0.1053	0.14	2.93	2.90	16.0	1.40	4.7		2,18,40
RXCJ0716.7+5324	Zw0712.9+5834	109.1776	53.4078	0.0644	0.19	4.30	4.18	28.7	0.75	6.9		2
RXCJ0721.3+5547	A0576	110.3426	55.7864	0.0381	1.03	22.72	22.54	7.0	1.41	5.7		2,6
RXCJ0724.9+6658	A0578	111.2298	66.9785	0.0863	0.13	2.78	2.70	16.3	0.88	4.4		2,34
RXCJ0726.0+4122	A0580	111.5022	41.3821	0.1120	0.18	3.98	3.95	15.8	2.15	6.8		1
RXCJ0728.9+2935	-	112.2379	29.5863	0.3976	0.04	0.95	0.95	25.7	6.36	6.0	?	1
RXCJ0729.7+7915	A0575	112.4419	79.2537	0.1058	0.09	1.95	1.89	16.8	0.93	3.8		1
RXCJ0732.3+3137	A0586	113.0916	31.6296	0.1710	0.37	7.91	7.94	9.1	9.84	4.9		2,6,3
RXCJ0736.4+3925	-	114.1059	39.4332	0.1177	0.34	7.59	7.59	8.8	4.49	6.4	C	1
RXCJ0737.6+5920	-	114.4223	59.3404	0.0384	0.09	1.93	1.47	29.1	0.09	4.9		2
RXCJ0740.9+5525	UGC03957	115.2476	55.4320	0.0340	0.85	18.09	17.60	7.5	0.88	4.6		2,11
RXCJ0741.5+2557	-	115.3757	25.9628	0.1577	0.05	0.96	0.94	24.5	1.04	4.8		1

TABLE 1—*Continued*

name	alt.name	RA	DEC	z	ctr	F_x	F_x^*	err	L_x	N_H	ID	ref
RXCJ0741.7+7414	Zw0735.7+7421	115.4367	74.2478	0.2149	0.19	4.06	4.08	11.4	7.94	4.1		1,5
RXCJ0746.6+3100	-	116.6554	31.0136	0.0579	0.10	2.27	2.11	21.0	0.31	5.1		1
RXCJ0748.1+1832	-	117.0394	18.5465	0.0400	0.18	3.72	2.82	21.0	0.20	4.1		1
RXCJ0751.3+5012	UGC04052	117.8437	50.2125	0.0228	0.38	8.20	6.22	29.6	0.14	5.1		1,41
RXCJ0756.9+3839	-	119.2316	38.6501	0.2203	0.07	1.51	1.51	35.1	3.17	5.1		1
RXCJ0758.3+2640	-	119.5888	26.6792	0.2315	0.05	1.05	1.04	24.3	2.43	3.9		1
RXCJ0759.7+5400	Zw0755.8+5408	119.9284	54.0016	0.1032	0.21	4.39	4.35	17.3	2.01	3.8		1,41
RXCJ0800.9+3602	A0611	120.2455	36.0471	0.2880	0.12	2.47	2.48	18.5	8.63	4.9		1,38,29
RXCJ0804.3+4646	A0616	121.0915	46.7823	0.1868	0.08	1.66	1.65	36.7	2.51	4.5		1
RXCJ0805.7+4541	A0620	121.4304	45.6903	0.1353	0.09	1.93	1.91	20.9	1.53	4.8		1
RXCJ0811.0+1644	A0635	122.7599	16.7349	0.0925	0.09	1.81	1.76	28.5	0.66	3.7		1
RXCJ0811.1+7002	A0621	122.7833	70.0395	0.2230	0.20	4.25	4.27	15.3	8.97	3.7		1,29
RXCJ0821.0+0751	d)	125.2574	7.8660	0.1100	0.18	3.56	3.53	15.5	1.86	1.8		1,29
RXCJ0822.1+4705	A0646	125.5404	47.0999	0.1303	0.34	7.19	7.19	9.1	5.25	3.8		2,6
RXCJ0825.5+4707	A0655	126.3761	47.1299	0.1267	0.35	7.45	7.45	10.9	5.13	4.3		2,6
RXCJ0825.7+8218	A0625	126.4360	82.3100	0.2000	0.12	2.45	2.45	27.6	4.20	2.9		1
RXCJ0828.6+3025	A0671	127.1621	30.4280	0.0503	0.35	7.28	7.08	9.6	0.78	3.9		2,6
RXCJ0830.9+6551	A0665	127.7428	65.8503	0.1818	0.53	11.18	11.23	7.5	15.69	4.3		2,6
RXCJ0840.5+0543	-	130.1302	5.7332	0.2651	0.08	1.67	1.67	22.8	5.03	3.8		1
RXCJ0842.9+3621	A0697	130.7362	36.3625	0.2820	0.28	5.74	5.77	15.6	19.15	3.5		1,41
RXCJ0844.9+4258	-	131.2361	42.9817	0.0541	0.08	1.63	1.23	18.6	0.16	2.8		2
RXCJ0847.7+7741	A0686	131.9414	77.6920	0.2600	0.11	2.13	2.14	20.0	6.17	2.0		1
RXCJ0850.2+3603	-	132.5501	36.0601	0.3780	0.15	3.03	3.05	19.3	17.94	3.0		1,38
RXCJ0856.1+3756	-	134.0356	37.9479	0.4107	0.11	2.24	2.26	38.7	15.76	2.9		1
RXCJ0909.1+1059	A0750	137.2832	10.9925	0.1751	0.32	6.54	6.57	10.4	8.54	3.2		2,6
RXCJ0917.8+5143	A0773	139.4624	51.7248	0.2172	0.31	6.08	6.11	9.0	12.11	1.3		1,19,29
RXCJ0920.0+0102	MKW1s	140.0020	1.0401	0.0175	0.06	1.21	0.85	23.7	0.01	3.2		2,23
RXCJ0920.4+3030	A0781	140.1087	30.5150	0.2952	0.10	1.91	1.91	25.2	7.06	1.9		1,41
RXCJ0921.1+4538	3C219	140.2857	45.6437	0.1745	0.09	1.67	1.65	21.6	2.20	1.5	?	2,16
RXCJ0924.0+1410	A0795	141.0238	14.1684	0.1357	0.36	7.47	7.49	9.6	5.91	3.5		2,6
RXCJ0928.6+3747	A0800	142.1573	37.7986	0.2472	0.09	1.76	1.76	29.0	4.61	1.4		1
RXCJ0938.2+7553	A0814	144.5666	75.8872	0.1503	0.06	1.20	1.19	40.3	1.17	2.1		2
RXCJ0942.2+1522	A0853	145.5605	15.3865	0.1664	0.15	3.12	3.12	14.0	3.69	3.4	o	1
RXCJ0943.1+4659	A0851	145.7795	46.9975	0.4069	0.05	1.03	1.04	32.1	7.27	1.3		1,8
RXCJ0944.0+6424	A0845	146.0074	64.4117	0.1200	0.11	2.38	2.36	16.8	1.47	4.8		1
RXCJ0949.8+1707	-	147.4698	17.1298	0.3826	0.18	3.61	3.63	13.2	21.95	3.1		1
RXCJ0958.1+2346	-	149.5430	23.7820	0.1471	0.11	2.18	2.16	26.2	2.04	2.9		1
RXCJ1000.5+4409	d)	150.1272	44.1543	0.1540	0.14	2.78	2.77	12.7	2.84	1.1		1,29
RXCJ1002.6+3241	Zw0959.6+3257	150.6609	32.6995	0.0499	0.26	5.16	5.01	11.1	0.54	1.6	B	1,41
RXCJ1003.0+3254	-	150.7672	32.9079	0.4161	0.06	1.14	1.15	22.4	8.29	1.6		1
RXCJ1006.6+2554	A0923	151.6647	25.9101	0.1162	0.17	3.48	3.45	14.0	2.01	2.8		2,6
RXCJ1009.3+7110	A0914	152.3348	71.1751	0.1927	0.15	3.15	3.15	20.4	5.00	4.0	C	1,12
RXCJ1016.6+2448	A0964	154.1503	24.8082	0.0811	0.14	2.79	2.71	18.3	0.78	2.3		1
RXCJ1017.5+5934	A0959	154.3981	59.5667	0.3530	0.22	4.16	4.19	54.9	21.56	0.9		2,12
RXCJ1019.9+4059	A0971	154.9992	40.9873	0.0922	0.16	3.11	3.02	16.4	1.12	1.1		1,27,40
RXCJ1022.0+3830	a)	155.5196	38.5120	0.0491	0.19	3.63	3.37	28.3	0.35	1.5		1
RXCJ1023.3+5948	A0983	155.8291	59.8085	0.2055	0.06	1.25	1.24	19.0	2.28	0.7		2,12
RXCJ1023.6+0411	Zw1021.0+0426	155.9117	4.1865	0.2850	0.43	8.77	8.82	8.2	29.91	2.9		2,20
RXCJ1023.6+4907	A0990	155.9220	49.1329	0.1440	0.40	7.77	7.80	8.2	6.88	1.0		2,32,29
RXCJ1025.9+1241	b)	156.4829	12.6852	0.1434	0.27	5.53	5.53	9.4	4.86	3.5	o	1,20
RXCJ1031.7+3502	A1033	157.9317	35.0495	0.1259	0.40	7.86	7.86	11.1	5.34	1.9		2,20
RXCJ1034.9+3041	A1045	158.7469	30.6944	0.1407	0.20	4.00	3.99	10.9	3.39	1.8		2,20
RXCJ1040.7+3956	A1068	160.1829	39.9481	0.1372	0.39	7.60	7.62	8.3	6.16	1.3		1,20
RXCJ1109.3+4133	A1173	167.3282	41.5624	0.0763	0.22	4.30	4.18	11.6	1.06	1.6		1,40
RXCJ1109.7+2145	A1177	167.4294	21.7620	0.0319	0.25	4.97	3.74	14.3	0.17	1.5		1,6,15
RXCJ1111.6+4050	A1190	167.9104	40.8424	0.0794	0.38	7.40	7.33	10.3	2.01	1.7		2,6,40
RXCJ1113.3+1735	A1204	168.3324	17.5937	0.1706	0.28	5.42	5.44	10.8	6.73	1.4		2,20
RXCJ1114.3+5823	Zw1111.0+5843	168.5993	58.3898	0.2065	0.17	3.24	3.25	10.7	5.92	0.7		1,29
RXCJ1115.5+5426	-	168.8865	54.4350	0.0691	0.18	3.49	3.39	13.8	0.70	0.9		1
RXCJ1121.7+0249	SHK352 f)	170.4280	2.8184	0.0468	0.27	5.76	5.60	11.8	0.53	4.4		1,31
RXCJ1122.2+6712	-	170.5604	67.2129	0.0560	0.06	1.25	0.93	20.3	0.13	1.2		1
RXCJ1123.2+1935	A1235	170.8049	19.5996	0.1042	0.19	3.75	3.71	13.2	1.75	1.7		2,6
RXCJ1123.9+2129	A1246	170.9912	21.4903	0.1904	0.22	4.23	4.24	14.9	6.52	1.4		20,2
RXCJ1131.3+3334	A1290	172.8433	33.5818	0.2212	0.10	2.10	2.10	22.3	4.39	2.1		2
RXCJ1132.3+5558	A1291	173.0817	55.9789	0.0527	0.22	4.33	4.21	12.3	0.51	1.0		2,26,14
RXCJ1143.5+4623	A1361	175.8762	46.3845	0.1167	0.43	8.63	8.63	34.9	5.02	2.2		2,20
RXCJ1149.5+2223	-	177.3898	22.3960	0.1761	0.06	1.28	1.27	20.6	1.73	2.3		1
RXCJ1155.3+2324	A1413	178.8270	23.4075	0.1427	0.64	12.61	12.69	6.4	10.91	1.6		2,6
RXCJ1156.9+2415	d)	179.2409	24.2581	0.1392	0.15	2.91	2.90	12.9	2.42	1.8		1,20
RXCJ1157.3+3336	-	179.3259	33.6121	0.2138	0.20	3.72	3.73	19.2	7.23	0.0		1,29
RXCJ1200.0+1122	-	180.0105	11.4041	0.2070	0.03	0.55	0.54	47.6	1.03	1.8	b	1

Table 1—*Continued*

name	alt.name	RA	DEC	z	ctr	F_x	F_x^*	err	L_x	N_H	ID	ref
RXCJ1200.4+0320	A1437	180.1057	3.3336	0.1339	0.44	8.73	8.75	8.6	6.72	1.9		2,6
RXCJ1201.3+2306	A1443	180.3257	23.1092	0.2690	0.13	2.61	2.63	14.8	7.99	2.4		1
RXCJ1201.9+5802	A1446	180.4997	58.0475	0.1031	0.15	2.97	2.94	19.3	1.35	1.5		2,12
RXCJ1203.0+2836	A1449	180.7615	28.6039	0.1341	0.12	2.39	2.37	15.7	1.86	1.7	B	1,45
RXCJ1204.0+2807	A1455	181.0133	28.1233	0.1631	0.07	1.42	1.41	19.3	1.63	1.7		1,5
RXCJ1204.4+0154	MKW4	181.1065	1.9010	0.0195	0.93	18.52	17.19	6.0	0.28	1.9		2,46,20
RXCJ1204.9+2237	A1466	181.2403	22.6167	0.2519	0.03	0.68	0.67	31.8	1.88	2.1		1
RXCJ1205.2+3920	d)	181.3021	39.3493	0.0381	0.52	10.33	10.04	7.4	0.63	2.1		1,41
RXCJ1206.9+7139	A1470	181.7431	71.6576	0.1912	0.09	1.67	1.67	14.2	2.63	1.6		2,12
RXCJ1210.0+0630	-	182.5231	6.5000	0.0000	0.07	1.43	1.43	21.9	0.00	1.5	bB	1
RXCJ1210.3+0523	a)	182.5783	5.3850	0.0748	0.30	5.81	5.76	10.4	1.40	1.4		1,41
RXCJ1217.6+0339	Zw1215.1+0400	184.4192	3.6624	0.0766	1.04	20.48	20.48	5.4	5.17	1.6		2,41
RXCJ1218.4+4013	a)	184.6204	40.2184	0.3038	0.09	1.81	1.82	16.7	7.13	2.0		1
RXCJ1223.1+1037	NGC4325	185.7772	10.6240	0.0258	0.47	9.32	7.01	7.8	0.20	2.2		2,41
RXCJ1225.2+3213	-	186.3001	32.2291	0.0594	0.19	3.62	3.52	12.5	0.54	1.4		1,45
RXCJ1227.4+0849	A1541	186.8667	8.8290	0.0896	0.13	2.61	2.53	19.7	0.89	1.7	B	2,21
RXCJ1227.8+6322	A1544	186.9603	63.3830	0.1454	0.12	2.36	2.34	15.5	2.15	1.9		1,12
RXCJ1229.7+0759	M49-Virgo	187.4403	7.9870	0.0033	1.00	19.70	13.57	6.2	0.01	1.6		2,17
RXCJ1229.9+1147	A1552	187.4966	11.7891	0.0852	0.18	3.60	3.50	34.0	1.12	2.4	o	2,6
RXCJ1230.7+3439	-	187.6792	34.6550	0.3331	0.10	1.98	1.99	16.4	9.29	1.4		1
RXCJ1231.3+8225	g)	187.8497	82.4280	0.2053	0.09	2.04	2.04	18.3	3.69	5.6		1
RXCJ1236.9+6311	A1576	189.2457	63.1907	0.3019	0.15	3.00	3.02	13.8	11.52	1.7		2,6
RXCJ1242.8+0241	NGC4636	190.7063	2.6856	0.0031	1.85	36.57	25.21	12.0	0.01	1.8	L	2,17
RXCJ1243.3+2716	A1602	190.8448	27.2757	0.1940	0.11	2.20	2.19	15.9	3.56	1.2		1
RXCJ1243.6+1133	M60-Vir	190.9182	11.5502	0.0037	0.37	7.43	5.13	9.1	0.00	1.9		2,48
RXCJ1255.5+3521	a)	193.8781	35.3602	0.1585	0.05	1.05	1.04	22.2	1.14	1.3		2,49
RXCJ1257.3+6930	Zw1255.4+6946	194.3337	69.5064	0.2270	0.09	1.68	1.68	16.4	3.71	1.7		1,29
RXCJ1259.7+2756	Coma	194.9294	27.9386	0.0231	15.80	304.94	305.89	12.4	7.01	0.9	L	2,21
RXCJ1303.0+5756	-	195.7614	57.9419	0.1961	0.08	1.48	1.48	18.4	2.45	1.2		1
RXCJ1303.7+1916	A1668	195.9398	19.2715	0.0643	0.51	10.14	10.05	8.1	1.79	2.3		1,6,40
RXCJ1304.4+3335	A1672	196.1147	33.5920	0.1882	0.15	2.90	2.90	15.3	4.39	1.0		2,20
RXCJ1305.9+3054	A1677	196.4778	30.9065	0.1832	0.20	3.87	3.89	11.6	5.58	1.0		2,20
RXCJ1306.9+4633	A1682	196.7278	46.5560	0.2259	0.21	4.05	4.07	11.2	8.78	1.4		2,20
RXCJ1311.7+2201	-	197.9300	22.0267	0.1716	0.07	1.31	1.30	17.3	1.67	1.9		1
RXCJ1314.2+4123	-	198.5611	41.3927	0.2011	0.08	1.52	1.52	16.7	2.66	1.3		1
RXCJ1315.1+5149	A1703	198.7776	51.8248	0.2836	0.13	2.53	2.54	13.9	8.66	1.2		20
RXCJ1320.0+7003	A1722	200.0183	70.0616	0.3275	0.11	2.14	2.15	12.9	9.70	1.5		2
RXCJ1320.9+3354	A1716	200.2374	33.9041	0.1820	0.10	1.97	1.97	15.0	2.82	1.0		1
RXCJ1322.8+3138	-	200.7179	31.6459	0.3083	0.09	1.73	1.74	15.9	7.02	1.1		1
RXCJ1324.1+1358	NGC5129	201.0497	13.9792	0.0230	0.22	4.29	2.96	17.1	0.07	1.8		2,46
RXCJ1325.8+5919	A1744	201.4572	59.3225	0.1515	0.16	3.20	3.19	9.9	3.16	1.8		1,12
RXCJ1326.2+0013	b)	201.5733	0.2251	0.0826	0.28	5.60	5.55	11.7	1.65	1.8		1,41
RXCJ1332.7+5032	A1758	203.1796	50.5496	0.2799	0.29	5.56	5.60	9.5	18.29	1.0	o	2,20
RXCJ1332.6+5419	-	203.1671	54.3205	0.1017	0.14	2.81	2.79	14.0	1.25	1.3		1
RXCJ1335.3+4059	A1763	203.8257	40.9970	0.2279	0.33	6.30	6.35	8.1	13.85	0.8		2,42
RXCJ1336.1+5912	A1767	204.0255	59.2079	0.0701	0.63	12.44	12.40	5.4	2.62	1.9		2,6
RXCJ1339.5+1830	-	204.8952	18.5122	0.1140	0.06	1.22	1.19	21.5	0.68	1.7		1
RXCJ1341.8+2622	A1775	205.4740	26.3720	0.0724	0.65	12.58	12.54	16.7	2.83	1.0		2,6
RXCJ1344.3+3906	-	206.0762	39.1120	0.2997	0.04	0.79	0.79	24.5	3.08	0.9		1
RXCJ1348.8+2635	A1795	207.2207	26.5956	0.0622	3.05	59.29	59.56	2.8	9.93	1.2		2,6
RXCJ1349.0+4918	A1804	207.2582	49.3047	0.1665	0.06	1.27	1.25	20.2	1.51	1.2		1
RXCJ1349.3+2806	A1800	207.3402	28.1036	0.0748	0.50	9.83	9.79	8.2	2.36	1.2		2,46,6
RXCJ1351.7+4622	-	207.9398	46.3668	0.0625	0.17	3.32	3.22	15.0	0.55	1.3		1
RXCJ1354.0+1455	A1814	208.5095	14.9231	0.1251	0.18	3.49	3.48	16.0	2.35	1.7		2
RXCJ1354.6+7715	-	208.6575	77.2596	0.3967	0.10	2.08	2.09	25.0	13.56	2.9		1
RXCJ1359.8+6231	Zw1358.1+6245	209.9711	62.5212	0.3259	0.10	1.97	1.98	12.1	8.83	1.9		2,50
RXCJ1400.2+7207	A1851	210.0598	72.1257	0.2143	0.09	1.78	1.78	20.0	3.52	1.8		2,12
RXCJ1401.0+0252	A1835	210.2595	2.8801	0.2528	0.61	12.12	12.21	7.3	32.56	2.2		2,20
RXCJ1411.4+5212	3C295	212.8515	52.2106	0.4599	0.05	1.00	1.00	17.6	8.88	1.3		2,51
RXCJ1413.7+4339	A1885	213.4313	43.6634	0.0890	0.27	5.25	5.20	7.8	1.77	1.1		2,32
RXCJ1415.8+0015	a)	213.9650	0.2589	0.1259	0.06	1.23	1.19	22.4	0.83	3.0		1
RXCJ1416.5+3045	A1889	214.1354	30.7621	0.1860	0.05	1.01	1.00	23.2	1.53	1.3		2,6
RXCJ1418.9+4903	-	214.7473	49.0504	0.2806	0.10	2.04	2.05	24.3	6.87	1.9		1
RXCJ1421.5+4933	Zw1420.2+4952	215.3981	49.5519	0.0716	0.34	6.75	6.69	8.0	1.48	1.9		1,29
RXCJ1421.6+3717	A1902	215.4226	37.2958	0.1813	0.22	4.25	4.26	10.8	5.99	0.9		1
RXCJ1423.1+2615	a)	215.7922	26.2556	0.0375	0.12	2.28	1.72	16.4	0.10	1.6		2,46
RXCJ1423.8+4015	a)	215.9685	40.2619	0.0822	0.12	2.36	2.29	13.1	0.68	1.0		1
RXCJ1425.3+6311	A1918	216.3447	63.1872	0.1394	0.28	5.52	5.52	11.2	4.58	1.8		2,12
RXCJ1426.0+3749	A1914	216.5068	37.8271	0.1712	0.66	12.81	12.90	5.2	15.91	1.0		2,6
RXCJ1428.4+5652	A1925	217.1171	56.8829	0.1051	0.19	3.62	3.59	17.1	1.72	1.4		2
RXCJ1431.1+2538	A1927	217.7794	25.6388	0.0908	0.31	6.18	6.12	10.5	2.18	2.1		1,18

TABLE 1—*Continued*

name	alt.name	RA	DEC	z	ctr	F_x	F_x^*	err	L_x	N_H	ID	ref
RXCJ1440.6+0328	MKW8	220.1592	3.4765	0.0263	0.63	12.75	11.84	8.7	0.35	2.6		2,52
RXCJ1442.3+2218	UGC09480	220.5768	22.3048	0.0901	0.32	6.47	6.45	9.0	2.24	2.5		1
RXCJ1447.4+0827	-	221.8568	8.4637	0.1954	0.24	4.85	4.87	12.1	7.87	2.1		1
RXCJ1452.9+5802	A1995	223.2337	58.0488	0.3179	0.16	3.18	3.20	12.4	13.42	1.5		2,12
RXCJ1452.9+1641	A1983	223.2449	16.6998	0.0444	0.29	5.81	5.64	15.5	0.48	1.8		2,21
RXCJ1453.1+2153	A1986	223.2798	21.8947	0.1186	0.13	2.65	2.63	28.2	1.60	2.8		2,6
RXCJ1454.4+1622	-	223.6166	16.3704	0.0456	0.13	2.48	1.86	41.5	0.17	1.8		1,53
RXCJ1454.5+1838	A1991	223.6309	18.6420	0.0586	0.49	9.88	9.79	9.0	1.46	2.4	B	2,6
RXCJ1457.2+2220	MS1455.0+2232	224.3163	22.3434	0.2579	0.24	4.89	4.92	11.6	13.73	3.3		1,20
RXCJ1501.2+0141	NGC5813	225.3016	1.6960	0.0065	0.85	17.94	12.68	6.8	0.02	4.2		2,17
RXCJ1501.3+4220	-	225.3466	42.3464	0.2917	0.11	2.22	2.23	15.1	7.96	1.5		1
RXCJ1506.4+0136	NGC5846	226.6241	1.6049	0.0060	0.51	10.78	7.62	10.3	0.01	4.3		2
RXCJ1510.1+3330	A2034	227.5489	33.5147	0.1130	0.61	11.94	11.97	6.4	6.49	1.5	BC	2,29,69
RXCJ1511.1+1802	A2036	227.7761	18.0437	0.1161	0.13	2.63	2.61	17.1	1.52	2.9		2,6
RXCJ1512.6+3451	A2046	228.1553	34.8601	0.1489	0.07	1.41	1.40	17.6	1.35	1.4		1
RXCJ1516.7+0701	A2052	229.1834	7.0185	0.0353	2.35	47.94	47.79	3.6	2.58	2.9		2,6
RXCJ1518.7+0613	A2055	229.6899	6.2312	0.1021	0.42	8.74	8.74	9.7	3.91	3.3	C	41
RXCJ1520.9+4840	A2064	230.2271	48.6693	0.1076	0.31	6.13	6.11	10.2	3.05	1.7		2,6
RXCJ1521.8+0742	MKW3s	230.4583	7.7088	0.0442	1.57	32.24	32.15	5.1	2.70	3.2		2,47
RXCJ1522.4+2742	A2065	230.6106	27.7095	0.0723	1.04	21.18	21.18	5.5	4.75	2.8		2,6
RXCJ1523.0+0836	A2063	230.7724	8.6025	0.0355	1.75	35.80	35.48	4.6	1.94	2.9		2,21
RXCJ1528.0+6956	a),h)	232.0156	69.9423	0.1136	0.14	2.84	2.82	16.3	1.57	2.4		1
RXCJ1539.7+3424	A2111	234.9337	34.4156	0.2290	0.19	3.89	3.91	19.3	8.68	2.1		2,6
RXCJ1539.8+3043	A2110	234.9530	30.7173	0.0980	0.46	9.26	9.26	10.7	3.81	2.4		2,6
RXCJ1553.3+5107	A2136	238.3353	51.1226	0.2354	0.06	1.17	1.17	17.0	2.81	1.3		1
RXCJ1554.2+3237	-	238.5734	32.6277	0.0750	0.13	2.52	2.45	23.3	0.60	2.5	?	1
RXCJ1556.1+6621	A2146	239.0369	66.3558	0.2339	0.20	3.99	4.01	8.2	9.31	2.8	C	2,20
RXCJ1557.7+3530	A2141	239.4382	35.5040	0.1549	0.16	3.17	3.16	16.5	3.28	1.9		1,46
RXCJ1558.3+2713	A2142	239.5857	27.2269	0.0894	2.88	60.46	60.83	3.0	20.52	4.1	L	2,6
RXCJ1601.3+5354	A2149	240.3474	53.9061	0.1068	0.24	4.68	4.66	7.9	2.30	1.1		2,18
RXCJ1604.5+1743	Hercules	241.1489	17.7244	0.0370	0.82	16.93	16.46	7.0	0.98	3.4	L	2,53
RXCJ1604.9+2355	AWM4	241.2377	23.9206	0.0326	0.57	12.31	11.98	97.9	0.55	4.8	L	2,23
RXCJ1605.5+7208	-	241.3822	72.1467	0.1332	0.12	2.46	2.43	9.5	1.88	3.0		1
RXCJ1615.5+1927	NGC6098	243.8947	19.4600	0.0308	0.16	3.46	2.62	14.0	0.11	4.2		2
RXCJ1617.5+3458	(NGC6107)	244.3635	34.9367	0.0315	0.42	8.39	7.78	8.0	0.33	1.5	bL	2,17
RXCJ1618.2+2938	-	244.5741	29.6400	0.2993	0.05	1.12	1.12	20.0	4.30	2.8	B	1
RXCJ1620.5+2953	A2175	245.1322	29.8953	0.0972	0.38	7.57	7.54	8.4	3.06	2.5		2,6
RXCJ1624.2+4114	A2187	246.0591	41.2383	0.1825	0.15	2.87	2.87	12.9	4.10	1.0		2,20
RXCJ1626.9+5528	A2201	246.7459	55.4802	0.1300	0.14	2.83	2.80	10.6	2.06	2.0		1,29
RXCJ1627.3+4240	A2192	246.8482	42.6784	0.0317	0.19	3.66	2.75	10.1	0.12	1.0		1
RXCJ1627.6+4055	A2197	246.9173	40.9197	0.0301	0.22	4.28	3.21	10.9	0.13	1.0		2,17
RXCJ1628.6+3932	A2199	247.1582	39.5487	0.0299	5.08	97.92	97.92	2.6	3.77	0.8	L	2,21
RXCJ1629.7+5831	A2208	247.4367	58.5241	0.1329	0.14	2.79	2.77	8.6	2.13	1.8		2,20
RXCJ1632.7+0534	A2204	248.1936	5.5705	0.1514	1.09	24.11	24.23	4.8	23.43	5.9		1,6
RXCJ1634.6+6738	A2216	248.6591	67.6370	0.1668	0.06	1.23	1.22	10.5	1.48	4.4		1
RXCJ1635.8+6612	A2218	248.9682	66.2144	0.1709	0.32	6.57	6.59	4.4	8.16	3.1		2,6
RXCJ1640.3+4642	A2219	250.0892	46.7058	0.2280	0.56	11.10	11.18	5.2	24.33	1.7		2,20
RXCJ1643.2+5114	A2227	250.8043	51.2498	0.1990	0.09	1.89	1.89	13.9	3.23	2.5		1
RXCJ1643.3+2131	-	250.8337	21.5261	0.1535	0.08	1.62	1.60	17.3	1.65	5.0		1
RXCJ1644.9+0140	-	251.2402	1.6677	0.0000	0.05	1.15	1.15	34.7	0.00	5.1	?	
RXCJ1647.4+0441	-	251.8644	4.6882	0.0000	0.06	1.29	1.29	25.6	0.00	6.2	?	
RXCJ1651.1+0459	Her A	252.7918	4.9961	0.1540	0.24	5.39	5.39	10.8	5.49	6.3		2,54
RXCJ1652.2+4449	-	253.0679	44.8203	0.1753	0.16	3.09	3.09	11.7	4.06	1.8		1
RXCJ1652.9+4009	-	253.2318	40.1535	0.1492	0.16	3.13	3.12	13.3	2.99	1.8		1
RXCJ1654.3+2334	-	253.5972	23.5699	0.0575	0.13	2.69	2.50	13.5	0.36	4.6		1
RXCJ1654.7+5854	A2239	253.6945	58.9016	0.0869	0.11	2.18	2.12	11.9	0.70	2.2		1
RXCJ1658.0+2751	AWM5	254.5032	27.8544	0.0337	0.37	7.89	7.33	8.2	0.36	5.0	L	2,23,46
RXCJ1659.6+6826	-	254.9042	68.4375	0.0504	0.12	2.44	1.85	7.7	0.21	3.8		1,55
RXCJ1659.7+3236	A2241,B	254.9365	32.6135	0.1013	0.24	4.72	4.68	9.9	2.08	2.2		2,6
RXCJ1700.7+6412	A2246	255.1949	64.2143	0.2250	0.07	1.39	1.39	8.7	3.04	2.5	C	2,6
RXCJ1702.7+3403	A2244	255.6786	34.0619	0.0953	0.95	19.02	19.08	3.8	7.39	2.1		2,3
RXCJ1703.8+7838	A2256	255.9532	78.6443	0.0581	2.29	48.08	48.19	2.1	7.01	4.0	L	5
RXCJ1709.8+3426	A2249	257.4535	34.4406	0.0802	0.60	12.11	12.07	6.1	3.36	2.5		2,6
RXCJ1711.0+3941	A2250	257.7616	39.6942	0.0647	0.16	3.20	3.11	9.5	0.57	2.6		2,6,26
RXCJ1712.7+6403	A2255	258.1968	64.0614	0.0809	1.01	20.44	20.50	4.2	5.77	2.5	L	2,6
RXCJ1714.3+4341	NGC6329	258.5775	43.6897	0.0276	0.19	3.82	2.88	9.9	0.09	2.2		2,56
RXCJ1715.2+0309	-	258.8033	3.1631	0.1647	0.21	4.65	4.65	12.3	5.38	5.7		1
RXCJ1715.3+5724	NGC6338 i)	258.8414	57.4074	0.0276	0.75	15.24	14.81	15.4	0.49	2.8	L	2,57
RXCJ1717.6+3627	a)	259.4002	36.4637	0.1709	0.07	1.38	1.37	15.0	1.75	3.4		1
RXCJ1717.8+1940	A2254	259.4554	19.6833	0.1780	0.29	6.30	6.32	9.3	8.51	5.4		1,32,29
RXCJ1717.8+3235	A2257	259.4731	32.5860	0.1054	0.19	3.80	3.77	12.6	1.82	3.2		2,6

TABLE 1—*Continued*

name	alt.name	RA	DEC	z	ctr	F_x	F_x^*	err	L_x	N_H	ID	ref
RXCJ1718.1+5639	Zw1717.9+5636	259.5410	56.6656	0.1138	0.28	5.66	5.64	8.5	3.13	2.9		1,41
RXCJ1718.1+7801	A2271	259.5424	78.0220	0.0584	0.25	5.21	5.07	6.5	0.75	4.0		2,6
RXCJ1720.1+2637	e)	260.0386	26.6272	0.1644	0.51	10.79	10.84	6.4	12.34	3.9	B	1,38
RXCJ1720.1+2740	A2259	260.0370	27.6702	0.1640	0.25	5.30	5.31	8.6	6.06	3.6		1,32,29
RXCJ1722.2+3042	-	260.5617	30.7041	0.0500	0.07	1.40	1.06	22.1	0.12	3.3	B	2,56
RXCJ1722.4+3208	A2261	260.6129	32.1338	0.2240	0.47	9.77	9.83	6.6	20.61	3.4		1,32,29
RXCJ1723.3+5658	NGC6370	260.8466	56.9784	0.0272	0.10	2.16	1.51	10.5	0.05	3.2		2
RXCJ1723.7+8553	A2294	260.9478	85.8850	0.1780	0.23	5.25	5.26	8.1	7.11	6.6		1,41,29
RXCJ1730.4+7422	i)	262.6207	74.3749	0.1100	0.08	1.63	1.58	10.3	0.84	3.8	B	1,45
RXCJ1733.0+4345	IC1262	263.2607	43.7629	0.0307	0.59	11.89	11.55	5.1	0.47	2.5		2,57,56
RXCJ1735.0+6406	A2276	263.7723	64.1015	0.1406	0.11	2.16	2.14	8.5	1.84	2.8		1
RXCJ1735.9+1659	-	263.9757	16.9943	0.0858	0.09	1.98	1.93	16.8	0.63	5.9		
RXCJ1736.3+6803	Zw1745.6+6703	264.0919	68.0572	0.0248	0.15	3.22	2.28	5.3	0.06	4.4	B	1,58
RXCJ1738.1+6006	-	264.5257	60.1014	0.0000	0.06	1.36	1.36	9.2	0.00	3.7	?	
RXCJ1740.5+3538	a)	265.1362	35.6475	0.0428	0.32	6.42	6.24	6.8	0.49	2.6		1,41,3
RXCJ1742.8+3900	-	265.7013	39.0097	0.0423	0.26	5.35	4.97	8.3	0.39	3.0		2
RXCJ1744.2+3259	Zw1742.1+3306	266.0624	32.9896	0.0757	0.85	17.73	17.73	4.6	4.37	3.6		2,41,59
RXCJ1747.2+4512	-	266.8202	45.2156	0.1565	0.13	2.55	2.54	18.4	2.69	2.9	B	1
RXCJ1749.3+4245	-	267.3406	42.7621	0.2296	0.07	1.43	1.43	21.8	3.27	3.1		1
RXCJ1749.6+5334	-	267.4225	53.5793	0.0909	0.10	1.99	1.93	10.6	0.70	3.5		1
RXCJ1750.2+3504	b)	267.5689	35.0817	0.1712	0.22	4.45	4.46	12.9	5.57	3.1		1,41,3
RXCJ1751.7+2304	NGC6482	267.9480	23.0705	0.0132	0.17	3.88	2.84	10.9	0.02	7.7		2,56
RXCJ1753.4+5205	A2286	268.3740	52.0920	0.0988	0.07	1.47	1.43	12.9	0.61	3.9		1
RXCJ1754.0+5805	A2289	268.5093	58.0886	0.2263	0.08	1.68	1.68	14.6	3.69	4.0		1,27
RXCJ1754.6+6803	Zw1754.5+6807	268.6647	68.0564	0.0770	0.20	4.28	4.16	26.7	1.08	4.7	B	4
RXCJ1755.8+6236	NGC6521	268.9564	62.6135	0.0266	0.19	3.84	2.90	5.4	0.09	3.4	B	1,58,60
RXCJ1800.5+6913	A2295	270.1284	69.2236	0.0823	0.11	2.28	2.21	6.5	0.66	4.5	C	2,6,33
RXCJ1802.7+4247	j)	270.6811	42.7962	0.0502	0.09	1.82	1.37	23.4	0.15	3.3		2,57,56
RXCJ1811.0+4954	-	272.7503	49.9110	0.0501	0.46	9.71	9.45	5.0	1.03	4.4		2,41
RXCJ1814.2+6939	A2301	273.5738	69.6594	0.0863	0.05	1.11	1.03	10.0	0.34	5.3		2,6
RXCJ1816.4+5314	-	274.1117	53.2377	0.2764	0.06	1.35	1.35	11.2	4.41	3.5		1
RXCJ1819.8+3307	-	274.9666	33.1331	0.2796	0.06	1.24	1.24	17.2	4.16	4.6		
RXCJ1819.9+5710	A2302	274.9807	57.1677	0.0000	0.13	2.71	2.71	15.2	0.00	3.7		1
RXCJ1820.1+6857	A2304	275.0444	68.9555	0.0870	0.10	2.12	2.07	13.4	0.69	5.6		2,6
RXCJ1827.2+6134	-	276.8168	61.5815	0.1014	0.09	1.94	1.88	11.5	0.85	4.5		1
RXCJ1832.5+6449	-	278.1400	64.8313	0.1623	0.09	1.95	1.94	6.7	2.23	5.2		1
RXCJ1832.5+6848	-	278.1440	68.8034	0.2050	0.15	3.33	3.34	5.3	5.98	6.1	C	1,61
RXCJ1834.1+7057	A2308	278.5392	70.9578	0.0824	0.11	2.37	2.31	7.5	0.69	5.7		2,18
RXCJ1836.5+6344	-	279.1311	63.7423	0.0484	0.19	4.19	4.08	4.6	0.41	4.9		1
RXCJ1843.6+5021	-	280.9128	50.3637	0.1158	0.12	2.51	2.48	11.3	1.44	5.4		1
RXCJ1844.0+4533	-	281.0076	45.5567	0.0918	0.17	3.76	3.73	9.9	1.36	6.5		2,46,62
RXCJ1847.2+7320	A2310	281.8169	73.3473	0.1125	0.12	2.75	2.73	7.6	1.49	6.8		1
RXCJ1852.1+5711	-	283.0390	57.1972	0.1094	0.17	3.78	3.75	8.1	1.95	5.3		1
RXCJ1853.9+6822	A2312	283.4920	68.3813	0.0928	0.26	5.67	5.62	5.4	2.09	5.3		2,18
RXCJ1854.1+6858	-	283.5274	68.9715	0.2415	0.07	1.59	1.59	9.6	3.95	5.3	?	1
RXCJ1900.4+6958	A2315	285.1195	69.9687	0.0877	0.23	5.25	5.21	5.6	1.73	6.8		2,18,40
RXCJ1908.3+6903	A2317	287.0997	69.0617	0.2103	0.08	1.91	1.90	13.1	3.65	7.0	B	2,6
RXCJ1910.4+6741	MS1910.5+6736	287.6136	67.6908	0.2471	0.10	2.32	2.33	8.6	6.04	6.0		1,5
RXCJ1920.1+6318	-	290.0330	63.3046	0.0000	0.09	2.00	2.00	13.6	0.00	6.3		1
RXCJ1921.3+7433	-	290.3389	74.5654	0.0000	0.13	2.97	2.97	9.1	0.00	7.9		1
RXCJ1927.5+6549	-	291.8758	65.8322	0.1886	0.08	1.71	1.71	9.4	2.61	7.2		1
RXCJ1935.3+6734	-	293.8340	67.5760	0.1706	0.09	2.01	2.01	10.3	2.52	7.8		1
RXCJ2035.7+0046	-	308.9382	0.7678	0.0000	0.05	1.03	1.03	29.0	0.00	7.5	?	1
RXCJ2041.7+0721	-	310.4251	7.3573	0.0639	0.05	1.07	0.82	24.8	0.15	7.9	?	1
RXCJ2050.7+0123	-	312.6898	1.3887	0.3334	0.05	1.24	1.24	25.8	5.88	7.5		1
RXCJ2051.1+0216	-	312.7806	2.2679	0.3211	0.07	1.68	1.68	20.6	7.36	8.1		1
RXCJ2057.5+1334	-	314.3892	13.5709	0.2232	0.04	0.91	0.91	27.6	1.99	10.5		1,43
RXCJ2103.8+0437	-	315.9612	4.6258	0.1694	0.04	0.79	0.77	25.9	0.99	7.0		1
RXCJ2104.9+1401	-	316.2260	14.0278	0.1615	0.14	3.24	3.24	13.4	3.66	7.3		1
RXCJ2113.8+0233	IC1365	318.4745	2.5555	0.0494	0.61	13.60	13.49	8.9	1.42	6.6		2,43
RXCJ2129.6+0005	e)	322.4186	0.0973	0.2347	0.34	7.18	7.22	11.2	16.70	4.2		1,38
RXCJ2151.4+1347	-	327.8595	13.7979	0.2076	0.10	2.21	2.21	22.0	4.09	6.3		1
RXCJ2153.5+1741	A2390	328.3980	17.6868	0.2329	0.49	11.01	11.06	10.3	25.15	6.7		2,6
RXCJ2155.6+1232	A2396	328.9198	12.5336	0.1920	0.16	3.49	3.49	16.8	5.51	6.3		2,27
RXCJ2200.8+2058	A2409	330.2201	20.9708	0.1470	0.37	8.32	8.34	12.0	7.68	6.7		2,20
RXCJ2214.8+1350	b)	333.7198	13.8468	0.0253	0.20	4.28	3.24	18.1	0.09	5.1		2,41,63
RXCJ2226.8+2550	A2445	336.7199	25.8432	0.1650	0.15	3.28	3.28	16.6	3.82	5.3		1
RXCJ2228.6+2036	-	337.1546	20.6087	0.4120	0.20	4.21	4.24	20.0	29.62	4.7		1
RXCJ2241.8+1732	A2472	340.4738	17.5416	0.3137	0.09	2.04	2.05	21.3	8.44	5.3		1
RXCJ2245.0+2637	-	341.2713	26.6304	0.3040	0.14	3.01	3.02	13.2	11.71	5.4		1
RXCJ2250.3+1054	A2495	342.5873	10.9024	0.0768	0.50	10.80	10.77	35.7	2.74	5.5		2,18

Table 1—*Continued*

name	alt.name	RA	DEC	z	ctr	F_x	F_x^*	err	L_x	N_H	ID	ref
RXCJ2256.8+0530	A2507	344.2195	5.5115	0.1960	0.04	0.88	0.87	43.0	1.46	5.6	B	3,64
RXCJ2300.2+2926	-	345.0579	29.4419	0.0688	0.14	2.93	2.85	15.0	0.59	5.7	o	1
RXCJ2307.0+1631	-	346.7632	16.5236	0.2502	0.16	3.45	3.46	23.8	9.16	6.0		1
RXCJ2307.6+2716	-	346.9169	27.2700	0.1100	0.07	1.51	1.47	26.4	0.78	5.6		1
RXCJ2310.4+0734	Pegasus II	347.6099	7.5769	0.0424	0.50	10.66	10.37	8.3	0.81	4.9		2,65,66
RXCJ2311.1+1137	-	347.7875	11.6317	0.2610	0.07	1.55	1.55	19.2	4.56	4.5		1
RXCJ2311.5+0338	A2552	347.8878	3.6437	0.1325	0.21	4.59	4.58	15.8	3.48	5.2		1,29,3
RXCJ2318.5+1842	A2572	349.6323	18.7054	0.0403	0.40	8.44	8.21	9.6	0.58	4.6		2,6,17
RXCJ2321.8+1505	-	350.4671	15.0430	0.1500	0.10	2.21	2.19	15.0	2.15	4.1	c	1
RXCJ2323.6+0908	A2588	350.9125	9.1480	0.1992	0.10	2.12	2.11	17.9	3.63	4.7		1
RXCJ2325.0+1841	-	351.2493	18.6971	0.2018	0.04	0.84	0.84	32.5	1.49	4.2		
RXCJ2333.8+2140	-	353.4712	21.6771	0.1022	0.14	2.96	2.94	17.2	1.33	4.3		1
RXCJ2334.0+0704	A2620	353.5203	7.0709	0.0990	0.08	1.82	1.82	19.4	0.76	5.6		69
RXCJ2336.5+2108	A2626	354.1261	21.1424	0.0565	0.54	11.32	11.22	7.5	1.55	4.3		2,6
RXCJ2337.6+0016	A2631	354.4206	0.2760	0.2780	0.17	3.56	3.58	20.1	11.60	3.8		1,67,29
RXCJ2338.4+2659	A2634	354.6071	27.0126	0.0309	1.01	21.87	21.29	5.1	0.88	5.2	bL	2,6,43,6
RXCJ2340.5+1029	A2639	355.1335	10.4910	0.1800	0.08	1.82	1.82	19.0	2.55	5.3		1
RXCJ2341.1+0018	-	355.2763	0.3148	0.1100	0.10	2.00	1.94	18.0	1.03	3.7		1,37
RXCJ2344.9+0911	A2657	356.2376	9.1980	0.0400	1.22	26.49	26.27	6.0	1.81	5.3	L	2,21,66,
RXCJ2350.5+2929	MS2348.0+2913	357.6400	29.4980	0.1498	0.17	3.69	3.68	16.9	3.56	5.3		1,5
RXCJ2350.8+0609	A2665	357.7109	6.1611	0.0562	0.60	13.34	13.24	11.7	1.81	6.2		2,6
RXCJ2355.6+1120	A2675	358.9094	11.3433	0.0726	0.31	6.70	6.64	10.2	1.51	4.5		2,6
RXCJ2355.8+3423	A2677	358.9572	34.3859	0.1480	0.11	2.52	2.51	20.2	2.37	6.3		1

RA and DEC for J2000; RA in decimal degrees

(a) see also Bade et al. 1998, (b) see also Ebeling et al. (1998), (c) Barton et al. 1996, (d) Crawford et al. 1995, (e) Cooray et al. 1998, (f) Stoll et al. 1995, (g) Struble & Rood 1991b, (h) see also Tucker et al. 1995, (i) Appenzeller et al. 1998, (j) Wegner et al. 1996

References.— (1) this work; (2) Huchra (priv. communication: Z-cat, A-cat), (3) Crawford et al. 1999, (4) Hopp et al. 1995, (5) Stocke et al. 1991, (6) Struble & Rood 1987, 1991, (7) Merrifield & Kent, 1991, (8) Gunn, Hoessel, & Oke, 1986, (9) Schmidt, Schneider, & Gunn, 1986, (10) Chapman, Geller, & Huchra, 1988, (11) Michel & Huchra, 1988, (12) Huchra et al 1990, (13) Capelato et al. 1991, (14) Maurogordato et al. 1995, (15) Batuski et al. 1991, (16) Hewitt & Burbidge, 1991, (17) de Vaucouleurs et al. 1991, (18) Postman, Huchra, & Geller, 1992, (19) Elvis et al. 1992, (20) Allen et al. 1992, (21) Zabludoff et al. 1993, (22) Braine & Dupraz, 1994, (23) Dell'Antonio, Geller, & Fabricant, 1994, (24) Sakai, Giovanelli, & Wegner, 1994, (25) Davoust & Considere, 1995, (26) Owen, Ledlow, & Keel, 1995, (27) Ledlow & Owen, 1995, (28) Davidge & Grinder, 1995, (29) Crawford et al. 1995, (30) Tomita et al. 1996, (31) Ledlow et al. 1996, (32) Ebelinget al. 1996, (33) Dale et al. 1997, (34) Owen et al. 1997, (35) Smith et al. 1997, (36) Pietsch et al. 1998, (37) Katgert et al. 1998, (38) Cooray et al. 1998, (39) Lozinskaya et al. 1998, (40) Slinglend et al. 1998, (41) Ebeling et al. 1998, (42) Cao, Wei, & Hu, 1999, (43) Huchra et al. 1999, (44) Gubanov & Reshetnikov, 1999, (45) Appenzeller, et al. 1998, (46) Beers et al. 1995, (47) Hill & Oegerle, 1993, (48) Huchtmeier, Sage, & Henkel, 1995, (49) Huchra et al. 1995, (50) Fisher et al. 1998, (51) Schade, Barrientos, & Lopez-Cruz, 1997, (52) Andersen, & Owen, 1994, (53) Dressler, & Shectman, 1988, (54) Spinrad et al. 1985, (55) Henstock et al. 1997, (56) Marzke, Huchra, & Geller, 1996, (57) Wegner et al. 1996, (58) Henry et al. 1995, (59) Ulrich, 1976, (60) Falco, Kochanek, & Munoz, 1998, (61) Moran et al. 1996, (62) Fisher et al. 1995, (63) Lacy et al. 1993, (64) Brandt et al. 1994, (65) Chincarini & Rood, 1976, (66) Trasarti-Battistoni, 1998, (67) Fetisova et al. 1993, (68) Barton et al. 1996, (69) Struble & Rood 1999.

TABLE 2
THE NON-CLUSTER X-RAY SOURCES AMONG THE EXTENDED RASS 1 SOURCES

name	alt.name	RA	DEC	ctr	F_x	F_x^*	err	P_{ext}	r_c	r_{min}	HR	err	ΔHR	N_H	ID
RXJ0013.4+0949	Star	3.3656	9.8272	0.16	3.54	0.00	11.50	0.7	0.0	0.0	0.95	0.07	1.02	6.0	
RXJ0029.3+4153	STAR	7.3304	41.8900	0.04	0.87	0.00	25.80	0.9	2.5	0.0	0.53	0.23	-1.56	6.4	
RXJ0042.6+4115	M31	10.6748	41.2569	1.47	33.04	0.00	4.10	-1.0	2.5	2.0	0.79	0.04	-2.58	6.6	
RXJ0053.5+1241	AGN	13.3951	12.6937	0.65	13.94	0.00	7.80	1.4	0.0	0.0	0.50	0.06	-5.62	5.0	
RXJ0053.8+2231	AGN?	13.4517	22.5314	0.09	1.94	0.00	21.50	0.7	0.0	0.0	-0.06	0.15	-5.43	3.7	
RXJ0208.5+3523	AGN	32.1490	35.3857	0.24	5.39	0.00	20.20	0.1	0.0	0.0	1.15	0.03	3.81	6.3	
RXJ0227.2+0201	AGN?	36.8191	2.0307	1.06	21.82	21.95	7.80	0.1	0.0	0.0	0.45	0.06	-4.21	3.1	
RXJ0300.1+1630	AGN	45.0308	16.5033	0.37	9.27	0.00	8.80	0.2	0.0	0.0	0.94	0.09	-0.10	10.8	
RXJ0319.8+1845	AGN	49.9661	18.7616	0.58	14.48	0.00	6.20	0.7	0.0	0.0	0.86	0.04	-2.20	10.6	
RXJ0326.5+2843	STAR	51.6470	28.7168	2.77	71.68	0.00	3.00	3.4	0.0	0.0	-0.07	0.02	-9.99	12.4	
RXJ0331.2+2659	STAR?	52.8051	26.9904	0.04	0.98	0.00	28.70	1.0	0.5	0.0	0.25	0.27	-2.60	11.1	
RXJ0344.3+2447	STAR	56.0799	24.7896	0.10	2.32	0.00	17.70	0.6	0.0	0.0	0.55	0.16	-2.43	9.6	
RXJ0405.3+2009	T-Tauri	61.3266	20.1567	0.12	3.28	0.00	18.10	1.2	0.5	0.0	0.23	0.15	-4.91	16.3	
RXJ0738.0+7443	AGN	114.5057	74.7280	0.12	2.53	0.00	14.40	0.2	0.0	0.0	0.54	0.13	-1.89	4.1	
RXJ0801.5+4736	AGN	120.3869	47.6031	0.24	5.14	0.00	10.60	0.7	0.0	0.0	0.49	0.09	-3.52	4.4	
RXJ0814.3+2940	AGN	123.5822	29.6728	0.05	1.11	0.00	36.40	1.0	1.0	0.0	0.42	0.31	-1.11	3.8	
RXJ0840.4+1824	STAR	130.1241	18.4054	0.20	4.09	0.00	18.20	0.3	0.5	0.0	-0.05	0.13	-5.48	2.8	
RXJ0842.1+0759	AGN	130.5311	7.9951	0.31	6.53	0.00	10.50	0.9	0.5	0.0	1.01	0.11	1.65	4.6	
RXJ0847.6+3445	AGN	131.9243	34.7511	0.32	6.59	0.00	13.30	1.8	0.5	0.5	0.10	0.07	-8.81	3.3	
RXJ0900.6+4147	STAR	135.1537	41.7857	0.22	4.30	0.00	12.10	1.3	0.5	0.5	-0.42	0.06	-9.99	2.1	
RXJ0907.3+1716	AGN	136.8495	17.2745	0.07	1.38	0.00	22.90	0.3	1.0	0.0	0.14	0.17	-3.65	3.8	
RXJ0909.9+5428	STARS	137.4907	54.4831	0.24	4.68	0.00	11.40	0.8	0.0	0.0	0.17	0.09	-3.95	1.9	
RXJ0924.2+0309	AGN	141.0664	3.1507	0.06	1.25	0.00	24.80	0.7	6.0	0.0	0.53	0.22	-1.00	3.6	
RXJ0933.9+2450	AGN	143.4984	24.8353	0.04	0.82	0.81	29.30	1.6	3.0	0.0	0.13	0.29	-1.43	2.0	
RXJ0933.9+8717	AGN	143.4946	87.2876	0.07	1.47	0.00	15.50	0.7	0.0	0.0	0.66	0.16	-1.42	6.3	
RXJ0955.8+6940	M82	148.9630	69.6796	1.15	24.24	0.00	7.10	7.9	0.5	0.5	0.90	0.05	2.05	4.3	
RXJ1008.5+4629	AGN	152.1325	46.4956	0.14	2.69	0.00	12.40	1.4	0.5	0.5	-0.37	0.07	-9.64	0.9	
RXJ1027.1+0609	STAR	156.7790	6.1530	0.17	3.56	0.00	13.20	3.4	1.0	0.5	0.09	0.10	-5.69	2.7	
RXJ1101.0+1102	Mrk728	165.2623	11.0499	0.15	3.09	2.33	17.80	0.6	0.5	0.0	0.45	0.15	-1.42	2.8	
RXJ1107.8+1502	AGN	166.9513	15.0370	0.20	3.98	0.00	13.60	0.3	0.0	0.0	-0.20	0.08	-8.02	1.5	
RXJ1109.5+8305	STAR	167.3774	83.0978	0.21	4.62	0.00	13.00	3.3	0.5	0.5	0.09	0.08	-9.84	6.0	
RXJ1110.1+0113	AGN	167.5436	1.2279	0.10	2.11	0.00	16.00	0.3	0.5	0.0	0.20	0.12	-4.96	4.2	
RXJ1110.5+7133	AGN	167.6449	71.5647	0.06	1.15	0.00	20.50	1.0	0.5	0.0	0.23	0.17	-2.32	2.5	
RXJ1119.1+2119	AGN	169.7857	21.3206	0.31	6.06	0.00	15.20	1.1	0.0	0.0	-0.49	0.05	-9.99	1.2	
RXJ1120.3+1259	M66	170.0773	12.9838	0.08	1.66	0.00	22.00	0.4	0.5	0.0	0.39	0.24	-1.06	2.6	
RXJ1123.8+1032	STARS	170.9738	10.5373	0.03	0.69	0.00	27.10	1.2	1.5	0.0	-0.64	0.10	-9.99	2.8	
RXJ1123.8+7230	AGN?	170.9535	72.5013	0.15	3.08	0.00	10.60	1.5	0.0	0.0	-0.09	0.07	-9.99	2.6	
RXJ1128.5+5833	Mrk171	172.1308	58.5595	0.12	2.23	0.00	19.10	1.2	0.0	0.0	0.73	0.23	1.70	1.1	
RXJ1145.2+7940	U06728	176.3075	79.6831	0.33	7.09	0.00	7.50	1.3	0.0	0.0	0.89	0.07	1.02	4.6	
RXJ1203.5+0249	STAR	180.8776	2.8220	0.14	2.69	0.00	14.00	2.5	1.0	0.5	0.97	0.16	2.83	1.8	
RXJ1215.1+3311	AGN	183.7763	33.1961	0.43	8.35	5.73	18.80	4.6	1.5	1.0	0.16	0.14	-1.56	1.2	
RXJ1218.9+4718	M106	184.7410	47.3039	0.23	4.46	0.00	11.10	3.3	0.5	0.5	0.54	0.13	1.25	1.2	
RXJ1221.7+7518	AGN	185.4379	75.3165	0.75	15.28	0.00	5.70	1.4	0.0	0.0	0.44	0.05	-4.52	2.8	
RXJ1222.5+2550	STAR	185.6289	25.8425	0.47	9.26	0.00	7.70	0.5	0.0	0.0	0.13	0.07	-5.59	1.9	
RXJ1257.0+2201	W.D.	194.2592	22.0310	0.00	0.02	0.00	0.00	1.0	3.0	0.0	-1.00	0.00	-9.99	2.6	o
RXJ1257.6+0917	AGN?	194.4137	9.2998	0.09	1.78	0.00	32.10	2.2	2.5	0.0	-0.36	0.16	-5.47	1.8	
RXJ1258.5+3816	STAR	194.6436	38.2754	0.19	3.75	0.00	13.70	2.8	0.5	0.5	-0.21	0.07	-9.46	1.5	
RXJ1259.4+2029	AGN	194.8598	20.4895	0.06	1.22	0.00	19.70	0.5	0.5	0.0	-0.17	0.13	-5.75	2.2	
RXJ1313.4+3635	AGN	198.3605	36.5962	0.25	4.91	0.00	9.80	1.4	0.5	0.0	0.17	0.09	-1.53	0.9	
RXJ1409.9+1604	STAR?	212.4900	16.0693	0.02	0.43	0.00	41.20	0.8	1.5	0.0	-0.15	0.26	-2.09	1.3	c
RXJ1422.6+5802	AGN	215.6646	58.0348	0.89	17.48	0.00	4.30	0.5	0.0	0.0	-0.11	0.03	-9.99	1.3	
RXJ1425.2+5151	STAR	216.3005	51.8531	1.01	19.66	0.00	4.00	0.3	0.0	0.0	0.00	0.03	-9.99	1.3	
RXJ1456.0+5048	AGN	224.0149	50.8072	0.75	14.83	0.00	4.80	5.4	0.5	0.5	0.03	0.04	-9.99	1.8	
RXJ1500.3+7636	AGN	225.0950	76.6126	0.07	1.35	0.00	14.90	0.0	0.0	0.0	0.20	0.12	-4.14	3.1	
RXJ1522.7+5040	STAR	230.6805	50.6780	0.04	0.83	0.00	25.80	1.1	0.5	0.5	-0.21	0.12	-5.76	1.6	
RXJ1531.5+0851	AGN	232.8991	8.8638	0.05	0.93	0.00	39.40	0.0	0.5	0.0	0.51	0.34	-0.64	3.4	
RXJ1533.1+1854	STAR	233.2955	18.9079	0.44	9.39	0.00	7.90	0.7	0.0	0.0	0.49	0.07	-4.31	4.2	
RXJ1535.0+5320	AGN	233.7521	53.3432	0.74	14.51	0.00	3.60	0.9	0.0	0.0	0.03	0.03	-9.99	1.3	
RXJ1535.3+0909	STAR	233.8435	9.1635	0.08	1.67	0.00	23.50	0.7	1.5	0.0	0.26	0.22	-2.14	3.4	
RXJ1601.7+5120	STAR	240.4429	51.3495	0.47	9.14	0.00	8.30	0.3	0.0	0.0	-0.06	0.06	-8.60	1.5	
RXJ1616.7+0412	AGN	244.1776	4.2084	0.05	1.17	0.00	22.20	0.0	0.5	0.0	0.85	0.19	0.05	5.1	
RXJ1625.5+8529	AGN	246.3905	85.4953	0.31	6.85	0.00	5.90	3.1	0.5	0.0	0.77	0.06	-1.97	6.3	
RXJ1637.9+7326	AGN	249.4887	73.4361	0.05	1.12	0.00	25.70	2.3	1.0	0.5	0.36	0.17	-2.31	3.7	
RXJ1639.8+7809	STAR	249.9712	78.1587	0.08	1.68	0.00	24.10	0.6	0.0	0.0	0.35	0.11	-3.94	4.1	
RXJ1642.3+0459	??	250.5791	4.9915	0.04	0.87	0.00	39.10	0.6	1.0	0.5	0.95	0.30	0.22	6.2	
RXJ1645.8+8202	STAR	251.4639	82.0378	0.70	15.41	0.00	3.50	0.9	0.0	0.0	0.27	0.03	-9.99	5.7	
RXJ1702.7+7222	AGN	255.6985	72.3756	0.03	0.53	0.00	16.00	0.1	0.5	0.0	0.57	0.19	-1.15	4.1	
RXJ1702.7+7253	AGN	255.6960	72.8915	0.37	7.69	0.00	4.70	2.3	0.0	0.0	0.68	0.05	-1.88	3.9	
RXJ1714.6+6441	AGN	258.6652	64.6997	0.04	0.82	0.00	10.30	0.0	0.0	0.0	-0.02	0.08	-8.76	2.9	
RXJ1717.1+2931	AGN	259.2778	29.5181	0.26	5.48	5.51	8.00	2.0	0.5	0.0	0.64	0.08	-1.27	3.5	
RXJ1719.1+0911	STAR	259.7885	9.1974	0.02	0.47	0.00	45.20	4.8	1.0	0.0	0.92	0.61	0.03	6.8	

TABLE 2—*Continued*

name	alt.name	RA	DEC	ctr	F_x	F_x^*	err	P_{ext}	r_c	r_{min}	HR	err	ΔHR	N_H	ID
RXJ1719.6+2228	AGN?	259.9024	22.4672	0.06	1.29	0.00	33.50	0.2	0.0	0.0	0.84	0.22	0.00	5.0	
RXJ1726.1+7431	AGN	261.5293	74.5177	0.18	3.71	0.00	5.60	2.2	0.0	0.0	0.32	0.05	-9.10	3.9	
RXJ1728.3+5013	AGN	262.0765	50.2197	1.24	24.99	0.00	2.70	0.8	0.0	0.0	0.29	0.02	-9.99	2.6	
RXJ1728.6+5901	STAR	262.1671	59.0326	0.56	11.39	0.00	3.40	3.9	0.0	0.0	0.25	0.03	-9.99	3.0	
RXJ1730.3+2202	STAR	262.5804	22.0340	0.25	5.48	0.00	10.70	1.0	0.0	0.0	0.36	0.07	-7.21	5.6	
RXJ1732.6+7413	STAR	263.1748	74.2275	0.75	15.66	0.00	8.90	3.3	0.0	0.0	0.14	0.02	-9.99	3.8	
RXJ1734.7+7844	STAR	263.6871	78.7373	0.06	1.19	0.00	10.90	0.2	0.0	0.0	-0.12	0.08	-9.99	4.3	
RXJ1737.4+7123	AGN?	264.3622	71.3988	0.06	1.25	1.22	18.60	0.9	0.5	0.0	0.32	0.10	-4.48	3.8	
RXJ1738.7+3223	AGN	264.6926	32.3839	0.10	2.13	2.11	17.30	1.4	0.5	0.5	0.15	0.11	-5.57	3.8	
RXJ1753.5+4937	STAR?	268.3771	49.6271	0.09	1.97	0.00	9.60	1.5	0.5	0.5	0.27	0.08	-6.26	3.9	
RXJ1756.2+5522	AGN	269.0655	55.3717	0.40	8.38	0.00	3.50	0.5	0.0	0.0	0.33	0.03	-9.99	3.7	
RXJ1757.2+7033	STAR	269.3029	70.5620	0.25	5.20	0.00	47.50	0.5	0.0	0.0	0.40	0.03	-9.99	4.4	
RXJ1757.3+7131	STAR	269.3322	71.5252	0.06	1.33	0.00	8.10	8.3	0.5	0.5	0.26	0.07	-7.47	4.1	
RXJ1758.6+2208	STAR	269.6563	22.1390	0.09	2.20	0.00	13.80	0.2	0.5	0.0	0.60	0.13	-2.51	8.3	
RXJ1803.4+6738	AGN?	270.8696	67.6345	0.20	4.35	0.00	2.00	2.5	0.0	0.0	0.44	0.02	-9.99	4.7	
RXJ1813.7+3001	AGN	273.4260	30.0267	0.16	3.59	0.00	12.80	1.1	0.0	0.0	1.05	0.14	0.64	7.3	
RXJ1823.9+5848	STAR	275.9911	58.8144	0.08	1.64	0.00	9.10	2.8	0.5	0.5	-0.11	0.06	-9.99	4.6	
RXJ1824.5+6350	STAR	276.1269	63.8344	0.02	0.34	0.00	12.50	-2.0	0.5	0.0	0.42	0.18	-2.09	4.2	
RXJ1829.4+5403	?	277.3573	54.0522	0.06	1.25	0.00	14.90	1.4	0.0	0.0	0.08	0.11	-6.05	3.6	
RXJ1831.3+6453	STAR	277.8400	64.8982	0.03	0.67	0.00	9.70	-1.2	0.5	0.5	-0.05	0.07	-9.99	5.2	
RXJ1842.8+5751	STAR	280.7062	57.8640	0.10	2.15	0.00	9.10	0.3	0.0	0.0	0.22	0.08	-7.69	4.9	
RXJ1843.7+5756	STAR	280.9490	57.9375	0.05	1.16	0.00	14.80	2.4	0.5	0.5	0.20	0.14	-4.54	4.9	
RXJ1927.3+6533	AGN?	291.8300	65.5656	1.12	25.47	0.00	2.30	3.2	0.0	0.0	0.84	0.01	-6.79	7.2	
RXJ2056.0+0349	STAR?	314.0062	3.8288	0.03	0.75	0.00	33.30	0.9	0.5	0.0	0.42	0.29	-1.67	7.0	
RXJ2103.9+0400	?	315.9810	4.0000	0.04	0.95	0.95	32.40	1.1	2.5	0.0	0.95	0.38	0.12	7.0	
RXJ2200.7+2715	STAR?	330.1837	27.2631	0.09	2.00	0.00	15.70	0.0	0.0	0.0	-0.20	0.10	-9.99	6.5	
RXJ2327.3+1524	AGN	351.8460	15.4113	0.25	5.11	0.00	12.00	1.2	0.5	0.0	1.06	0.02	9.99	3.8	
RXJ2356.8+1518	AGN	359.2181	15.3165	0.12	2.54	2.54	15.10	0.2	0.0	0.0	0.07	0.11	-6.39	3.9	

RA and DEC for J2000; RA in decimal degrees

TABLE 3

THE AGN IN CLUSTERS AND NON-CLUSTER-SOURCES IN THE LINE OF SIGHT WITH PROBABLE CLUSTERS

name	alt.name	RA	DEC	ctr	F_x	F_x^*	err	P_{ext}	r_c	r_{min}	HR	err	ΔHR	N_H	ID
RXJ0020.3+1034	AGN-Cl	5.0893	10.5793	0.28	5.99	6.00	12.5	2.2	0.5	0.5	0.71	0.10	-1.27	5.0	
RXJ0216.5+2314	AGN-Cl	34.1338	23.2460	0.34	7.86	0.00	12.4	0.3	0.0	0.0	0.71	0.10	-2.15	8.3	
RXJ1107.8+7105	AGN-Cl	166.9616	71.0968	0.10	2.08	1.93	23.5	1.1	0.0	0.0	0.45	0.15	-0.83	2.2	
RXJ1117.0+2014	AGN-Cl	169.2746	20.2364	2.16	42.35	0.00	4.0	2.4	0.0	0.0	-0.03	0.03	-9.99	1.4	
RXJ1207.2+3648	AGN-Cl	181.8179	36.8051	0.05	0.99	0.00	28.4	0.1	0.5	0.0	0.14	0.23	-1.60	1.8	
RXJ1209.9+0628	AGN-Cl	182.5000	6.4956	0.11	2.14	2.08	19.6	3.7	2.0	1.0	-0.09	0.13	-4.11	1.5	b
RXJ1315.9+2125	AGN-Cl	198.9840	21.4184	0.21	4.16	0.00	13.7	1.1	0.5	0.5	0.10	0.10	-4.12	1.8	
RXJ1346.1+7331	AGN-Cl	206.5355	73.5230	0.09	1.89	0.00	30.3	0.1	0.5	0.0	0.18	0.27	-1.36	2.0	
RXJ1353.0+6918	AGN-Cl	208.2701	69.3082	1.39	27.43	0.00	3.5	1.3	0.0	0.0	-0.03	0.03	-9.99	1.8	
RXJ1421.4+4747	AGN-Cl	215.3709	47.7870	0.53	10.49	10.45	7.3	4.4	0.5	0.5	-0.07	0.05	-9.99	1.6	
RXJ1427.6+1833	AGN-Cl	216.9067	18.5636	0.05	1.01	0.99	22.4	1.0	0.5	0.0	-0.27	0.14	-5.86	2.0	
RXJ1449.5+2746	AGN	222.3855	27.7758	0.34	6.74	6.26	8.0	1.2	0.5	0.5	0.46	0.08	-1.27	2.1	
RXJ1746.1+6737	AGN-Cl	266.5419	67.6224	0.11	2.26	1.71	3.8	1.2	0.0	0.0	0.35	0.04	-9.99	4.5	
RXJ1747.0+7240	STAR+Cl	266.7512	72.6753	0.21	4.47	0.00	4.0	-1.8	0.0	0.0	0.19	0.03	-9.99	3.8	
RXJ1747.0+6836	AGN-Cl	266.7508	68.6073	0.14	2.85	2.78	23.5	2.1	0.0	0.0	0.24	0.04	-9.99	4.2	
RXJ1756.4+5235	AGN-Cl	269.1133	52.5857	0.05	1.09	1.06	19.0	0.3	0.0	0.0	0.92	0.27	0.53	4.0	
RXJ1830.3+7312	AGN-Cl	277.5959	73.2119	0.06	1.36	0.00	9.7	1.8	0.5	0.5	0.66	0.13	-1.56	5.6	
RXJ1905.7+7804	AGN-Cl	286.4339	78.0782	0.21	4.49	4.49	7.2	1.1	0.0	0.0	0.57	0.07	-3.76	4.9	

RA and DEC for J2000; RA in decimal degrees

Table 4

X-ray properties of the non-cluster X-ray source cluster combinations

name	redshift of AGN	comments
RXJ0020.3+1034	0.1691	–
RXJ0216.5+2314	0.2890	AGN in a group
RXJ1107.8+7105	0.0600	AGN possibly in a group
RXJ1117.0+2014	0.1392	BL Lac in cluster at same redshift
RXJ1207.2+3648	2.4896	AGN - no z for cluster
RXJ1209.9+0628	0.0804	AGN in cluster
RXJ1315.9+2125	0.0896	–
RXJ1346.1+7331	0.0889	AGN in group
RXJ1353.0+6918	0.0305	AGN in a group
RXJ1421.4+4747	0.0732	AGN in a group (2 redshifts)
RXJ1427.6+1833	0.1015	AGN in a cluster
RXJ1449.5+2746	-	AGN in group (z=0.0314)
RXJ1746.1+6737	0.0415	AGN in a group
RXJ1747.0+7240	0.0632	AGN in a group
RXJ1747.0+6836	0.0000	cluster behind a bright star
RXJ1756.4+5235	0.0943	AGN in a loose group
RXJ1830.3+7312	0.1200	Sy 1 in a cluster
RXJ1905.7+7804	0.1394	AGN in a cluster

TABLE 5
X-RAY PROPERTIES OF THE NORAS CLUSTER X-RAY SOURCES

name	L_x	R_x ($'$)	R_x (Mpc)	P_{ext}	r_c	r_{min}	HR	err	ΔHR
RXCJ0000.1+0816	0.37	13.5	0.87	3.0	1.0	1.0	0.70	0.13	-1.33
RXCJ0001.9+1204	3.24	4.5	1.15	1.2	0.0	0.0	0.62	0.15	-1.49
RXCJ0004.9+1142	0.93	8.0	0.93	2.3	0.5	0.5	0.88	0.12	0.24
RXCJ0005.3+1612	2.88	10.0	1.67	7.0	5.0	2.5	0.78	0.14	0.18
RXCJ0006.3+1052	4.05	10.0	2.25	3.8	1.0	0.5	0.84	0.14	-0.16
RXCJ0011.7+3225	4.75	12.5	1.96	10.1	1.0	1.0	0.67	0.09	-2.10
RXCJ0016.7+0646	0.59	8.5	1.07	6.0	4.0	1.5	0.59	0.19	-1.04
RXCJ0019.6+2517	2.60	9.0	1.70	1.6	0.5	0.0	0.92	0.25	0.69
RXCJ0020.1+0005	1.08	3.0	0.79	0.2	0.5	0.0	0.20	0.31	-1.49
RXCJ0020.6+2840	2.68	12.5	1.75	13.9	2.5	2.0	0.59	0.11	-2.00
RXCJ0021.5+2803	1.80	11.0	1.55	3.6	0.5	0.5	1.05	0.19	1.11
RXCJ0024.5+3312	5.10	8.0	2.20	2.1	1.5	1.0	0.63	0.18	-1.23
RXCJ0027.8+2616	12.93	6.0	2.21	0.9	0.5	0.0	0.78	0.21	0.05
RXCJ0039.6+2114	0.36	6.5	0.63	1.4	0.0	0.0	0.81	0.24	0.34
RXCJ0040.4+2933	1.80	14.0	1.54	14.6	2.5	2.0	0.66	0.11	-1.74
RXCJ0041.7+2124	1.82	9.0	1.34	3.7	6.0	1.5	0.47	0.15	-1.70
RXCJ0058.9+2657	0.43	11.0	0.80	16.4	6.0	4.5	1.22	0.16	0.82
RXCJ0105.0+0201	4.38	7.5	1.88	3.8	2.0	1.0	1.23	0.30	1.12
RXCJ0106.8+0103	8.65	5.5	1.64	0.4	0.0	0.0	0.68	0.12	-0.22
RXCJ0108.1+0210	0.37	11.5	0.83	12.5	3.5	2.0	0.61	0.15	-0.53
RXCJ0110.0+1358	0.14	7.5	0.69	1.7	0.0	0.0	0.82	0.25	0.19
RXCJ0110.9+3308	0.04	9.5	0.28	4.0	1.5	0.5	0.96	0.15	0.58
RXCJ0112.2+3302	1.08	4.5	0.80	1.8	1.5	1.0	0.89	0.19	0.09
RXCJ0113.0+1531	0.37	11.0	0.79	7.1	6.0	4.0	1.02	0.17	1.14
RXCJ0114.9+0021	0.92	24.0	1.74	20.9	6.0	5.0	0.44	0.10	-2.82
RXCJ0121.9+0021	1.85	6.5	1.50	2.7	6.0	0.0	1.01	0.34	0.82
RXCJ0123.1+3327	0.04	11.0	0.29	3.6	1.0	1.0	1.00	0.08	1.89
RXCJ0125.5+0145	0.06	11.0	0.34	7.2	2.0	1.0	0.80	0.13	0.79
RXCJ0142.0+2130	0.69	6.5	0.70	1.3	0.5	0.5	1.07	0.15	0.60
RXCJ0152.7+0100	9.37	8.5	2.35	3.4	1.5	1.0	0.42	0.13	-1.93
RXCJ0152.7+3609	0.81	38.0	1.05	30.0	4.0	3.5	0.90	0.05	0.79
RXCJ0152.9+3732	7.71	3.5	1.15	0.2	1.0	0.5	1.21	0.23	0.63
RXCJ0155.1+3355	1.90	9.0	1.18	5.7	1.5	1.0	0.72	0.19	-0.77
RXCJ0200.2+3126	0.04	5.5	0.16	1.2	0.5	0.5	0.96	0.16	0.64
RXCJ0209.5+1946	1.00	10.5	1.08	4.4	3.5	1.0	0.74	0.16	-1.21
RXCJ0228.1+2811	0.30	12.5	0.72	7.0	4.0	2.5	0.92	0.21	0.00
RXCJ0246.0+3653	1.36	16.5	1.29	26.3	3.5	3.0	0.77	0.08	-1.60
RXCJ0255.8+0918	0.07	6.0	0.26	0.1	0.0	0.0	0.95	0.17	-0.02
RXCJ0257.8+1302	6.79	17.5	1.95	30.0	3.0	2.5	0.85	0.07	-1.40
RXCJ0258.9+1334	11.76	25.5	2.90	30.0	2.5	2.5	0.99	0.04	1.13
RXCJ0301.6+0155	6.08	6.0	1.35	0.2	0.0	0.0	0.99	0.17	0.43
RXCJ0311.5+0714	1.47	3.0	0.59	2.9	1.5	0.5	0.63	0.19	-1.74
RXCJ0313.3+2624	2.04	5.0	1.10	1.6	0.5	0.5	0.48	0.20	-2.37
RXCJ0338.6+0958	4.21	16.5	0.94	30.0	1.0	1.0	0.96	0.02	-0.48
RXCJ0341.2+1524	0.73	17.5	0.90	21.2	3.5	3.0	1.08	0.12	0.27
RXCJ0352.9+1941	3.96	9.0	1.42	2.3	0.5	0.5	1.00	0.11	0.35
RXCJ0404.6+1109	10.10	4.5	1.63	1.4	1.5	0.5	0.76	0.22	-0.91
RXCJ0413.4+1028	13.32	15.5	2.06	18.1	1.0	1.0	1.02	0.05	0.72
RXCJ0419.6+0224	0.28	30.0	0.63	25.2	3.0	2.5	1.02	0.06	0.79
RXCJ0439.0+0520	8.47	12.5	3.25	4.2	1.0	0.5	0.88	0.13	-0.47
RXCJ0439.0+0715	11.38	6.0	1.75	2.3	0.5	0.5	1.03	0.14	0.37
RXCJ0448.0+1037	0.84	6.5	0.91	1.9	0.5	0.0	0.97	0.26	0.03
RXCJ0448.2+0952	0.00	5.5	0.00	3.0	1.0	0.5	1.10	0.18	0.21
RXCJ0454.1+0255	14.52	12.5	3.20	10.5	1.5	1.0	0.72	0.10	-1.99
RXCJ0459.1+0846	1.66	8.5	1.29	5.2	1.5	1.0	0.67	0.20	-1.42
RXCJ0503.1+0607	1.77	10.0	1.32	9.1	2.5	1.5	1.07	0.15	0.41
RXCJ0506.9+0257	1.47	4.5	0.91	1.5	2.5	0.5	0.88	0.25	-0.20
RXCJ0618.5+6724	1.55	7.0	1.14	1.7	1.0	0.5	0.86	0.18	-0.30
RXCJ0704.4+6318	2.94	12.5	1.81	8.2	2.0	1.5	0.56	0.10	-2.82
RXCJ0708.1+7151	1.40	8.5	1.31	5.6	1.5	1.0	0.90	0.18	0.44
RXCJ0716.7+5324	0.76	13.5	1.36	4.9	3.5	1.5	0.53	0.17	-2.18
RXCJ0721.3+5547	1.41	17.0	1.06	26.8	3.5	3.0	0.88	0.08	0.16
RXCJ0724.9+6658	0.89	10.5	1.37	2.6	3.0	1.0	0.50	0.19	-1.61
RXCJ0726.0+4122	2.16	10.0	1.62	2.1	0.5	0.5	0.99	0.15	0.60
RXCJ0728.9+2935	6.36	4.5	1.73	0.5	0.5	0.0	0.92	0.36	0.12
RXCJ0729.7+7915	0.93	6.5	1.01	1.1	0.5	0.0	0.62	0.17	-0.87
RXCJ0732.3+3137	9.84	9.5	2.15	4.3	0.5	0.5	0.75	0.08	-1.04
RXCJ0736.4+3925	4.49	9.0	1.52	2.5	0.5	0.5	0.67	0.09	-2.42
RXCJ0737.6+5920	0.09	13.0	0.81	1.5	4.0	0.5	1.27	0.52	0.32
RXCJ0740.9+5525	0.88	14.5	0.81	17.8	1.5	1.5	0.86	0.05	0.86
RXCJ0741.5+2557	1.04	3.0	0.64	1.1	2.5	0.5	0.59	0.26	-0.92

Table 5—*Continued*

name	L_x	R_x (′)	R_x (Mpc)	P_{ext}	r_c	r_{min}	HR	err	ΔHR
RXCJ0741.7+7414	7.94	5.5	1.47	1.5	0.0	0.0	0.72	0.11	-0.60
RXCJ0746.6+3100	0.31	7.5	0.69	2.5	5.0	0.5	1.01	0.35	0.44
RXCJ0748.1+1832	0.20	9.5	0.62	6.9	2.0	1.5	1.07	0.23	0.94
RXCJ0751.3+5012	0.14	15.0	0.57	9.4	2.5	2.0	1.05	0.13	1.23
RXCJ0756.9+3839	3.17	7.5	2.03	1.5	0.5	0.0	0.84	0.23	-0.02
RXCJ0758.3+2640	2.43	3.5	0.98	0.6	0.0	0.0	0.78	0.28	0.04
RXCJ0759.7+5400	2.01	10.5	1.59	4.8	1.5	1.0	0.66	0.14	-0.74
RXCJ0800.9+3602	8.63	6.5	2.09	0.5	0.5	0.5	0.63	0.13	-1.56
RXCJ0804.3+4646	2.51	9.0	2.17	1.7	1.0	0.0	1.66	0.32	0.59
RXCJ0805.7+4541	1.53	6.5	1.23	1.0	0.5	0.0	0.75	0.22	-0.36
RXCJ0811.0+1644	0.66	10.0	1.38	2.0	6.0	0.0	0.15	0.22	-2.76
RXCJ0811.1+7002	8.97	7.5	2.05	1.6	0.5	0.5	0.70	0.13	-0.43
RXCJ0821.0+0751	1.86	5.5	0.88	2.3	0.5	0.5	0.75	0.16	1.50
RXCJ0822.1+4705	5.26	8.0	1.47	3.5	0.5	0.5	0.81	0.10	0.43
RXCJ0825.5+4707	5.13	14.5	2.60	12.4	3.0	2.0	0.66	0.15	-0.92
RXCJ0825.7+8218	4.20	11.0	2.79	3.1	1.0	0.5	0.90	0.22	1.01
RXCJ0828.6+3025	0.78	13.5	1.09	15.6	3.5	3.0	0.84	0.13	0.54
RXCJ0830.9+6551	15.69	10.5	2.48	21.5	2.0	1.5	0.79	0.07	-0.13
RXCJ0840.5+0543	5.03	4.0	1.22	1.5	0.5	0.5	0.59	0.23	-0.77
RXCJ0842.9+3621	19.15	7.0	2.22	1.3	0.5	0.5	0.81	0.11	0.66
RXCJ0844.9+4258	0.16	5.5	0.47	0.4	0.0	0.0	1.15	0.26	1.30
RXCJ0847.7+7741	6.17	6.5	1.96	3.5	2.0	1.0	0.71	0.24	0.66
RXCJ0850.2+3603	17.94	18.0	6.75	2.6	1.5	1.0	0.45	0.20	-1.20
RXCJ0856.1+3756	15.76	9.5	3.71	1.2	2.0	0.5	0.57	0.22	-0.48
RXCJ0909.1+1059	8.54	10.0	2.30	8.7	1.5	1.5	0.82	0.14	0.78
RXCJ0917.8+5143	12.11	9.0	2.41	4.3	0.5	0.5	0.62	0.11	1.89
RXCJ0920.0+0102	0.01	3.5	0.10	0.7	1.0	0.5	1.06	0.36	0.82
RXCJ0920.4+3030	7.06	7.0	2.29	1.3	2.0	0.5	0.46	0.32	-0.23
RXCJ0921.1+4538	2.20	4.0	0.92	0.3	0.0	0.0	0.42	0.17	-0.24
RXCJ0924.0+1410	5.91	12.5	2.37	6.0	1.0	1.0	0.64	0.10	-1.01
RXCJ0928.6+3747	4.61	9.0	2.63	0.4	0.0	0.0	0.10	0.16	-1.98
RXCJ0938.2+7553	1.17	7.5	1.54	1.6	1.5	0.0	0.22	0.27	-1.28
RXCJ0942.2+1522	3.70	7.0	1.55	6.4	2.0	1.0	0.70	0.16	-0.19
RXCJ0943.1+4659	7.27	4.0	1.56	0.8	0.0	0.0	0.44	0.25	0.18
RXCJ0944.0+6424	1.47	10.0	1.72	1.3	1.0	0.5	1.05	0.32	0.53
RXCJ0949.8+1707	21.95	5.0	1.89	3.3	1.0	0.5	0.85	0.13	1.15
RXCJ0958.1+2346	2.04	11.0	2.22	4.2	2.0	1.0	0.18	0.18	-2.79
RXCJ1000.5+4409	2.84	5.0	1.04	2.9	0.5	0.5	0.34	0.12	-0.06
RXCJ1002.6+3241	0.54	10.0	0.80	14.4	3.0	2.5	0.60	0.16	0.77
RXCJ1003.0+3254	8.29	4.5	1.77	0.6	1.0	0.5	0.90	0.40	1.06
RXCJ1006.6+2554	2.01	5.5	0.92	0.9	0.5	0.0	0.69	0.15	0.15
RXCJ1009.3+7110	5.00	11.0	2.71	1.2	0.5	0.5	0.82	0.21	0.19
RXCJ1016.6+2448	0.78	10.0	1.23	3.5	1.0	1.0	0.58	0.17	-0.08
RXCJ1017.5+5934	21.56	15.5	5.61	3.9	1.0	0.5	0.09	0.14	-1.56
RXCJ1019.9+4059	1.12	8.0	1.10	4.7	1.5	1.0	0.31	0.16	-0.32
RXCJ1022.0+3830	0.35	13.0	1.02	5.4	2.0	1.0	0.76	0.23	1.41
RXCJ1023.3+5948	2.28	5.0	1.29	1.3	1.0	0.5	0.37	0.21	0.63
RXCJ1023.6+0411	29.91	11.5	3.68	1.2	0.0	0.0	0.62	0.07	-0.77
RXCJ1023.6+4907	6.88	9.5	1.88	12.1	1.5	1.5	0.29	0.08	-0.55
RXCJ1025.9+1241	4.87	7.0	1.38	5.4	0.0	0.0	0.82	0.10	0.08
RXCJ1031.7+3502	5.35	12.5	2.23	5.7	1.0	0.5	0.33	0.10	-2.03
RXCJ1034.9+3041	3.40	6.0	1.17	3.4	1.0	0.5	0.53	0.12	0.12
RXCJ1040.7+3956	6.16	6.5	1.24	5.3	0.5	0.5	0.31	0.08	-1.24
RXCJ1109.3+4133	1.06	6.5	0.76	6.5	1.5	1.0	0.42	0.12	-0.51
RXCJ1109.7+2145	0.17	13.5	0.71	3.0	4.0	1.5	0.27	0.17	-1.12
RXCJ1111.6+4050	2.01	13.5	1.63	15.2	2.5	2.0	0.91	0.18	2.34
RXCJ1113.3+1735	6.73	6.0	1.35	1.9	0.0	0.0	0.37	0.11	-0.46
RXCJ1114.3+5823	5.92	11.5	2.98	0.0	0.0	0.0	0.31	0.11	0.73
RXCJ1115.5+5426	0.71	15.0	1.61	11.3	4.0	2.5	0.65	0.24	1.52
RXCJ1121.7+0249	0.53	11.5	0.87	8.3	6.0	5.0	0.84	0.19	0.17
RXCJ1122.2+6712	0.13	4.0	0.35	0.7	0.5	0.5	-0.04	0.13	-3.17
RXCJ1123.2+1935	1.75	9.0	1.38	4.9	1.5	0.5	0.17	0.13	-2.41
RXCJ1123.9+2129	6.52	7.0	1.71	6.4	1.5	1.0	0.35	0.12	-0.57
RXCJ1131.3+3334	4.39	6.5	1.76	0.4	0.0	0.0	0.55	0.19	-0.09
RXCJ1132.3+5558	0.51	7.0	0.59	9.2	3.0	2.0	0.65	0.15	2.23
RXCJ1143.5+4623	5.02	10.0	1.68	2.2	1.0	0.0	0.60	0.23	0.07
RXCJ1149.5+2223	1.73	5.5	1.27	0.4	0.5	0.0	0.52	0.23	-0.35
RXCJ1155.3+2324	10.91	12.5	2.46	11.1	1.0	1.0	0.44	0.06	-0.58
RXCJ1156.9+2415	2.42	4.5	0.87	3.0	1.0	1.0	0.63	0.14	0.80
RXCJ1157.3+3336	7.23	10.5	2.79	6.8	2.0	1.0	0.30	0.13	2.26
RXCJ1200.0+1122	1.04	1.0	0.26	0.9	0.0	0.0	0.50	0.43	0.00

TABLE 5—*Continued*

name	L_x	R_x (′)	R_x (Mpc)	P_{ext}	r_c	r_{min}	HR	err	ΔHR
RXCJ1200.4+0320	6.72	13.0	2.43	16.1	2.5	2.0	0.46	0.09	-0.70
RXCJ1201.3+2306	7.99	6.5	2.01	2.0	1.0	0.5	0.32	0.15	-1.91
RXCJ1201.9+5802	1.35	11.5	1.74	3.4	2.5	1.0	0.70	0.25	0.97
RXCJ1203.0+2836	1.86	5.0	0.94	3.6	1.5	1.0	0.65	0.19	0.79
RXCJ1204.0+2807	1.63	6.0	1.31	1.2	0.5	0.0	0.71	0.27	0.80
RXCJ1204.4+0154	0.28	17.0	0.56	25.2	2.0	2.0	0.71	0.09	2.09
RXCJ1204.9+2237	1.88	4.5	1.33	0.8	1.0	0.0	0.48	0.33	-0.24
RXCJ1205.2+3920	0.63	14.0	0.87	8.4	1.0	1.0	0.91	0.11	3.15
RXCJ1206.9+7139	2.63	8.0	1.96	5.2	1.5	1.0	0.59	0.24	0.52
RXCJ1210.0+0630	0.00	7.5	0.00	3.8	1.5	0.0	0.26	0.24	-0.77
RXCJ1210.3+0523	1.40	13.0	1.50	11.5	2.5	2.0	0.49	0.13	0.51
RXCJ1217.6+0339	5.17	16.0	1.88	30.0	2.5	2.5	0.38	0.06	-1.65
RXCJ1218.4+4013	7.13	6.5	2.16	0.5	0.5	0.0	1.07	0.19	2.36
RXCJ1223.1+1037	0.20	10.0	0.43	4.2	0.5	0.5	0.86	0.10	2.84
RXCJ1225.2+3213	0.54	5.5	0.51	0.7	0.0	0.0	0.59	0.12	1.41
RXCJ1227.4+0849	0.89	7.5	1.01	2.7	1.5	1.0	0.67	0.33	0.52
RXCJ1227.8+6322	2.15	6.0	1.20	4.1	1.0	0.5	0.73	0.21	0.95
RXCJ1229.7+0759	0.01	14.0	0.08	30.0	2.0	1.5	0.64	0.06	2.85
RXCJ1229.9+1147	1.12	8.0	1.03	2.6	0.0	0.0	0.80	0.65	0.29
RXCJ1230.7+3439	9.29	7.5	2.63	3.7	1.5	1.0	0.29	0.16	-0.79
RXCJ1231.3+8225	3.69	11.0	2.84	4.6	1.0	0.0	0.56	0.17	-1.79
RXCJ1236.9+6311	11.52	9.0	2.98	2.5	0.5	0.5	0.47	0.18	-0.09
RXCJ1242.8+0241	0.01	22.0	0.12	7.8	0.0	0.0	0.62	0.09	1.32
RXCJ1243.3+2716	3.55	7.0	1.74	2.4	1.0	0.5	0.23	0.17	-0.80
RXCJ1243.6+1133	0.00	7.0	0.05	1.2	0.5	0.5	0.65	0.10	1.14
RXCJ1255.5+3521	1.15	5.0	1.07	1.6	1.0	0.5	0.70	0.38	0.81
RXCJ1257.3+6930	3.71	8.5	2.35	1.9	1.0	0.5	0.01	0.13	-3.70
RXCJ1259.7+2756	7.01	70.0	2.71	30.0	6.0	6.0	0.23	0.01	-6.20
RXCJ1303.0+5756	2.45	4.5	1.12	1.8	1.0	0.5	0.11	0.17	-1.63
RXCJ1303.7+1916	1.79	15.5	1.56	14.9	2.0	1.5	0.68	0.12	0.76
RXCJ1304.4+3335	4.39	5.5	1.33	3.1	1.5	1.0	0.25	0.15	-0.51
RXCJ1305.9+3054	5.58	9.0	2.14	5.9	1.5	1.0	0.21	0.11	-1.08
RXCJ1306.9+4633	8.79	9.5	2.62	11.3	2.0	1.5	0.23	0.11	-1.69
RXCJ1311.7+2201	1.67	4.5	1.02	1.4	1.0	0.0	0.31	0.16	-1.35
RXCJ1314.2+4123	2.66	5.0	1.27	2.8	1.5	0.5	0.23	0.17	-1.04
RXCJ1315.1+5149	8.66	5.5	1.75	3.7	1.0	0.5	0.41	0.14	0.21
RXCJ1320.0+7003	9.70	6.0	2.08	5.2	1.0	0.5	0.06	0.11	-3.47
RXCJ1320.9+3354	2.82	5.5	1.30	2.8	1.5	1.0	0.21	0.15	-0.72
RXCJ1322.8+3138	7.02	5.0	1.68	4.1	2.5	1.0	0.34	0.17	-0.14
RXCJ1324.1+1358	0.07	11.0	0.42	2.6	6.0	0.5	0.31	0.17	-1.12
RXCJ1325.8+5919	3.16	7.5	1.55	3.7	0.5	0.5	0.61	0.14	0.78
RXCJ1326.2+0013	1.65	9.0	1.13	6.5	1.5	0.5	0.53	0.12	0.18
RXCJ1332.7+5032	18.29	11.5	3.64	7.0	5.5	3.0	0.72	0.18	2.17
RXCJ1332.6+5419	1.25	10.5	1.57	1.6	1.0	0.5	0.26	0.18	-0.84
RXCJ1335.3+4059	13.85	10.5	2.91	13.7	1.5	1.0	0.26	0.08	-0.21
RXCJ1336.1+5912	2.62	16.5	1.79	30.0	2.5	2.0	0.43	0.06	-1.56
RXCJ1339.5+1830	0.68	3.0	0.49	0.4	1.0	0.5	-0.12	0.16	-3.83
RXCJ1341.8+2622	2.83	16.0	1.79	17.9	1.5	1.5	0.20	0.06	-2.05
RXCJ1344.3+3906	3.08	4.0	1.32	0.1	0.0	0.0	0.89	0.48	1.23
RXCJ1348.8+2635	9.93	15.5	1.51	30.0	1.5	1.5	0.23	0.02	-7.40
RXCJ1349.0+4918	1.51	8.0	1.77	1.3	1.0	0.0	-0.02	0.19	-2.11
RXCJ1349.3+2806	2.36	12.0	1.38	17.5	2.0	1.5	0.33	0.08	-0.53
RXCJ1351.7+4622	0.55	11.0	1.08	10.1	2.5	2.0	0.55	0.16	0.96
RXCJ1354.0+1455	2.35	8.5	1.51	2.9	1.0	0.5	0.40	0.16	-0.58
RXCJ1354.6+7715	13.57	9.0	3.46	3.2	1.0	0.5	1.00	0.20	1.64
RXCJ1359.8+6231	8.83	5.5	1.90	3.4	1.0	1.0	0.53	0.16	-0.04
RXCJ1400.2+7207	3.52	7.0	1.86	2.5	1.5	0.5	0.09	0.19	-2.19
RXCJ1401.0+0252	32.56	9.0	2.67	3.5	0.5	0.5	0.43	0.07	-2.24
RXCJ1411.4+5212	8.88	2.5	1.03	0.7	0.0	0.0	0.14	0.16	-1.70
RXCJ1413.7+4339	1.77	7.0	0.94	7.3	1.0	0.5	0.14	0.07	-3.20
RXCJ1415.8+0015	0.83	6.0	1.07	1.3	5.5	1.0	0.48	0.24	-0.88
RXCJ1416.5+3045	1.53	4.5	1.08	1.4	1.0	0.5	0.51	0.27	0.42
RXCJ1418.9+4903	6.87	6.5	2.06	0.3	1.0	0.0	0.16	0.16	-2.30
RXCJ1421.5+4933	1.48	12.0	1.33	10.4	1.0	1.0	0.50	0.11	-0.26
RXCJ1421.6+3717	5.99	9.5	2.24	4.8	1.0	1.0	0.12	0.09	-2.05
RXCJ1423.1+2615	0.11	5.5	0.34	0.9	0.5	0.0	0.26	0.16	-1.29
RXCJ1423.8+4015	0.68	5.5	0.69	2.3	0.5	0.5	0.06	0.11	-2.35
RXCJ1425.3+6311	4.58	8.0	1.55	10.8	2.0	1.5	0.70	0.12	1.63
RXCJ1426.0+3749	15.91	9.5	2.15	9.7	0.5	0.5	0.22	0.05	-1.92
RXCJ1428.4+5652	1.72	11.5	1.77	8.4	2.5	2.0	0.19	0.13	-1.76
RXCJ1431.1+2538	2.18	10.0	1.36	4.7	0.5	0.5	0.69	0.10	1.32

Table 5—*Continued*

name	L_x	R_x (′)	R_x (Mpc)	P_{ext}	r_c	r_{min}	HR	err	ΔHR
RXCJ1440.6+0328	0.35	15.5	0.68	13.0	4.0	3.0	0.47	0.09	-1.89
RXCJ1442.3+2218	2.24	6.0	0.81	4.8	1.0	0.5	0.63	0.10	0.09
RXCJ1447.4+0827	7.87	6.0	1.50	0.4	0.0	0.0	0.50	0.11	-0.60
RXCJ1452.9+5802	13.42	9.5	3.24	4.1	1.0	0.5	0.17	0.14	-2.03
RXCJ1452.9+1641	0.48	11.0	0.79	6.9	2.0	1.0	0.44	0.12	-0.65
RXCJ1453.1+2153	1.60	8.0	1.36	2.0	0.5	0.0	0.55	0.19	-0.64
RXCJ1454.4+1622	0.17	9.5	0.70	1.6	2.0	1.0	0.03	0.19	-2.57
RXCJ1454.5+1838	1.46	14.5	1.34	2.7	0.5	0.5	0.27	0.07	-4.86
RXCJ1457.2+2220	13.73	5.5	1.65	3.3	0.5	0.5	0.70	0.11	-0.19
RXCJ1501.2+0141	0.02	12.5	0.14	14.0	1.0	1.0	0.88	0.06	1.46
RXCJ1501.3+4220	7.96	7.0	2.27	5.0	1.0	0.5	0.05	0.13	-3.03
RXCJ1506.4+0136	0.01	10.5	0.11	5.9	0.5	0.5	1.04	0.08	2.55
RXCJ1510.1+3330	6.49	13.5	2.20	20.4	1.5	1.5	0.36	0.06	-1.27
RXCJ1511.1+1802	1.52	5.5	0.92	5.1	2.0	1.0	0.91	0.28	0.82
RXCJ1512.6+3451	1.35	3.5	0.71	0.4	0.5	0.0	0.40	0.16	-0.20
RXCJ1516.7+0701	2.58	17.0	0.99	30.0	1.5	1.5	0.56	0.04	-2.93
RXCJ1518.7+0613	3.91	8.0	1.20	2.0	0.5	0.5	0.35	0.07	-5.27
RXCJ1520.9+4840	3.05	9.0	1.41	4.1	0.5	0.5	0.31	0.09	-2.10
RXCJ1521.8+0742	2.70	15.5	1.11	30.0	1.5	1.5	0.73	0.05	0.50
RXCJ1522.4+2742	4.75	12.0	1.34	30.0	2.5	2.5	0.72	0.06	0.83
RXCJ1523.0+0836	1.94	13.5	0.79	30.0	3.0	2.5	0.63	0.05	-0.99
RXCJ1528.0+6956	1.57	11.5	1.89	7.1	1.5	1.0	0.71	0.17	0.54
RXCJ1539.7+3424	8.68	10.5	2.92	3.6	1.5	1.0	0.59	0.19	0.16
RXCJ1539.8+3043	3.81	7.0	1.02	4.0	0.5	0.5	0.74	0.11	1.15
RXCJ1553.3+5107	2.81	6.0	1.70	0.7	0.5	0.5	0.08	0.16	-1.98
RXCJ1554.2+3237	0.60	9.5	1.10	2.2	1.5	0.5	0.64	0.19	0.05
RXCJ1556.1+6621	9.31	8.5	2.40	3.3	0.5	0.5	0.60	0.09	-0.77
RXCJ1557.7+3530	3.28	7.0	1.47	1.3	0.5	0.0	0.64	0.19	0.62
RXCJ1558.3+2713	20.52	28.0	3.76	30.0	2.0	2.0	0.72	0.03	-2.09
RXCJ1601.3+5354	2.30	11.5	1.79	29.4	3.5	3.0	0.52	0.13	1.35
RXCJ1604.5+1743	0.98	20.0	1.21	22.3	3.0	2.5	0.76	0.08	0.43
RXCJ1604.9+2355	0.55	20.0	1.08	27.3	2.5	2.5	1.15	0.13	1.30
RXCJ1605.5+7208	1.88	10.5	1.96	3.6	0.5	0.5	0.74	0.13	0.37
RXCJ1615.5+1927	0.11	10.5	0.54	5.9	6.0	3.5	0.88	0.22	0.40
RXCJ1617.5+3458	0.33	21.0	1.09	18.0	6.0	5.5	0.38	0.10	-0.74
RXCJ1618.2+2938	4.30	4.5	1.48	1.1	0.5	0.5	0.80	0.24	0.54
RXCJ1620.5+2953	3.06	14.0	2.02	28.2	2.0	2.0	0.77	0.09	1.59
RXCJ1624.2+4114	4.10	6.0	1.42	8.4	1.5	1.0	0.17	0.10	-1.56
RXCJ1626.9+5528	2.06	6.0	1.10	11.4	1.5	1.0	0.33	0.12	-1.79
RXCJ1627.3+4240	0.12	11.0	0.58	2.8	1.0	0.5	0.46	0.17	0.77
RXCJ1627.6+4055	0.13	15.5	0.77	3.5	1.5	1.0	0.36	0.18	0.16
RXCJ1628.6+3932	3.77	39.5	1.96	30.0	2.0	2.0	0.25	0.01	-2.70
RXCJ1629.7+5831	2.13	7.0	1.30	5.6	1.0	0.5	0.27	0.10	-2.46
RXCJ1632.7+0534	23.43	9.5	1.96	7.0	0.5	0.5	0.99	0.04	2.87
RXCJ1634.6+6738	1.48	5.5	1.22	6.8	1.5	1.0	1.14	0.23	0.83
RXCJ1635.8+6612	8.16	9.0	2.03	24.2	1.0	1.0	0.50	0.05	-4.03
RXCJ1640.3+4642	24.33	15.5	4.30	24.6	1.0	1.0	0.68	0.08	2.29
RXCJ1643.2+5114	3.23	7.0	1.77	3.0	1.0	0.5	0.25	0.12	-3.09
RXCJ1643.3+2131	1.65	6.0	1.25	3.9	4.0	1.5	0.74	0.17	-0.58
RXCJ1644.9+0140	0.00	5.5	0.00	0.5	1.0	0.5	1.39	0.55	0.28
RXCJ1647.4+0441	0.00	4.0	0.00	0.8	1.0	0.0	1.00	0.24	0.49
RXCJ1651.1+0459	5.49	6.5	1.36	3.2	0.5	0.5	0.85	0.09	-0.40
RXCJ1652.2+4449	4.06	9.5	2.19	7.7	2.5	1.5	0.24	0.13	-2.02
RXCJ1652.9+4009	3.00	9.5	1.94	4.4	1.5	1.0	0.35	0.17	-0.95
RXCJ1654.3+2334	0.36	10.0	0.91	4.4	1.5	1.0	0.89	0.23	0.32
RXCJ1654.7+5854	0.70	8.5	1.11	10.6	1.5	1.5	0.25	0.13	-2.51
RXCJ1658.0+2751	0.36	21.5	1.19	17.7	5.0	4.0	0.71	0.10	-1.27
RXCJ1659.6+6826	0.21	14.5	1.17	13.4	2.0	1.5	1.33	0.26	0.90
RXCJ1659.7+3236	2.08	11.0	1.64	8.7	1.0	1.0	1.01	0.12	3.52
RXCJ1700.7+6412	3.04	7.0	1.92	8.9	1.5	1.0	0.30	0.10	-3.21
RXCJ1702.7+3403	7.39	12.5	1.77	30.0	1.5	1.5	0.50	0.04	-1.49
RXCJ1703.8+7838	7.01	33.5	3.08	30.0	3.5	3.5	0.83	0.02	2.46
RXCJ1709.8+3426	3.36	14.5	1.77	30.0	3.5	3.0	0.60	0.06	-0.47
RXCJ1711.0+3941	0.57	6.0	0.61	14.9	2.0	1.5	0.80	0.11	1.43
RXCJ1712.7+6403	5.77	30.0	3.69	30.0	3.5	3.5	0.61	0.03	-0.60
RXCJ1714.3+4341	0.10	13.5	0.62	6.8	2.0	1.5	0.03	0.09	-6.10
RXCJ1715.2+0309	5.38	7.0	1.54	1.5	0.5	0.5	1.04	0.09	1.49
RXCJ1715.3+5724	0.49	22.0	1.01	30.0	2.0	2.0	0.91	0.06	4.17
RXCJ1717.6+3627	1.75	4.5	1.02	1.9	0.5	0.5	0.80	0.19	0.39
RXCJ1717.8+1940	8.51	12.0	2.80	11.7	1.5	1.5	0.90	0.15	0.29
RXCJ1717.8+3235	1.82	9.0	1.39	8.1	1.5	1.0	0.69	0.10	-0.17

TABLE 5—*Continued*

name	L_x	R_x (′)	R_x (Mpc)	P_{ext}	r_c	r_{min}	HR	err	ΔHR
RXCJ1718.1+5639	3.13	11.0	1.81	12.1	0.5	0.5	0.62	0.06	-1.01
RXCJ1718.1+7801	0.75	15.0	1.38	26.9	3.0	2.5	0.74	0.10	-0.41
RXCJ1720.1+2637	12.34	9.5	2.09	5.9	0.5	0.5	1.00	0.08	2.85
RXCJ1720.1+2740	6.06	8.0	1.75	6.9	1.0	0.5	0.64	0.10	-1.05
RXCJ1722.2+3042	0.12	11.0	0.88	1.8	0.0	0.0	0.70	0.25	-0.07
RXCJ1722.4+3208	20.61	14.5	3.97	9.8	1.0	0.5	0.72	0.09	-0.06
RXCJ1723.3+5658	0.05	9.0	0.41	7.0	1.5	1.0	1.06	0.22	1.33
RXCJ1723.7+8553	7.11	9.5	2.21	17.7	1.5	1.0	0.99	0.09	1.08
RXCJ1730.4+7422	0.84	8.0	1.28	23.3	6.0	6.0	1.00	0.22	1.08
RXCJ1733.0+4345	0.47	17.0	0.86	30.0	1.5	1.5	0.54	0.07	-1.15
RXCJ1735.0+6406	1.84	14.0	2.73	11.3	1.0	1.0	0.45	0.13	-1.70
RXCJ1735.9+1659	0.63	7.5	0.97	2.6	1.0	0.0	0.64	0.19	-1.23
RXCJ1736.3+6803	0.06	18.0	0.75	6.0	5.0	4.5	1.00	0.16	1.22
RXCJ1738.1+6006	0.00	7.5	0.00	2.0	0.5	0.5	1.00	0.19	1.27
RXCJ1740.5+3538	0.49	9.5	0.66	19.9	1.5	1.5	0.63	0.08	-0.17
RXCJ1742.8+3900	0.39	11.0	0.75	10.0	1.0	1.0	1.11	0.11	2.87
RXCJ1744.2+3259	4.37	16.0	1.86	25.7	1.0	1.0	0.82	0.05	1.52
RXCJ1747.2+4512	2.69	6.0	1.27	17.4	3.0	2.0	0.65	0.11	-0.25
RXCJ1749.3+4245	3.27	8.5	2.37	2.1	1.0	0.5	0.59	0.17	-0.64
RXCJ1749.6+5334	0.70	11.5	1.57	11.1	2.5	2.0	0.79	0.19	0.28
RXCJ1750.2+3504	5.57	10.0	2.26	1.6	0.5	0.0	0.65	0.09	-0.57
RXCJ1751.7+2304	0.02	6.0	0.14	3.1	0.5	0.5	0.98	0.10	0.64
RXCJ1753.4+5205	0.61	7.5	1.10	4.9	1.0	1.0	0.80	0.21	0.14
RXCJ1754.0+5805	3.69	10.5	2.90	16.6	2.0	1.5	0.99	0.15	1.43
RXCJ1754.6+6803	1.08	9.0	1.06	30.0	2.0	2.0	1.00	0.65	0.27
RXCJ1755.8+6236	0.09	15.5	0.69	30.0	3.0	2.5	0.88	0.10	1.51
RXCJ1800.5+6913	0.66	17.0	2.12	22.9	1.5	1.5	1.18	0.21	0.90
RXCJ1802.7+4247	0.15	8.5	0.68	3.4	1.5	0.5	0.33	0.15	-2.62
RXCJ1811.0+4954	1.03	17.0	1.36	30.0	3.0	3.0	0.69	0.06	-1.89
RXCJ1814.2+6939	0.34	6.5	0.85	11.2	1.5	1.0	0.96	0.17	0.64
RXCJ1816.4+5314	4.41	7.0	2.20	4.2	1.5	1.0	0.81	0.19	0.39
RXCJ1819.8+3307	4.16	5.0	1.58	1.6	1.0	0.5	0.93	0.27	0.41
RXCJ1819.9+5710	0.00	11.0	0.00	15.8	2.0	1.5	1.18	0.21	1.15
RXCJ1820.1+6857	0.69	7.0	0.92	28.4	1.5	1.5	1.32	0.14	0.97
RXCJ1827.2+6134	0.85	11.0	1.64	11.0	2.0	1.5	0.60	0.17	-1.25
RXCJ1832.5+6449	2.23	10.5	2.28	26.9	1.5	1.5	1.00	0.16	0.95
RXCJ1832.5+6848	5.98	5.5	1.42	6.6	0.5	0.5	0.83	0.06	-0.85
RXCJ1834.1+7057	0.69	9.0	1.13	30.0	2.5	2.0	0.93	0.12	0.54
RXCJ1836.5+6344	0.41	12.5	0.97	30.0	2.5	2.0	0.69	0.06	-2.38
RXCJ1843.6+5021	1.44	6.0	1.00	0.9	0.5	0.5	0.89	0.14	0.25
RXCJ1844.0+4533	1.36	11.0	1.51	6.9	1.0	1.0	0.89	0.14	-0.01
RXCJ1847.2+7320	1.49	7.5	1.22	6.3	0.5	0.5	0.95	0.10	0.52
RXCJ1852.1+5711	1.95	12.0	1.91	5.7	1.0	1.0	0.63	0.12	-1.83
RXCJ1853.9+6822	2.09	13.5	1.87	30.0	1.5	1.5	0.83	0.09	-0.24
RXCJ1854.1+6858	3.95	6.0	1.73	2.1	0.5	0.5	0.77	0.15	-0.54
RXCJ1900.4+6958	1.73	11.5	1.52	30.0	3.0	3.0	0.80	0.09	-1.09
RXCJ1908.3+6903	3.65	7.0	1.84	4.3	0.5	0.5	1.00	0.27	0.36
RXCJ1910.4+6741	6.04	12.5	3.65	5.3	1.0	0.5	0.83	0.18	-0.27
RXCJ1920.1+6318	0.00	11.5	0.00	10.3	4.0	2.5	1.38	0.36	0.32
RXCJ1921.3+7433	0.00	11.0	0.00	17.6	2.0	1.5	0.91	0.13	-0.07
RXCJ1927.5+6549	2.61	6.5	1.58	11.7	1.5	1.5	1.21	0.16	0.58
RXCJ1935.3+6734	2.52	7.5	1.69	10.5	1.5	1.0	0.90	0.15	-0.12
RXCJ2035.7+0046	0.00	7.5	0.00	2.1	4.0	0.0	0.64	0.33	-0.83
RXCJ2041.7+0721	0.15	3.5	0.35	1.8	3.0	1.0	0.75	0.22	-0.78
RXCJ2050.7+0123	5.88	4.5	1.58	1.6	1.0	0.0	1.11	0.27	0.32
RXCJ2051.1+0216	7.36	8.5	2.92	0.6	0.0	0.0	1.15	0.21	0.36
RXCJ2057.5+1334	1.99	4.5	1.23	1.2	0.5	0.0	0.76	0.34	-0.55
RXCJ2103.8+0437	0.99	4.0	0.90	2.8	6.0	0.0	1.21	0.21	0.46
RXCJ2104.9+1401	3.66	6.5	1.41	1.9	1.5	1.0	1.17	0.10	0.90
RXCJ2113.8+0233	1.42	18.0	1.42	25.6	4.0	3.5	0.68	0.08	-2.68
RXCJ2129.6+0005	16.70	8.0	2.26	3.0	0.5	0.5	0.66	0.12	-1.12
RXCJ2151.4+1347	4.10	4.5	1.17	0.9	0.5	0.0	1.04	0.20	0.75
RXCJ2153.5+1741	25.15	11.0	3.09	3.2	0.5	0.5	1.03	0.07	1.48
RXCJ2155.6+1232	5.51	6.5	1.60	2.0	0.5	0.5	0.99	0.13	0.81
RXCJ2200.8+2058	7.68	7.0	1.41	6.8	1.5	1.0	1.00	0.08	1.25
RXCJ2214.8+1350	0.09	14.0	0.59	5.7	4.0	2.0	0.92	0.22	0.36
RXCJ2226.8+2550	3.82	6.0	1.32	3.3	0.5	0.5	1.36	0.17	0.87
RXCJ2228.6+2036	29.62	9.0	3.52	2.6	1.0	0.5	0.59	0.19	-1.22
RXCJ2241.8+1732	8.44	4.0	1.35	1.3	1.0	0.0	0.74	0.20	-0.55
RXCJ2245.0+2637	11.71	5.5	1.83	0.3	0.0	0.0	1.07	0.12	1.19
RXCJ2250.3+1054	2.74	9.0	1.06	13.2	1.5	1.0	0.74	0.07	-1.69

TABLE 5—*Continued*

name	L_x	R_x ($'$)	R_x (Mpc)	P_{ext}	r_c	r_{min}	HR	err	ΔHR
RXCJ2256.8+0530	1.46	10.0	2.50	2.2	0.5	0.0	1.00	0.28	0.48
RXCJ2300.2+2926	0.59	8.0	0.85	3.6	2.5	1.5	0.21	0.12	-5.50
RXCJ2307.0+1631	9.16	8.5	2.51	2.4	1.0	0.5	0.80	0.11	-0.71
RXCJ2307.6+2716	0.78	5.5	0.88	2.9	3.5	1.0	1.37	0.28	0.48
RXCJ2310.4+0734	0.81	17.0	1.17	15.2	5.5	4.0	0.98	0.13	1.14
RXCJ2311.1+1137	4.56	11.0	3.33	1.5	0.5	0.0	1.83	0.34	0.55
RXCJ2311.5+0338	3.48	12.5	2.32	3.1	0.5	0.5	0.97	0.15	0.82
RXCJ2318.5+1842	0.58	10.0	0.66	16.8	2.5	2.0	0.89	0.10	0.75
RXCJ2321.8+1505	2.15	6.0	1.23	1.7	1.0	0.5	0.74	0.19	-0.21
RXCJ2323.6+0908	3.63	4.5	1.14	3.0	1.0	0.5	0.64	0.16	-1.15
RXCJ2325.0+1841	1.49	7.0	1.78	0.2	0.5	0.0	0.81	0.27	0.07
RXCJ2333.8+2140	1.33	13.5	2.03	2.5	1.0	0.5	1.11	0.29	0.70
RXCJ2334.0+0704	0.76	5.0	0.73	3.9	2.0	1.0	0.66	0.19	-1.06
RXCJ2336.5+2108	1.55	10.5	0.94	12.5	1.0	1.0	0.76	0.07	-0.54
RXCJ2337.6+0016	11.60	10.0	3.15	3.0	1.5	1.0	0.55	0.15	-1.45
RXCJ2338.4+2659	0.88	30.5	1.56	30.0	6.0	6.0	0.80	0.05	-0.91
RXCJ2340.5+1029	2.55	5.5	1.29	3.9	1.5	1.0	0.72	0.20	-0.64
RXCJ2341.1+0018	1.03	5.0	0.80	0.0	0.0	0.0	0.76	0.16	0.04
RXCJ2344.9+0911	1.81	31.0	2.02	30.0	3.0	2.5	0.94	0.05	1.80
RXCJ2350.5+2929	3.56	7.5	1.53	1.2	0.5	0.5	0.81	0.16	-0.25
RXCJ2350.8+0609	1.81	13.5	1.20	8.6	1.5	1.0	0.90	0.09	0.18
RXCJ2355.6+1120	1.52	13.5	1.51	11.0	3.0	2.5	0.64	0.12	-1.41
RXCJ2355.8+3423	2.37	10.0	2.03	0.8	0.5	0.0	1.26	0.23	0.49

TABLE 6

ADDITIONAL ACO CLUSTERS DETECTED AS X-RAY SOURCES IN THE 9^h TO 14^h REGION

name	alt.name	RA	DEC	z	ctr	F_x	F_x^*	err	L_x	N_H	ID	ref
RXCJ0913.5+8133	A723	138.3937	81.5528	0.0000	0.18	3.65	3.65	13.2	0.00	2.3		
RXCJ0901.1+6239	A725	135.2982	62.6560	0.0900	0.11	2.32	2.26	18.3	0.80	4.5		1
RXCJ0906.4+1020	A743	136.6097	10.3492	0.0000	0.09	1.89	1.89	18.5	0.00	3.1	?	
RXCJ0907.3+1639	A744	136.8430	16.6566	0.0730	0.09	1.98	1.92	17.9	0.45	3.6		2
RXCJ0909.3+5133	A746	137.3444	51.5629	0.0000	0.14	2.80	2.80	18.3	0.00	1.6		
RXCJ0910.0+3533	A752	137.5187	35.5563	0.0000	0.35	6.92	6.92	9.8	0.00	2.1	?	
RXCJ0913.0+4742	A757	138.2586	47.7059	0.0510	0.23	4.61	4.47	15.0	0.50	1.6		3
RXCJ0920.3+7350	A765	140.0940	73.8367	0.1330	0.09	1.74	1.73	19.5	1.33	2.3		4
RXCJ0919.8+3345	A779	139.9550	33.7603	0.0230	0.21	4.12	2.84	13.4	0.06	1.6		3
RXCJ0928.0+7446	A786	142.0206	74.7828	0.1240	0.12	2.32	2.30	14.7	1.53	2.2		3
RXCJ0922.2+1225	A791	140.5729	12.4304	0.0000	0.08	1.62	1.62	21.8	0.00	3.5		
RXCJ0926.6+1741	A797	141.6697	17.6903	0.1170	0.13	2.79	2.77	26.1	1.64	3.7		5
RXCJ0928.1+2032	A801	142.0325	20.5422	0.1920	0.08	1.77	1.76	21.4	2.80	4.0		3
RXCJ0935.4+0729	A830	143.8705	7.4925	0.2610	0.08	1.62	1.62	39.7	4.76	3.6		6
RXCJ0942.0+0857	A854	145.5149	8.9632	0.2060	0.17	3.46	3.47	16.0	6.29	3.1		3
RXCJ0957.5+1938	A903	149.3946	19.6462	0.0000	0.08	1.71	1.71	23.8	0.00	2.9		
RXCJ0959.7+2223	A908	149.9387	22.3934	0.3900	0.08	1.63	1.64	21.3	10.30	2.8		7
RXCJ1003.1+6709	A910	150.7830	67.1576	0.2060	0.13	2.69	2.69	14.7	4.90	3.7		3
RXCJ1007.8+0031	A933	151.9539	0.5170	0.0960	0.09	1.89	1.84	21.5	0.74	2.9		8
RXCJ1009.0+1400	A937	152.2501	14.0045	0.0000	0.08	1.65	1.65	21.5	0.00	3.8		
RXCJ1012.2+0625	A949	153.0749	6.4216	0.0000	0.12	2.35	2.35	17.9	0.00	2.3		
RXCJ1013.7+1946	A952	153.4298	19.7752	0.0000	0.25	5.14	5.14	18.5	0.00	2.6		
RXCJ1016.2+4108	A958	154.0716	41.1382	0.0000	0.25	4.78	4.78	11.0	0.00	1.2		
RXCJ1016.3+3338	A961	154.0940	33.6347	0.1240	0.19	3.65	3.63	11.9	2.41	1.6		9
RXCJ1017.0+3902	A963	154.2600	39.0484	0.2060	0.25	4.82	4.84	17.9	8.72	1.4		3
RXCJ1022.5+5006	A980	155.6275	50.1017	0.1580	0.29	5.72	5.74	9.2	6.13	1.0		10
RXCJ1025.0+4750	A1003	156.2743	47.8373	0.0520	0.08	1.62	1.21	18.1	0.14	1.2		3
RXCJ1028.3+0346	A1024	157.0884	3.7690	0.0730	0.10	2.16	2.10	20.0	0.49	3.2		4
RXCJ1032.2+4015	A1035	158.0616	40.2647	0.0790	0.30	5.78	5.72	10.4	1.55	1.2	D	5,3
RXCJ1039.4+0510	A1066	159.8661	5.1795	0.0700	0.30	6.20	6.14	17.2	1.30	3.0		3
RXCJ1047.5+1513	A1095	161.8849	15.2329	0.2108	0.09	1.85	1.85	24.2	3.56	2.8		15
RXCJ1048.7+2214	A1100	162.1904	22.2402	0.0450	0.09	1.78	1.34	20.0	0.12	1.8		3
RXCJ1053.8+1650	A1126	163.4514	16.8403	0.0852	0.21	4.19	4.15	19.6	1.31	2.3		3
RXCJ1058.4+5647	A1132	164.6077	56.7917	0.1369	0.40	7.62	7.65	7.3	6.15	0.6		3
RXCJ1058.1+0135	A1139	164.5446	1.5871	0.0380	0.15	3.15	2.38	20.0	0.15	4.0	B	3
RXCJ1100.8+1033	A1142	165.2037	10.5596	0.0353	0.27	5.51	5.12	13.7	0.28	2.8		3
RXCJ1110.5+2842	A1185	167.6357	28.7164	0.0220	0.35	6.99	5.26	11.9	0.11	1.8		3
RXCJ1112.9+1326	A1201	168.2287	13.4448	0.1690	0.17	3.31	3.31	13.1	4.04	1.6		3
RXCJ1113.3+0231	A1205	168.3362	2.5323	0.0780	0.37	7.84	7.78	9.2	2.05	4.4		6
RXCJ1121.5+4803	A1227	170.3977	48.0629	0.1120	0.15	2.96	2.94	15.2	1.60	1.5		3
RXCJ1122.8+0106	A1238	170.7066	1.1076	0.0720	0.11	2.34	2.27	19.6	0.51	3.7		5
RXCJ1125.2+4229	A1253	171.3064	42.4876	0.0000	0.13	2.59	2.59	38.5	0.00	2.0		
RXCJ1128.0+7529	A1255	172.0055	75.4904	0.1650	0.10	2.07	2.06	26.3	2.41	3.8		11,3
RXCJ1126.9+1706	A1264	171.7483	17.1149	0.1270	0.20	3.98	3.96	12.7	2.76	2.5		3
RXCJ1129.8+2347	A1272	172.4682	23.7919	0.1371	0.16	3.09	3.09	26.1	2.51	1.6		15
RXCJ1130.0+3637	A1275	172.5073	36.6303	0.0600	0.14	2.87	2.79	23.6	0.44	2.1		3
RXCJ1130.0+2028	A1278	172.5199	20.4771	0.1290	0.20	4.02	4.01	17.2	2.88	1.8	D	3
RXCJ1133.9+7506	A1301	173.4875	75.1162	0.1220	0.09	1.84	1.82	19.3	1.18	3.8		11,3
RXCJ1133.2+6622	A1302	173.3197	66.3786	0.1160	0.24	4.68	4.66	9.9	2.69	0.9		11,3
RXCJ1132.8+1428	A1307	173.2208	14.4690	0.0834	0.63	12.90	12.90	8.2	3.87	2.8		3
RXCJ1134.8+4903	A1314	173.7103	49.0577	0.0341	0.18	3.57	2.68	14.9	0.14	1.7		3
RXCJ1141.2+1044	A1345	175.3063	10.7413	0.1090	0.10	2.16	2.11	21.0	1.10	3.3	D	3
RXCJ1142.5+5832	A1351	175.6284	58.5389	0.3220	0.10	1.90	1.91	21.9	8.31	1.8		11,3
RXCJ1144.6+6724	A1366	176.1677	67.4099	0.1159	0.25	4.93	4.91	8.8	2.83	1.5		5
RXCJ1144.7+1949	A1367	176.1790	19.8188	0.0276	2.29	46.24	45.83	3.5	1.51	2.5		3
RXCJ1145.3+1529	A1371	176.3440	15.4948	0.0670	0.17	3.51	3.41	14.0	0.67	3.1		3
RXCJ1147.3+5544	A1377	176.8363	55.7433	0.0510	0.18	3.41	3.17	14.8	0.36	1.1		3
RXCJ1149.0+5135	A1387	177.2715	51.5855	0.1320	0.09	1.85	1.85	20.2	1.39	1.6		15
RXCJ1156.0+7325	A1412	179.0181	73.4181	0.0830	0.15	2.94	2.86	11.0	0.87	2.5		11,3
RXCJ1157.4+0503	A1424	179.3696	5.0629	0.0770	0.20	3.98	3.86	13.4	1.00	1.6		3
RXCJ1159.2+4947	A1430	179.8225	49.7937	0.2110	0.15	2.93	2.94	17.0	5.60	2.1		3
RXCJ1200.3+5613	A1436	180.0918	56.2303	0.0650	0.29	5.66	5.49	12.1	1.01	1.3		3
RXCJ1211.0+3519	A1483	182.7585	35.3324	0.1380	0.10	2.06	2.04	22.9	1.69	1.5		13
RXCJ1213.0+3411	A1492	183.2648	34.1869	0.0000	0.10	1.88	1.88	31.3	0.00	1.3	?	
RXCJ1228.8+1924	A1548	187.2201	19.4077	0.1610	0.08	1.65	1.64	39.5	1.86	2.9		3
RXCJ1229.0+4737	A1550	187.2590	47.6251	0.2540	0.10	2.04	2.04	16.2	5.62	1.1		3
RXCJ1230.7+1033	A1553	187.6959	10.5606	0.1650	0.31	6.22	6.24	10.9	7.21	2.1		3
RXCJ1233.9+1511	A1560	188.4935	15.1916	0.0000	0.25	4.94	4.94	16.0	0.00	2.3		
RXCJ1236.4+1631	A1569	189.1003	16.5284	0.0780	0.19	3.91	3.80	23.1	1.01	2.3		3
RXCJ1241.3+1834	A1589	190.3296	18.5711	0.0730	0.37	7.20	7.14	9.3	1.65	1.7		3
RXCJ1247.3+5500	A1616	191.8426	55.0108	0.0830	0.12	2.30	2.23	17.1	0.67	1.5		3

TABLE 6—*Continued*

name	alt.name	RA	DEC	z	ctr	F_x	F_x^*	err	L_x	N_H	ID	ref
RXCJ1310.4+2151	A1686	197.6093	21.8637	0.0000	0.09	1.73	1.73	16.1	0.00	1.9		
RXCJ1311.1+3913	A1691	197.7911	39.2176	0.0720	0.25	4.89	4.75	9.9	1.07	1.1		5
RXCJ1313.1+4616	A1697	198.2768	46.2810	0.1830	0.17	3.24	3.24	16.9	4.67	1.4		3
RXCJ1314.4+6434	A1704	198.6021	64.5779	0.2200	0.17	3.37	3.38	11.2	6.94	1.8		11
RXCJ1320.6+3746	A1715	200.1678	37.7744	0.0000	0.09	1.83	1.83	18.1	0.00	1.1		
RXCJ1323.5+1117	A1728	200.8751	11.2967	0.0000	0.18	3.65	3.65	16.8	0.00	1.9		
RXCJ1326.2+1230	A1735	201.5716	12.5009	0.2040	0.38	7.49	7.54	11.7	13.21	2.0		14
RXCJ1327.3+0337	A1743	201.8401	3.6301	0.0000	0.11	2.16	2.16	19.3	0.00	1.9		
RXCJ1331.5+0451	A1753	202.8878	4.8607	0.0000	0.11	2.28	2.28	21.9	0.00	2.2		
RXCJ1334.1+2013	A1759	203.5290	20.2309	0.1710	0.13	2.61	2.60	15.2	3.28	1.8		3
RXCJ1342.0+0213	A1773	205.5223	2.2261	0.0765	0.29	5.84	5.84	12.9	1.46	1.8		15
RXCJ1353.0+0509	A1809	208.2540	5.1550	0.0788	0.37	7.31	7.24	9.5	1.95	2.0		12,3
RXCJ1358.0+2038	A1825	209.5083	20.6365	0.0620	0.08	1.65	1.24	22.0	0.21	2.4		3
RXCJ1359.2+2758	A1831	209.8230	27.9729	0.0612	0.61	11.87	11.76	8.9	1.91	1.4		3

RA and DEC for J2000; RA in decimal degrees

REFERENCES.—(1) Owen Ledlow & Keel 1995, (2) Stocke et al. 1991, (3) Strubel & Rood 1991, (4) Ledlow & Owen 1995, (5) Slinglend et al. 1998, (6) Quintana & Ramirez 1995, (7) Lin & Daly 1996, (8) Postman, Huchra & Geller 1992, (9) Ebeling et al. 1998, (10) Ebeling et al. 1996, (11) Huchra et al. 1990, (12) Katgert et al. 1996, (13) Appenzeller et al. 1998, (14) Cao et al. 1999, (15) Strubel & Rood 1999.

Table 7

X-ray properties of the additionally found ACO clusters

name	L_x	R_x ($'$)	R_x (Mpc)	KS-prop	r_c	r_c(min)	HR	err	ΔHR
RXCJ0913.5+8133	0.00	12.0	0.00	0.7	0.0	0.0	0.60	0.17	0.03
RXCJ0901.1+6239	0.80	9.5	1.28	1.7	1.0	0.0	0.91	0.28	0.34
RXCJ0906.4+1020	0.00	4.5	0.00	1.2	1.0	0.5	0.45	0.18	-1.38
RXCJ0907.3+1639	0.45	3.5	0.39	0.9	0.5	0.5	0.38	0.15	-2.46
RXCJ0909.3+5133	0.00	9.5	0.00	5.2	5.0	2.0	0.21	0.16	-1.63
RXCJ0910.0+3533	0.00	11.5	0.00	0.8	0.0	0.0	0.04	0.07	-7.40
RXCJ0913.0+4742	0.51	13.0	1.06	5.0	6.0	3.5	0.16	0.13	-2.39
RXCJ0920.3+7350	1.33	8.5	1.58	3.3	0.5	0.0	0.30	0.20	-1.44
RXCJ0919.8+3345	0.07	10.5	0.41	9.1	2.5	1.5	0.20	0.14	-2.01
RXCJ0928.0+7446	1.53	6.0	1.06	1.4	0.5	0.5	0.69	0.19	0.60
RXCJ0922.2+1225	0.00	8.0	0.00	1.7	0.5	0.0	0.40	0.26	-1.29
RXCJ0926.6+1741	1.64	5.0	0.84	0.5	0.0	0.0	1.00	0.27	0.92
RXCJ0928.1+2032	2.80	6.0	1.48	0.3	0.0	0.0	0.77	0.22	-0.06
RXCJ0935.4+0729	4.76	9.0	2.73	0.8	1.0	0.0	0.94	0.31	0.62
RXCJ0942.0+0857	6.29	6.5	1.68	3.0	1.5	1.0	0.68	0.17	-0.10
RXCJ0957.5+1938	0.00	5.5	0.00	1.7	2.5	0.0	0.72	0.29	0.15
RXCJ0959.7+2223	10.30	4.5	1.71	1.2	0.5	0.0	0.24	0.18	-2.37
RXCJ1003.1+6709	4.90	9.5	2.46	5.6	1.5	1.0	0.91	0.25	0.61
RXCJ1007.8+0031	0.74	9.5	1.36	4.2	6.0	3.0	1.00	0.54	0.61
RXCJ1009.0+1400	0.00	6.5	0.00	5.2	3.0	0.5	0.72	0.24	-0.17
RXCJ1012.2+0625	0.00	9.0	0.00	4.1	6.0	4.0	0.39	0.21	-0.98
RXCJ1013.7+1946	0.00	8.0	0.00	5.3	2.5	1.0	0.62	0.19	-0.11
RXCJ1016.2+4108	0.00	5.5	0.00	2.2	0.5	0.0	0.02	0.08	-4.37
RXCJ1016.3+3338	2.41	7.5	1.32	11.4	2.5	1.5	0.12	0.10	-3.61
RXCJ1017.0+3902	8.72	10.0	2.59	0.9	0.5	0.0	0.38	0.11	-0.41
RXCJ1022.5+5006	6.13	10.5	2.24	7.2	1.0	1.0	0.28	0.09	-0.60
RXCJ1025.0+4750	0.14	6.5	0.54	3.3	1.5	0.5	0.62	0.27	0.87
RXCJ1028.3+0346	0.49	6.0	0.68	2.4	0.5	0.0	1.00	0.35	0.83
RXCJ1032.2+4015	1.55	13.5	1.63	5.9	4.0	1.5	0.60	0.20	1.15
RXCJ1039.4+0510	1.30	9.5	1.03	7.2	6.0	3.5	0.43	0.17	-1.52
RXCJ1047.5+1513	3.56	7.5	1.97	6.5	6.0	0.5	0.42	0.28	-0.86
RXCJ1048.7+2214	0.12	5.5	0.40	3.5	1.5	0.5	0.45	0.25	-0.23
RXCJ1053.8+1650	1.31	10.5	1.35	2.3	0.5	0.0	0.41	0.15	-1.21
RXCJ1058.4+5647	6.15	8.5	1.62	14.2	1.0	1.0	0.24	0.07	0.52
RXCJ1058.1+0135	0.15	6.5	0.40	9.5	6.0	3.0	0.53	0.19	-1.30
RXCJ1100.8+1033	0.28	17.0	0.99	3.0	6.0	5.0	0.55	0.21	-0.54
RXCJ1110.5+2842	0.11	12.0	0.44	7.9	6.0	4.0	0.71	0.19	1.03
RXCJ1112.9+1326	4.04	7.0	1.57	3.1	1.0	0.5	0.20	0.12	-2.24
RXCJ1113.3+0231	2.05	13.0	1.55	17.8	4.5	3.5	0.71	0.11	-0.90
RXCJ1121.5+4803	1.60	8.5	1.38	5.4	5.0	0.5	0.53	0.23	0.35
RXCJ1122.8+0106	0.51	12.0	1.33	4.4	3.0	1.5	0.62	0.27	-0.52
RXCJ1125.2+4229	0.00	7.5	0.00	3.1	1.0	0.5	0.89	0.27	1.27
RXCJ1128.0+7529	2.41	9.0	1.98	1.2	0.5	0.0	0.71	0.23	-0.22
RXCJ1126.9+1706	2.76	9.5	1.71	6.1	1.5	1.0	0.58	0.16	-0.31
RXCJ1129.8+2347	2.51	11.5	2.20	6.9	6.0	1.5	0.23	0.16	-1.49
RXCJ1130.0+3637	0.44	11.0	1.04	3.2	6.0	1.0	0.75	0.30	0.64
RXCJ1130.0+2028	2.88	12.0	2.18	9.8	5.0	3.0	0.96	0.29	1.53
RXCJ1133.9+7506	1.18	7.5	1.30	3.4	2.0	1.0	0.47	0.22	-1.33
RXCJ1133.2+6622	2.69	9.0	1.50	4.6	1.0	1.0	0.25	0.10	-0.51
RXCJ1132.8+1428	3.87	13.5	1.71	21.4	2.0	1.5	0.69	0.07	0.43
RXCJ1134.8+4903	0.14	6.5	0.37	15.8	6.0	3.5	0.24	0.14	-1.75
RXCJ1141.2+1044	1.10	10.0	1.59	1.8	2.0	0.5	0.17	0.21	-2.62
RXCJ1142.5+5832	8.31	6.0	2.06	1.1	1.0	0.5	0.03	0.19	-2.50
RXCJ1144.6+6724	2.83	9.5	1.58	8.8	1.0	1.0	0.08	0.08	-4.58
RXCJ1144.7+1949	1.51	18.0	0.83	10.0	6.0	6.0	0.44	0.03	-6.44
RXCJ1145.3+1529	0.67	7.0	0.73	11.3	4.0	2.5	0.43	0.14	-1.91
RXCJ1147.3+5544	0.36	12.5	1.02	9.7	6.0	3.5	0.06	0.14	-2.00
RXCJ1149.0+5135	1.39	8.5	1.57	2.7	3.0	1.0	0.16	0.20	-1.54
RXCJ1156.0+7325	0.87	5.5	0.69	9.9	2.0	1.5	0.72	0.13	0.73
RXCJ1157.4+0503	1.00	10.5	1.24	12.3	5.0	3.0	0.68	0.20	1.02
RXCJ1159.2+4947	5.60	10.5	2.76	4.9	2.5	1.5	0.48	0.19	-0.44
RXCJ1200.3+5613	1.01	14.0	1.42	5.2	6.0	4.5	0.42	0.15	0.19
RXCJ1211.0+3519	1.69	6.5	1.25	1.1	0.5	0.0	1.00	0.36	1.52
RXCJ1213.0+3411	0.00	14.0	0.00	0.2	0.5	0.0	0.69	0.34	0.82
RXCJ1228.8+1924	1.86	8.0	1.73	3.4	6.0	1.0	0.48	0.27	-0.71
RXCJ1229.0+4737	5.62	9.5	2.83	0.9	0.5	0.5	0.30	0.18	-0.36
RXCJ1230.7+1033	7.21	8.0	1.76	6.8	1.0	1.0	0.64	0.13	0.59
RXCJ1233.9+1511	0.00	16.0	0.00	3.9	6.0	4.5	0.64	0.25	0.16
RXCJ1236.4+1631	1.01	9.0	1.07	1.7	2.5	0.5	0.39	0.27	-0.74
RXCJ1241.3+1834	1.65	13.0	1.46	16.8	3.5	2.5	0.25	0.09	-2.68
RXCJ1247.3+5500	0.68	11.0	1.38	3.3	6.0	1.5	-0.01	0.16	-2.89

TABLE 7—*Continued*

name	L_x	R_x (′)	R_x (Mpc)	KS-prop	r_c	r_c(min)	HR	err	ΔHR
RXCJ1310.4+2151	0.00	7.0	0.00	4.7	2.0	1.0	0.49	0.21	-0.17
RXCJ1311.1+3913	1.07	11.0	1.22	12.1	2.5	1.5	0.16	0.10	-1.80
RXCJ1313.1+4616	4.67	12.5	2.97	4.9	1.0	1.0	-0.01	0.12	-3.53
RXCJ1314.4+6434	6.94	6.5	1.76	9.0	1.0	0.5	0.28	0.10	-2.32
RXCJ1320.6+3746	0.00	10.0	0.00	6.9	6.0	3.0	-0.02	0.16	-2.33
RXCJ1323.5+1117	0.00	6.5	0.00	3.2	1.5	1.0	0.54	0.19	0.06
RXCJ1326.2+1230	13.21	13.0	3.34	0.3	0.0	0.0	0.22	0.11	-2.89
RXCJ1327.3+0337	0.00	5.0	0.00	1.8	0.5	0.0	0.77	0.26	0.90
RXCJ1331.5+0451	0.00	8.5	0.00	4.7	3.5	1.0	0.45	0.24	-0.51
RXCJ1342.0+0213	1.46	11.5	1.35	9.9	3.5	2.0	0.57	0.16	0.35
RXCJ1353.0+0509	1.95	12.0	1.44	13.0	2.5	2.0	0.84	0.15	1.93
RXCJ1358.0+2038	0.21	6.5	0.63	2.3	1.0	0.5	0.72	0.39	0.27
RXCJ1359.2+2758	1.91	14.0	1.35	17.6	1.5	1.5	0.46	0.08	0.55

TABLE 8
ADDITIONAL CLUSTERS DETECTED AS EXTENDED X-RAY SOURCES IN THE 9^h TO 14^h REGION

name	alt.name	RA	DEC	z	ctr	F_x	F_x^*	err	L_x	N_H	ref
RXCJ0907.8+4936	VV196	136.9622	49.6066	0.0352	0.17	3.27	2.45	27.3	0.13	1.8	1
RXCJ0916.1+1736		139.0286	17.6017	0.0292	0.16	3.24	2.44	15.4	0.09	3.5	2
RXCJ0923.1+2217	UGC04991	140.7833	22.2979	0.0316	0.11	2.27	1.59	20.0	0.07	3.4	3
RXCJ0933.4+3403	UGC05088	143.3539	34.0521	0.0269	0.08	1.63	1.12	20.5	0.04	1.5	4
RXCJ1008.7+1147	Zw1006.1+1201	152.1995	11.7926	0.2245	0.14	2.98	2.99	16.1	6.40	3.7	5
RXCJ1010.2+5429	RIXOS F231-526	152.5667	54.4883	0.0470	0.11	2.15	1.61	17.0	0.14	0.7	6
RXCJ1053.7+5452	a)	163.4331	54.8721	0.0704	0.21	4.01	3.89	11.5	0.84	0.8	7
RXCJ1057.7+3738		164.4325	37.6351	0.0353	0.09	1.71	1.18	19.8	0.06	1.9	8
RXCJ1116.0+2441		169.0135	24.6885	0.1021	0.11	2.17	2.11	23.2	0.96	1.0	9
RXCJ1122.3+2419	HCG 51	170.5846	24.3167	0.0258	0.15	2.97	2.04	18.4	0.06	1.4	10
RXCJ1122.8+3407	UGC06394	170.7080	34.1232	0.0430	0.10	1.92	1.44	36.5	0.12	2.1	11
RXCJ1204.1+2020	NGC 4066	181.0483	20.3481	0.0252	0.21	4.19	3.15	13.0	0.09	2.4	11,12
RXCJ1206.4+2215	PGC 038401	181.6167	22.2525	0.0656	0.08	1.62	1.50	19.8	0.28	2.1	13
RXCJ1206.6+2811	NGC 4104	181.6560	28.1835	0.0283	0.26	5.23	3.93	12.5	0.14	1.7	14
RXCJ1224.6+3159	SHK 245	186.1673	31.9865	0.0630	0.09	1.82	1.69	19.4	0.29	1.4	15
RXCJ1227.1+1951	MS1224.7+2007	186.7751	19.8538	0.3241	0.09	1.94	1.95	20.0	8.59	2.9	5
RXCJ1231.0+0037	NGC 4493	187.7734	0.6290	0.0232	0.13	2.66	1.84	20.1	0.04	1.9	16
RXCJ1234.2+0947	Zw1231.4+1007	188.5665	9.7835	0.2290	0.14	2.71	2.72	17.5	6.08	1.8	17
RXCJ1320.2+3308	NGC 5098	200.0642	33.1417	0.0362	0.25	4.79	3.59	10.1	0.20	1.0	4,18
RXCJ1329.5+1147	MKW 11	202.3836	11.7892	0.0220	0.38	7.57	5.70	13.4	0.12	2.0	3
RXCJ1334.3+3441	NGC 5223	203.5992	34.6912	0.0240	0.19	3.75	2.57	11.9	0.06	0.9	11

RA and DEC for J2000; RA in decimal degrees

REFERENCES.— (1) Davoust & Considere 1995, (2) Ledlow et al. 1996, (3) Beers et al. 1995, (4) Ramella et al. 1995, (5) Stocke et al. 1991, (6) Caballo et al. 1995, (7) Crawford et al. 1999, (8) Huchra, Geller, & Corwin 1995, (9) Klemola, Jones, & Hansen 1987, (10) Hickson et al. 1992, (11) DeVaucouleur et al. 1991 (RC3), (12) Mahtessian 1998, (13) Fouque et al. 1992, (14) Dell'Antonio, Geller, & Fabricant 1994, (15) Appenzeller et al. 1998, (16) Grogin, Geller, & Huchra 1998, (17) Ebeling et al. 1998, (18) Bade et al. 1998

NOTE.—(a) see also Ebeling et al. 1998

Table 9

X-ray properties of the additional extended cluster sources

name	L_x	R_x ($'$)	R_x (Mpc)	KS-prop	r_c	r_c(min)	HR	err	ΔHR
RXCJ0907.8+4936	0.13	10.5	0.61	2.4	1.0	0.5	0.66	0.23	0.67
RXCJ0916.1+1736	0.09	9.0	0.44	4.5	3.5	0.5	0.33	0.16	-2.58
RXCJ0923.1+2217	0.07	11.5	0.60	3.0	6.0	2.5	0.50	0.28	-0.82
RXCJ0933.4+3403	0.04	7.5	0.34	3.6	1.5	0.5	0.14	0.19	-1.61
RXCJ1008.7+1147	6.40	9.5	2.61	3.2	1.0	0.5	0.59	0.19	-0.87
RXCJ1010.2+5429	0.14	10.0	0.73	5.0	6.0	1.0	0.23	0.21	-0.06
RXCJ1053.7+5452	0.84	11.0	1.20	13.6	3.5	2.5	0.07	0.10	-1.96
RXCJ1057.7+3738	0.06	6.5	0.38	2.3	1.5	0.0	0.31	0.22	-0.96
RXCJ1116.0+2441	0.96	8.5	1.28	4.6	2.0	0.5	1.00	0.45	1.51
RXCJ1122.3+2419	0.06	11.0	0.47	5.7	6.0	2.5	0.38	0.21	-0.16
RXCJ1122.8+3407	0.12	7.0	0.49	2.5	1.0	0.0	0.42	0.27	-0.56
RXCJ1204.1+2020	0.09	13.0	0.55	4.2	6.0	4.5	0.93	0.30	1.04
RXCJ1206.4+2215	0.28	7.5	0.77	2.7	0.0	0.0	1.00	0.40	1.10
RXCJ1206.6+2811	0.14	12.5	0.59	5.1	2.5	1.5	0.20	0.10	-2.85
RXCJ1224.6+3159	0.30	9.0	0.89	5.9	5.5	2.5	0.69	0.38	0.71
RXCJ1227.1+1951	8.59	9.5	3.28	4.1	6.0	3.0	0.81	0.38	0.36
RXCJ1231.0+0037	0.04	10.5	0.41	6.2	4.5	2.0	0.58	0.28	0.20
RXCJ1234.2+0947	6.08	8.5	2.36	5.0	2.5	1.0	0.01	0.15	-3.31
RXCJ1320.2+3308	0.20	11.0	0.65	5.1	1.0	0.5	0.38	0.13	0.35
RXCJ1329.5+1147	0.12	15.5	0.57	2.6	6.0	3.0	0.75	0.24	0.88
RXCJ1334.3+3441	0.06	11.5	0.46	4.0	3.0	1.5	0.32	0.16	0.10